PROPERTIES OF MOLECULES IN WEAK AND STRONG MAGNETIC FIELDS

MARIA DIMITROVA

Dissertation for the degree of *Doctor Philosophiae*

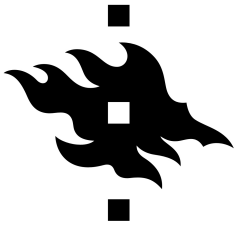

HELSINGIN YLIOPISTO
HELSINGFORS UNIVERSITET
UNIVERSITY OF HELSINKI

MATEMAATTIS-LUONNONTIETEELLINEN TIEDEKUNTA
MATEMATISK-NATURVETENSKAPLIGA FAKULTETEN
FACULTY OF SCIENCE

To be presented for public examination with the permission of the Faculty of Science of the University of Helsinki in Auditorium A129, Chemicum, A. I. Virtasen aukio 1, Helsinki on 27 September 2019 at 12 o'clock.

SUPERVISOR:
Dage Sundholm
University of Helsinki

PRE-REVIEWERS:
Andrew Teale
University of Nottingham

Juha Vaara
University of Oulu

OPPONENT:
Raphael Berger
Universität Salzburg

CUSTOS:
Dage Sundholm
University of Helsinki

ISBN 978-951-51-5400-2 (paperback)
ISBN 978-951-51-5401-9 (PDF)
Unigrafia, Helsinki 2019

Maria Dimitrova: *Properties of Molecules in Weak and Strong Magnetic Fields,* Dissertation for the degree of *Doctor Philosophiae*.

Art is science made clear.
— Jean Cocteau

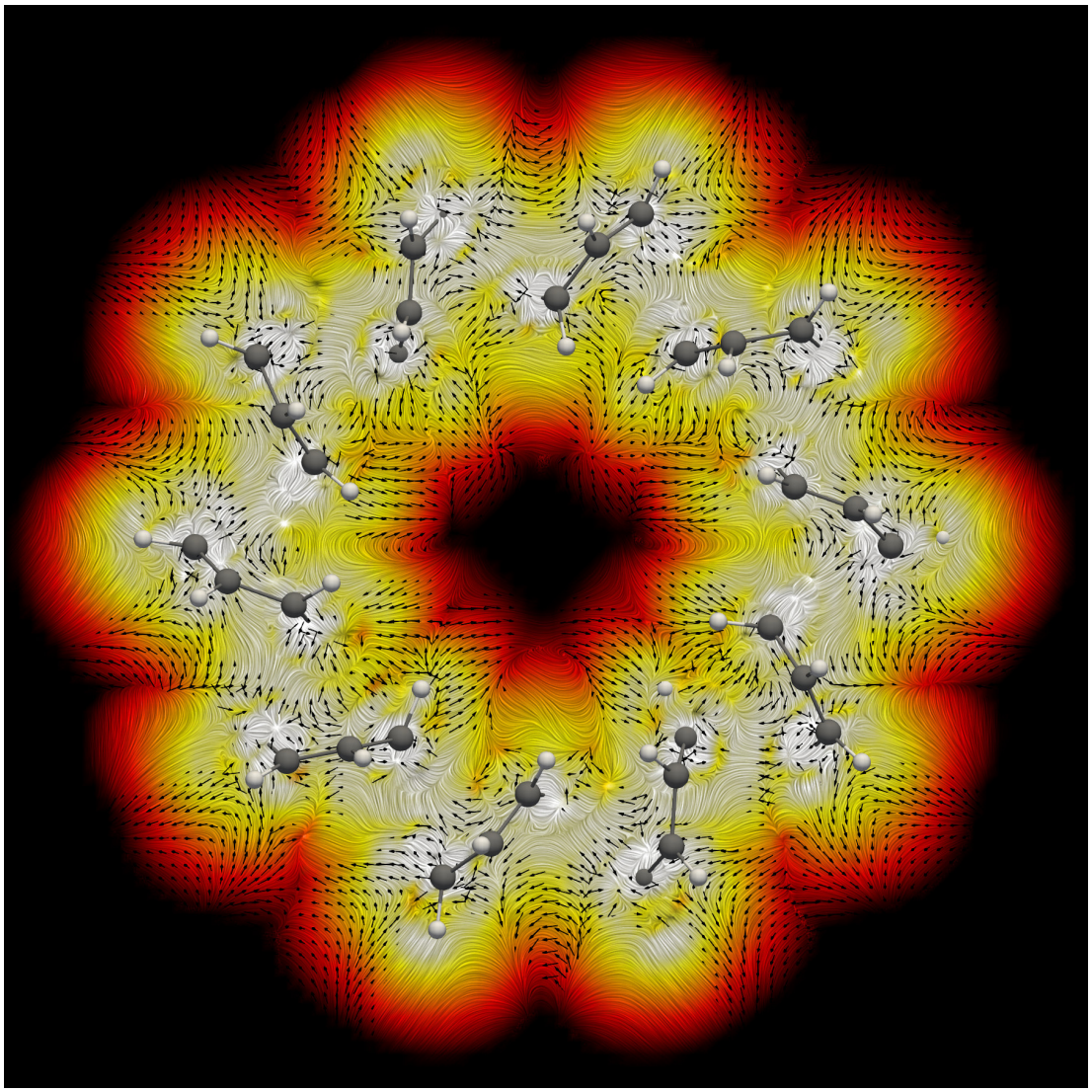

ABSTRACT

Magnetic fields alter the properties of molecules, affecting the electron distribution, the electron configuration and the molecular geometry. In weak magnetic fields, the changes are subtle. Electrons as charged particles placed in magnetic field start following specific pathways, giving rise to magnetically induced ring currents. They follow the contour of the molecule, as well as form vortices around certain molecular rings and chemical bonds. Strong ring currents arise near atomic nuclei due to the core electrons. Magnetically induced currents are a unique fingerprint of the molecular structure but they also serve as an indicator for electron delocalisation, aromatic properties and applicability in optoelectronics. Various organic molecules were investigated using the gauge-including magnetically-induced current density approach. It has been demonstrated that heteroatoms alter the ring-current pathways and the current strength, and thereby affect molecular aromaticity. The topology of Möbius systems has been shown to depend both on the twist of the molecular rings of a series of [4o]annulenes, as well as on their spatial folding (writhe). The investigation of a series of toroidal carbon nanotubes showed helical current flow in one of the chiral molecules in the study, which is a pre-requisite for the generation of anapole moment when the molecule is placed in a magnetic field.

Very strong magnetic fields beyond achievable on Earth cause major changes in the electron configuration of atoms and molecules. Orbitals with high angular momentum and high-spin configurations become lower in energy than the typical zero-field occupation. Weak magnetic fields can be studied as a perturbation to the zero-field Hamiltonian. However, as the field strength increases, the magnetic interaction becomes equally strong as the electrostatic one. The explicit treatment of the magnetic field strength involves the angular momentum operator in the Schrödinger equation, thus leading to complex orbitals. Therefore, new quantum chemistry software is necessary. A benchmark study for the performance of a traditional implementation based on Gaussian-type orbitals versus a fully numerical code has been done at the Hartree–Fock level. After determining the accuracy of the method, small hydrocarbon molecules have been investigated, which showed that they exist as bound molecules in high-spin configurations where only the core electrons of the carbon atom are paired.

YLEISTAJUINEN TIIVISTELMÄ

Kuten tiedämme, magneetti vetää rautaesineitä puoleensa. Magneettien avulla kiinnitetään lappuja jääkaapin oveen, suljetaan kaappien ovet ja älypuhelimen kotelo. Lääkärit tutkivat potilaita vahvan magneettikentän avulla, magnetisoitunut neula kompassissa osoittaa pohjoiseen, ja tietokoneen kovalevy lukee sille talletetut tiedot magneetin avulla. Näiden ilmiöiden salaisuus piilee elektronien ja magneettikentän välisissä vuorovaikutuksissa. Molekyylitasolla magnetismi aikaansaa elektroniliikkeen molekyylin ympäri. Elektronit kiertävät myös tiettyjä atomiryhmiä renkaanmuotoisilla poluilla. Koska jokaisella molekyylillä on omanlainen elektronijakauma, niin näitä elektronipolkuja tutkimalla saadaan tietoja molekyylin ominaisuuksista. Polut kertovat mm. molekyylin soveltuvuudesta aurinkokenno- ja akkukäyttöön. Väitöskirjassa on tutkittu erilaisia orgaanisia molekyylejä sekä toroidimaisia – eli renkaankaltaisia – hiilinanoputkia. Laitetta, joka suoraan pystyisi mittaamaan elektroniliikettä magneettikentässä ei ainakaan vielä ole olemassa, joten tutkimus on suoritettu teoreettisen mallinnuksen avulla, kvanttikemiallisia menetelmiä käyttäen.

Laboratoriossa valmistetut magneetit voivat olla jopa miljoona kertaa maapallon omaa magneettikenttää voimakkaampia. Sellaista ainetta, joka kestäisi sitä valtavaa voimaa, jolla vahva magneettikenttä vaikuttaa kappaleeseen, ei ole olemassa. Maailmankaikkeudesta, tiettyjen tähtien läheisyydessä, löytyy kuitenkin jopa miljardikertaisesti vahvempia magneettikenttiä. Elämänsä loppuvaiheessa tähti voi kutistua pieneksi, erittäin tiheäksi kappaleeksi – niin sanotuksi valkoiseksi kääpiöksi. Mikäli alkuperäinen tähti on ollut riittävän iso, lopuksi jää kappale, joka on niin tiheä, että atomitkin hajoavat. Tällaista taivaankappaletta kutsutaan neutronitähdeksi. Erittäin vahva magneettikenttä aiheuttaa huomattavia muutoksia molekyylien elektronirakenteissa, mikä puolestaan johtaa uusiin ja pääosin arvaamattomiin ominaisuuksiin. Näiden ominaisuuksien tutkiminen onkin väitöskirjan toinen aihe. Perinteiset kvanttikemian ohjelmistot eivät pysty mallintamaan magneettikentän aiheuttamia muutoksia elektronirakenteessa. Väitöskirjassa tutkittiin uudentyyppisten ohjelmistojen tarkkuutta vahvassa magneettikentässä olevien molekyylien mallinnuksessa. Tutkimuksen kohteena oli pienten molekyylien elektronikonfiguraatio, geometria ja sidosten vahvuus; ominaisuuksia, joita ei aikaisemmin juurikaan ole tutkittu.

ACKNOWLEDGMENTS

First and foremost, I would like to express my gratitude to my supervisor, Prof. Dage Sundholm, who has given me the opportunity to obtain new skills and to start the track towards becoming an independent researcher, as well as for the numerous possibilities to travel and present my work at international conferences. I would like to thank my co-workers and friends Markus Rauhalahti, Lukas Wirz and Heike Fliegl for their support, and the rest of the members of the Laboratory for Instruction in Swedish (nowadays Theoretical and Computational Chemistry group) for the friendly atmosphere during my studies as a Master's degree student and as a doctoral candidate. I am greatful for the thorough constructive comments by Prof. Pekka Pyykkö, Lukas Wirz, and Susi Lehtola who volunteered to read the manuscript of my doctoral thesis. Thanks to Mikael Johansson for correcting my mistakes in the abstract in Finnish. I would like to thank Stella Stopkowicz, Andy Teale and Trygve Helgaker for the fruitful discussions, as well as the rest of the members of the project "Molecules in Extreme Environments" for the advice and guidance. It was an enlightening experience to do research in the Centre for Advanced Studies at the Norwegian Academy of Science and Letters. I thank Andy Teale and Juha Vaara for their detailed reviews of my work, and Raphael Berger for agreeing to be my opponent at the defence of my doctoral thesis in a short notice. I thank Erik Tellgren for the copy of the London program, and Stella Stopkowicz and Florian Hampe for sharing their tool to determine orbital symmetry. The template for my doctoral thesis is originally created and made freely available online by André Miede and Ivo Pletikosić. My research would not have been possible without the financial support of the Magnus Ehrnrooth foundation and the Finnish cultural foundation. The computational resources provided by the Finnish IT Centre for Science (CSC) and the Finnish Grid and Cloud Infrastructure were likewise indispensable. I also thank my partner and my parents for the kind support and understanding during my studies.

Maria Dimitrova

September 13, 2019
Helsinki, Finland

PUBLICATIONS INCLUDED IN THE THESIS

[1] M. Dimitrova and D. Sundholm. The aromatic character of [10]annulenes and dicupra[10]annulenes from current density calculations. *Phys. Chem. Chem. Phys.* **20** (2018), 1337.

[2] M. Dimitrova, H. Fliegl, and D. Sundholm. The influence of heteroatoms on the aromatic character and the current pathways of B_2N_2-dibenzo[a,e]pentalenes. *Phys. Chem. Chem. Phys.* **19** (2017), 20213.

[3] L. N. Wirz, M. Dimitrova, H. Fliegl, and D. Sundholm. Magnetically Induced Ring-Current Strengths in Möbius Twisted Annulenes. *J. Phys. Chem. Lett.* **9** (2018), 1627.

[4] K. Reiter, F. Weigend, L. N. Wirz, M. Dimitrova, and D. Sundholm. Magnetically Induced Current Densities in Toroidal Carbon Nanotubes. *J. Phys. Chem. C* **123** (2019), 15354.

[5] S. Lehtola, M. Dimitrova, and D. Sundholm. Fully numerical electronic structure calculations on diatomic molecules in weak to strong magnetic fields. *Mol. Phys. (published online)* (2019).

[6] M. Dimitrova, S. Lehtola, D. Sundholm, T. Helgaker, and S. Stopkowicz. Small hydrocarbons in strong magnetic fields: CH and CH_2. *(in preparation)* (2019).

OTHER PUBLICATIONS

[1] D. Jia, Y. Yang, M. Dimitrova, Y. Man, and D. Sundholm. Nuclear versus electronic currents in torsional molecules induced by magnetic fields: Quantum model simulations for $C_6H_2F_3CH_3$. *(in preparation)* (2019).

[2] K. Bartkowski, M. Dimitrova, P. J. Chmielewski, D. Sundholm, and M. Pawlicki. Aromatic and Antiaromatic Pathways in a Triphyrin(2.1.1) Fused with Benzo[b]heterocycles. *(submitted)* (2019).

AUTHOR CONTRIBUTIONS

Article I	MD developed a visualisation procedure and an interactive interface to the GIMIC program, performed all calculations, prepared the figures, and participated in the analysis of the results and the preparation of the manuscript.
Article II	MD performed all calculations, prepared the figures, and participated in the analysis of the results and the preparation of the manuscript.
Article III	MD introduced LNW to the computational method, performed the calculations of the magnetically induced current-density vector field, prepared the figures, and participated in the analysis of the results and the preparation of the manuscript.
Article IV	MD introduced KR to the method, performed some of the calculations of the magnetically induced current-density vector field, prepared some of the figures, and participated in the analysis of the results and the preparation of the manuscript.
Article V	MD performed the calculations with the LONDON program and participated in the analysis of the results and the preparation of the manuscript.
Article VI	MD performed all calculations with the exception of the benchmarks obtained with the HELFEM code, prepared the figures, and participated in the analysis of the results and the preparation of the manuscript.

CONTENTS

ABSTRACT v

YLEISTAJUINEN TIIVISTELMÄ vii

1 INTRODUCTION 1

2 QUANTUM CHEMISTRY METHODS 5

2.1 The Schrödinger Equation . . . 5
2.2 The Hamiltonian Operator . . . 6
2.3 The Self-consistent Field Method . . . 7
2.4 Hartree–Fock Equations . . . 7
2.5 Basis Set Expansion . . . 9
2.6 Linear Combinations of Atomic Orbitals . . . 10
2.7 Electron Correlation . . . 11
2.8 Perturbation Theory . . . 12
2.9 Configuration Interaction . . . 13
2.10 Coupled Cluster . . . 14
2.11 Electron Density . . . 15
2.11.1 The Thomas–Fermi model . . . 15
2.11.2 Hohenberg–Kohn theorems . . . 16
2.12 Kohn–Sham Equations . . . 16
2.13 Density Functional Theory . . . 17
2.13.1 Local-density approximation . . . 17
2.13.2 Generalised-gradient approximation . . . 18
2.13.3 Hybrid functionals . . . 19
2.14 Methodological Errors and Corrections . . . 19
2.14.1 Basis-set problems . . . 19
2.14.2 System-size problems . . . 20
2.14.3 Problems in density functional theory . . . 20
2.14.4 Dispersion correction . . . 21
2.14.5 Resolution-of-the-identity approximation . . . 22
2.14.6 Spin-component-scaled electron correlation . . . 22
2.14.7 Explicitly correlated methods . . . 22
2.15 Molecular Properties . . . 23

3 MAGNETIC FIELDS 25

3.1 Classical Electromagnetism . . . 25
3.1.1 Notation and units . . . 26
3.1.2 Maxwell's equations . . . 26
3.1.3 Electromagnetic induction . . . 27
3.1.4 Electrostatic fields . . . 27
3.1.5 Magnetostatic fields . . . 28
3.1.6 Magnetic pressure . . . 29
3.1.7 Precession in a magnetic field . . . 29
3.1.8 Classical diamagnetism . . . 30
3.1.9 Magnetisation . . . 30

3.1.10 Magnetic permeability . . . 31
3.2 Quantum-mechanical Treatment of Magnetic Fields . . 32
3.2.1 Angular momentum in quantum mechanics . . 32
3.2.2 Quantisation of angular momentum . . . 33
3.2.3 Spin angular momentum . . . 33
3.2.4 Total angular momentum . . . 34
3.2.5 Zeeman effect . . . 35
3.2.6 The Hamiltonian in a uniform magnetic field . 35
3.2.7 Magnetically induced current density . . . 37
3.2.8 Current density topology . . . 39
3.2.9 Nuclear magnetic vector potential . . . 40
3.2.10 Nuclear shielding . . . 41
3.2.11 The gauge-including magnetically induced currents method . . . 43
3.2.12 Molecular aromaticity . . . 44
3.2.13 Anapole moment . . . 45
3.2.14 The strong-magnetic-field regime . . . 46
3.2.15 Atoms and molecules in strong and ultrastrong magnetic fields . . . 46
4 INVESTIGATIONS AND RESULTS 49
4.1 Electronic Flow in Weak Magnetic Fields . . . 49
4.1.1 Visualisation of the current density field . . . 49
4.1.2 Calculation of the strength of the current density 51
4.1.3 Applications of the current density analysis . . 55
4.2 Small Molecules in Strong Magnetic Fields . . . 58
4.2.1 Basis set evaluation . . . 58
4.2.2 Atoms . . . 59
4.2.3 Diatomic molecules . . . 61
4.2.4 Polyatomic molecules . . . 62
5 CONCLUSION 63

BIBLIOGRAPHY 65
APPENDIX 77
Article I . . . 79
Article II . . . 91
Article III . . . 103
Article IV . . . 109
Article V . . . 121
Article VI . . . 135

LIST OF FIGURES

Figure 1.1 Orders of magnitude of magnetic field strength. 2
Figure 4.1 The current density in ethane illustrated with the line-integral convolution method. 50
Figure 4.2 The current density in the T-shaped benzene dimer. 50
Figure 4.3 The current density in a triphyrin illustrated with streamlines. 52
Figure 4.4 A streamline representation of the global ring current in a toroidal carbon nanotube. 52
Figure 4.5 An integration plane in the toluene molecule showing the current density flow. 54
Figure 4.6 Ring currents in naphthalene. 54
Figure 4.7 The structure of the corners of some of the investigated toroidal carbon nanotubes. 57
Figure 4.8 Basis-set truncation errors for the quintet state of BeH^+ with a series of correlation-consistent basis sets. 60
Figure 4.9 The energy of the carbon atom in strong magnetic fields. 60
Figure 4.10 The p orbital of the carbon atom at $B = 0$ and at $B = 10\,B_0$. 61

LIST OF TABLES

Table 3.1 Commonly used units in electromagnetism. . . 26

ACRONYMS

AO atomic orbital

BSIE basis-set incompleteness error

BSSE basis-set superposition error

BSTE basis-set truncation error

CC coupled cluster

CCD coupled cluster doubles

CCSD coupled cluster singles and doubles

CCSD-F12 explicitly correlated coupled cluster

CCSD(T) coupled cluster singles and doubles with perturbative inclusion of triples

CGTO contracted Gaussian–type orbital

CI configuration interaction

CID configuration interaction doubles

CISD configuration interaction singles and doubles

DFT density functional theory

DZ double-ζ

ECP effective core potential

FCI full configuration interaction

FEM finite-element method

GGA generalised-gradient approximation

GIAO gauge-including atomic orbital

GIMIC gauge-including magnetically induced currents

GTO Gaussian-type orbital

HF Hartree–Fock

HK Hohenberg–Kohn

KS Kohn–Sham

LCAO linear combination of atomic orbitals

LSDA local-spin-density approximation

MGGA meta-generalised-gradient approximation

MO molecular orbital

MP2 second-order Møller–Plesset perturbation theory

NICS nucleus-independent chemical shift

NMR nuclear magnetic resonance

PES potential energy surface

POST-HF post-Hartree–Fock

PPM parts per million

QZ quadruple-ζ

RI resolution of the identity

SCF self-consistent field

SCS spin-component scaled correlation

STO Slater–type orbital

SV split valence

TF Thomas–Fermi

TZ triple-ζ

UHF unrestricted Hartree–Fock

XC exchange–correlation

1 INTRODUCTION

Magnetic fields perturb atoms and molecules, leading to shifts and/or splitting of their energy levels. For open-shell atoms, such Zeeman splittings were observed for the first time in the atomic emission spectra of sunspots in the beginning of the 20$^{\text{th}}$ century [1, 2]. Molecules with anisotropic magnetic susceptibility have a preferred orientation with respect to the magnetic field lines even in weak magnetic fields [3]. Functionalised carbon nanotubes were observed to become longer and higher in quality in a magnetic field of about 1 T [4]. Phthalocyanine moieties align favourably in a magnetic field of 12 T and form nanowires with increased conductivity on a suitable surface template [5]. There are indications that the properties of water such as its melting point, surface tension and hydrogen bond strength are altered in the presence of magnetic fields of the order of 10 T [6–8]. However, the spatial motion of molecules is not restricted in a magnetic field of such magnitude, and they are able to take any spatial orientation thanks to thermal motion.

The magnetic moment of an electron with an orbital angular momentum of $\hbar$ is quantified in *Bohr magnetons*, μ_B. The spin angular momentum of an electron gives rise to magnetic moment which is approximately equal to $\pm 1/2 \mu_B$. The Bohr magneton is rather small in magnitude, ($\mu_B = 9.274\,010\,078\,3 \times 10^{-24}\ \text{J} \cdot \text{T}^{-1}$) [9].

In fact, the ratio between the electron magnetic moment and the Bohr magneton is 1.001 159 652(10). *The difference is the quantum-electrodynamic correction.*

The strength of magnetic fields can be classified by the relative magnitude of the Coulomb interactions and the magnetic interactions between the particles and the electromagnetic field. In the weak-field limit, magnetic interactions of an electron are a small perturbation to Coulomb interactions. However, in semiconductors with a high dielectric constant, the Coulomb force is attenuated and the magnetic field acts as if it were very strong [10].

A graphical representation of the scale of magnetic field strength found in nature and in laboratory conditions is given in Figure 1.1. The strongest continuous magnetic field made in laboratory conditions is barely 45.5 T, produced at the National High Magnetic Field Laboratory in Tallahassee, Florida [11]. An alternative technique for achieving higher magnetic field strength is by producing pulsed fields in millisecond-long bursts or shorter. The present record for the strongest non-destructive pulsed magnet is held by the Pulsed Field Facility at Los Alamos National Laboratory in Los Alamos, New Mexico (100 T). However, there are reports of up to 2000 T having been reached at the All-Russian Scientific Research Institute of Experimental Physics (VNIIEF) [12]. Other reports of self-destructive magnetic field appa-

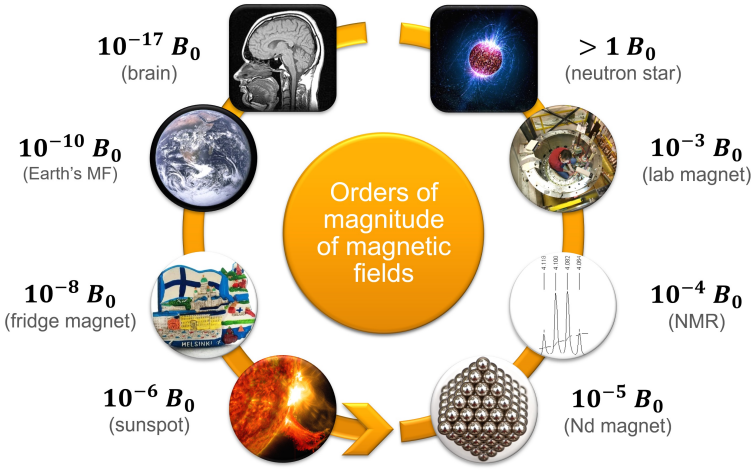

Figure 1.1: Orders of magnitude of magnetic field strength. The atomic unit of magnetic field strength has been employed, where $B_0 = 2.350\ 517\ 42 \times 10^5$ T. Pictures obtained from Wikimedia Commons.

ratuses have been given for example by Fowler and Nakamuna [13, 14].

Magnetic fields beyond achievable on Earth exist on magnetic white dwarfs [15–18]. At the end of the scale lie neutron stars [19]. They are stars at the end of their lifespan with extremely high density and high angular momentum. The magnetic field strength on these bodies can reach millions of tesla [20]. In spite of the high surface temperature of more than 10 000 K [18], molecular hydrogen has been found in the spectra of white dwarfs [21]. Other elements and molecular species have also been identified, including H, He, O, CH, and C_2 [16, 22–26]. The extremely strong gravity and temperature on neutron stars makes it highly unlikely for any molecular species to exist.

The work presented in this doctoral thesis is focused on some properties of molecules in weak and strong external magnetic fields. We have investigated the magnetically induced current density in various molecules at the limit of infinitely weak magnetic field. The results of the studies are presented in Article I, Article II, Article III, and Article IV. According to the ring-current model [27], magnetically induced current-density vortices arise when a molecule is placed in a magnetic field. The current density distribution reflects the electronic structure of the molecule, giving a unique representation of its properties. Molecules sustaining non-zero net current strength exhibit aromatic or antiaromatic character depending on the direction of the current flow with respect to the external magnetic field. A typical structural feature of aromatic and antiaromatic molecules is the presence of conjugated π-electron pathways in the molecular rings. Aromaticity can be reliably studied using the ring-current criterion. Therefore, organic and inorganic structures with one or more molecular rings are

often the subject of interest in current-density studies [28]. Although traditionally associated with the stability and chemical properties of molecules, the significance of the abstract concept of aromaticity goes beyond chemical reactivity. Highly delocalised excited states usually make molecules suitable as conductive or semi-conductive materials, as well as chromophores which are of practical interest in light harvesting. They are suitable for the purpose of optoelectronics, spintronics, photovoltaics and non-linear optics [29]. Therefore current-density studies are a valuable tool for the development of new materials.

The strong-magnetic-field regime has been studied experimentally to a limited extent due to the aforementioned difficulties in the construction of the necessary laboratory equipment. Theoretical studies have recently started gaining popularity. The explicit treatment of the magnetic field in the calculations brings various challenges to accurately model the environment which is potentially impossible to study in the lab. New quantum-chemistry programs are necessary for the explicit treatment of the magnetic field. The majority of prior studies in the literature are focused on atoms or diatomic molecules. In Article V, we performed a benchmark study on the performance of a traditional versus a fully-numerical implementation to describe small diatomic molecules. Subsequently in Article VI, we investigated chemical bonding in small polyatomic molecules consisting of carbon and hydrogen. Their electron configurations and geometry do not match prior chemical intuition. Such studies may contribute to fundamental science and can be potentially useful in astrophysics.

2

QUANTUM CHEMISTRY METHODS

Quantum chemistry is the application of quantum mechanics to molecular systems. Electronic structure methods describe molecular systems across different scales – from a single atom to macromolecules of a million atoms [30]. Quantum chemistry calculations typically aim for obtaining an accurate value for the energy of the investigated molecule after applying a set of approximations. Various other properties can be subsequently calculated.

The wave function is a vector in the Hilbert space – a multi-dimensional linear vector space.

2.1 THE SCHRÖDINGER EQUATION

In the Copenhagen interpretation of quantum mechanics, the wave function is an abstract entity which fully describes the state of a quantum object. The time-independent Schrödinger equation can be used to calculate the energy spectrum of a quantum mechanical system [31–34],

Spectral (eigenvalue) decomposition implies that a linear operator or a matrix is symmetrical and can be diagonalised.

$$\hat{H}\psi = E\psi, \tag{2.1}$$

where $\hat{H}$ is the Hamiltonian operator, ψ is the wave function, and E is the energy. The Hamiltonian consists of kinetic and potential energy terms. Formally, if the wave function were known, it would be possible to calculate the exact energy of the molecule which is ultimately its most important characteristic.

As noted by Schrödinger back in 1926 [35], his concept of wave mechanics is identical to the matrix mechanics approach developed by Born, Heisenberg, and Jordan [36–39]. An observable A is a property which can be measured experimentaly. Measurement causes the wave function collapse into one of its eigenstates. The possible outcomes of a measurement are the set of eigenvalues A_i which correspond to a Hermitian operator $\hat{A}$. This reflects the statistical, nondeterministic nature of quantum mechanics as there is a probability amplitude associated with the collapse to each eigenstate. The probability for obtaining an experimental outcome A_i is given by the squared modulus of the wave function, also known as *Born's rule* [40]. In Dirac (bra-ket) notation the expectation value of the observable is expressed as the normalized integral of the inner product of the complex conjugate of the wave function with the state vector obtained when the operator $\hat{A}$ is applied to the wave function [41],

The bra-vector $\langle\psi|$ is the complex conjugate of the state ket-vector $|\psi\rangle$.

$$\langle A \rangle = \frac{\langle \psi \,|\hat{A}|\, \psi \rangle}{\langle \psi \,|\psi\rangle}. \tag{2.2}$$

2.2 THE HAMILTONIAN OPERATOR

In quantum mechanics the Hamiltonian operator gives the energy spectrum of the system. The molecular Hamiltonian for a molecule in vacuum is the sum of the kinetic energy of the electrons $\hat{T}_e$, the kinetic energy of the nuclei $\hat{T}_N$, the electron-electron repulsion $\hat{V}_{ee}$, the nuclear repulsion $\hat{V}_{NN}$, and the Coulomb attraction between the nuclei and the electrons $\hat{V}_{eN}$,

$$\hat{H} = \hat{T}_e + \hat{T}_N + \hat{V}_{ee} + \hat{V}_{eN} + \hat{V}_{NN}. \tag{2.3}$$

Nuclear mass is at least three orders of magnitude larger than the mass of the electron which makes it possible to separate the total wave function into a product of electronic and nuclear components. This is known as the *Born–Oppenheimer approximation* [42]. The non-relativistic electronic Hamiltonian $\hat{H}_e$ for a molecule with n electrons and N atoms excluding the nuclear kinetic energy $\hat{T}_N$ and the nuclear repulsion $\hat{V}_{NN}$ is given by the expression

It is common to work in atomic units where the constants $m_e = e = \hbar = 4\pi\varepsilon_0 = 1$.

$$\hat{H}_e = \underbrace{-\sum_i^n \frac{\hbar}{2m_e}\nabla_i^2}_{\text{kinetic energy}} + \underbrace{\sum_{i<j} \frac{e^2}{4\pi\varepsilon_0}\frac{1}{|\boldsymbol{r}_i - \boldsymbol{r}_j|}}_{\text{potential energy (repulsion)}} - \underbrace{\sum_i^n \sum_A^N \frac{Z_A e^2}{4\pi\varepsilon_0}\frac{1}{|\boldsymbol{r}_i - \boldsymbol{R}_A|}}_{\text{potential energy (attraction)}}, \tag{2.4}$$

Generally, the Laplacian ∇^2 is the second derivative over each spatial dimension,

$$\frac{\partial^2}{\partial x^2} + \frac{\partial^2}{\partial y^2} + \frac{\partial^2}{\partial z^2}$$

where the following quantities are defined:

$\hbar$	reduced Planck constant
m_e	rest mass of the electron
∇_i^2	Laplacian acting on the position of electron i
e	elementary charge
Z_A	nuclear charge of atom A
ε_0	dielectric constant of the vacuum
$\lvert\boldsymbol{r}_i - \boldsymbol{r}_j\rvert$	distance between electrons i and j
$\lvert\boldsymbol{r}_i - \boldsymbol{R}_A\rvert$	distance between electron i and nucleus A

The Schrödinger equation can be solved analytically only for a handful of models such as the particle in a box [32], the harmonic oscillator [32, 38] and for hydrogen-like atoms.

The electronic repulsion term in the Hamiltonian includes the distance between each pair of electrons. Therefore, the molecular Schrödinger equation is not separable into a set of one-electron differential equations and its analytical solution becomes intractable. The motion of one electron depends on the instantaneous position of all the other electrons. In other words, electronic motion is *correlated*.

2.3 THE SELF-CONSISTENT FIELD METHOD

The motion of an electron depends on the potential generated by the electron density of the neighbouring electrons. When the probability distribution of one of them changes, the motion of all the other electrons is affected. The explicit interaction between the electrons in a molecule can be simplified to the interaction of an electron i with the mean electrostatic field V_{eff} of the other $(N-1)$ electrons as if their distribution were fixed [43, 44]. The effective potential for electron 1 can be expressed as a function of the charge density of each electron i, $\rho_i = |\varphi_i|^2$, in the elementary volume v as

$$V_{\text{eff}}(1,i) = \sum_{i=2}^{N} \int_V \frac{\rho_i}{r_{1,i}} dv. \tag{2.5}$$

Effectively, the above integral expresses that the charge of electron i is smeared out in space. This fairly crude approximation allows the many-electron wave function to be written as a *Hartree product* – a product of independent one-particle wave functions [43],

$$\Psi(\boldsymbol{r_1}, \boldsymbol{r_2}, \ldots, \boldsymbol{r_N}) = \varphi_1(\boldsymbol{r_1})\varphi_2(\boldsymbol{r_2}) \ldots \varphi_N(\boldsymbol{r_N}). \tag{2.6}$$

The N-body molecular electronic Hamiltonian is then the sum of the single-particle Hamiltonians $\hat{h}(i)$. Thus, the *mean-field approximation* makes it possible to separate the Schrödinger equation into one-electron equations. They are solved iteratively because the Hamiltonian depends on the occupied orbitals. As suggested by Slater, this approach reduces the differential-equation problem into a variational minimisation problem solved using the method of Lagrange multipliers λ_{ij} [45],

$$\delta\mathcal{L} = \delta E - \sum_{i,j}^{N} \lambda_{ij} \left(\langle \delta\chi_i | \chi_j \rangle - \langle \chi_i | \delta\chi_j \rangle \right) = 0. \tag{2.7}$$

The Lagrange multipliers ensure orthogonality between the orbitals.

Therefore the self-consistent field (SCF) method by Hartree is a *variational method*. Consequently, the best approximation of the ground-state wave function is obtained by minimising the expectation value ε of the energy [46]. The variational theorem states that the true energy of a system always lies lower than the approximate one ($\varepsilon \geq E_0$).

2.4 HARTREE–FOCK EQUATIONS

The disadvantage of the Hartree product (eq. 2.6) is that the molecular wave function $\Psi(\boldsymbol{r_1}, \boldsymbol{r_2}, \ldots, \boldsymbol{r_N})$ is not antisymmetric, which is required for fermions, such as electrons. An improved antisymmetrised linear

According to Fermi-Dirac spin statistics, the sign of the wave function changes upon permutation of two electrons [47, 48].

combination of one-electron wave functions depending both on the spatial and the spin coordinate $\chi_i(\boldsymbol{r}_j;\sigma_j)$ (spin-orbitals) is known as a *Slater determinant* [49, 50],

The Slater determinant vanishes for any two electrons with identical coordinates.

$$\begin{aligned}\Psi(\boldsymbol{r_1},\boldsymbol{r_2},\ldots,\boldsymbol{r}_N;\sigma_1,\sigma_2,\ldots,\sigma_N) &= \\ &= \frac{1}{\sqrt{N!}}\begin{vmatrix}\chi_1(\boldsymbol{r}_1;\sigma_1) & \chi_1(\boldsymbol{r}_2;\sigma_2) & \cdots & \chi_1(\boldsymbol{r}_N;\sigma_N)\\ \chi_2(\boldsymbol{r}_1;\sigma_1) & \chi_2(\boldsymbol{r}_2;\sigma_2) & \cdots & \chi_2(\boldsymbol{r}_N;\sigma_N)\\ \vdots & \vdots & \ddots & \vdots\\ \chi_N(\boldsymbol{r}_1;\sigma_1) & \chi_N(\boldsymbol{r}_2;\sigma_2) & \cdots & \chi_N(\boldsymbol{r}_N;\sigma_N)\end{vmatrix}.\end{aligned} \tag{2.8}$$

Describing the total wave function as a Slater determinant makes it consistent with the Pauli exclusion principle [51] which states that it is impossible to have two electrons with the same spatial and spin coordinates.

When the Hartree products are replaced with Slater determinants, the approach is called the Hartree–Fock (HF) method. The molecular Hamiltonian becomes the sum of the one-electron (core) Hamiltonians $\hat{h}_{\text{core}}(i)$, the two-electron effective potential terms and the nuclear repulsion,

$$\hat{H}_{\text{HF}} = \sum_i^n \hat{h}_{\text{core}}(i) + \sum_{i<j} V_{\text{eff}}(i,j) + V_{NN}\ \text{, where} \tag{2.9}$$

$$\hat{h}_{\text{core}}(i) = -\frac{1}{2}\nabla_i^2 - \sum_A^N \frac{Z_A}{r_{iA}}. \tag{2.10}$$

The indices i and j denote the set of electrons, while the index A refers to the nuclei. The effective potential V_{eff} is the two-electron interaction, which is expressed as two-electron integrals. By applying the variational principle, the energy expression is obtained as

The notation $\langle pq\,||rs\,\rangle$ implies that the integrals are antisymmetrised: $\langle pq\,|rs\,\rangle - \langle pq\,|sr\,\rangle$. The letters refer to the index of the spin-orbital χ.

$$E_{\text{HF}} = \sum_i \langle i|\hat{h}|i\rangle + \sum_{i,j}\frac{1}{2}\,\langle ij\,||ij\,\rangle\,. \tag{2.11}$$

The two-electron integrals $\langle ij\,||ij\,\rangle$ can be split into two sets. The Coulomb integrals J_{ij} describe the repulsion between two electrons in orbitals i and j,

$$J_{ij} = \langle ij\,|ij\,\rangle = \int \chi_i^*(\boldsymbol{r}_1)\chi_i(\boldsymbol{r}_1)\frac{1}{\boldsymbol{r}_{12}}\chi_j^*(\boldsymbol{r}_2)\chi_j(\boldsymbol{r}_2)\mathrm{d}\boldsymbol{r}_1\mathrm{d}\boldsymbol{r}_2. \tag{2.12}$$

The other set of integrals, the exchange integrals K_{ij}, defines the exchange interaction occurring when swapping electrons 1 and 2,

$$K_{ij} = \langle ij\,|ji\,\rangle = \int \chi_i^*(\boldsymbol{r}_1)\chi_j(\boldsymbol{r}_1)\frac{1}{\boldsymbol{r}_{12}}\chi_j^*(\boldsymbol{r}_2)\chi_i(\boldsymbol{r}_2)\mathrm{d}\boldsymbol{r}_1\mathrm{d}\boldsymbol{r}_2. \tag{2.13}$$

The two-electron integrals are used in the expression for the *Fock operator*,

$$\hat{f}(i) = \hat{h}_{\text{core}}(i) + \sum_{j=1}^{N} \left(\hat{J}_j - \hat{K}_j \right). \tag{2.14}$$

The Coulomb operator $\hat{J}_j$ and the exchange operator $\hat{K}_j$ are applied to the orbital $\chi_i(\boldsymbol{r}_1)$ as

The Coulomb operator expresses the interaction between an electron with the smeared charge density of the other electrons.

$$\hat{J}_j \chi_i(\boldsymbol{r}_1) = \chi_i(\boldsymbol{r}_1) \int |\chi_j(\boldsymbol{r}_2)|^2 \frac{1}{r_{12}} \mathrm{d}\boldsymbol{r}_1 \mathrm{d}\boldsymbol{r}_2; \tag{2.15}$$

$$\hat{K}_j \chi_i(\boldsymbol{r}_1) = \chi_j(\boldsymbol{r}_1) \int \chi_j^*(\boldsymbol{r}_2) \chi_i(\boldsymbol{r}_1) \frac{1}{r_{12}} \mathrm{d}\boldsymbol{r}_1 \mathrm{d}\boldsymbol{r}_2. \tag{2.16}$$

There is no analogue for the exchange interaction in classical physics.

In the case of $i = j$, the Coulomb and the exchange terms cancel. This prevents the unphysical repulsion between an electron and its own electron density known as *self-interaction error*.

2.5 BASIS SET EXPANSION

The Hartree–Fock problem is usually implemented in the linear combination of atomic orbitals (LCAO) approximation [52, 53]. Each molecular orbital (MO) is expanded into a set of basis functions,

$$\psi_i(\boldsymbol{r}) = \sum_{\mu} c_{\mu i} \chi_\mu(\boldsymbol{r}). \tag{2.17}$$

In principle, if one could use an infinite number of basis functions, the expansion would produce the exact Hartree–Fock energy. For practical purposes, the basis set is truncated to a feasible size.

The LCAO approximation allows the Hartree–Fock equations to be expressed in a matrix form. Also, it allows for the calculations to be efficiently carried out on a computer using linear algebra. The expression is known as the Hartree–Fock–Roothaan equations,

Mulliken notation $(\mu\lambda|\nu\sigma)$ is the analogue of bra-ket notation, however there are spatial orbitals ψ instead of spin-orbitals χ, and the order is different, $\langle ij|kl\rangle = (ik|lj)$.

$$\boldsymbol{FC} = \boldsymbol{SC\varepsilon} \;\Leftrightarrow\; \sum_{\mu} \left(F_{\mu\nu} - \varepsilon_i S_{\mu\nu} \right) c_{\mu i} = 0. \tag{2.18}$$

where $\boldsymbol{F}$ is the Fock matrix with matrix elements $F_{\mu\nu}$,

$$F_{\mu\nu} = h_{\mu\nu} + \sum_{\lambda\sigma} D_{\lambda\sigma} \left[(\mu\nu|\lambda\sigma) - \frac{1}{2} (\mu\lambda|\nu\sigma) \right], \tag{2.19}$$

$\boldsymbol{C}$ represents the matrix of orbital coefficients $c_{\mu i}$, $\boldsymbol{S}$ is the overlap matrix with matrix elements $S_{\mu\nu} = \langle \chi_\mu | \chi_\nu \rangle$, and $\boldsymbol{\varepsilon}_i$ is the diagonal

matrix of orbital energies. The overlap matrix arises because the employed basis functions are non-orthogonal while the molecular orbitals need to be orthonormal. The matrix elements of the Hamiltonian are expressed as $h_{\mu\nu} = \langle\mu|\hat{h}_{\text{core}}|\nu\rangle$. The sum of the products of orbital coefficients $D_{\mu\nu} = 2\sum_i c^*_{\mu i} c_{\nu i}$ is the density matrix, and the terms in square brackets are the two-electron integrals in Mulliken notation. The Greek letters refer to basis functions.

Instead of minimising the orbitals as in eq. 2.7, the SCF procedure minimises the energy by varying the orbital expansion coefficients c according to the Rayleigh–Ritz variational formalism [46],

$$\begin{aligned} \mathcal{L} &= c^*_{i\mu} c_{j\nu} \left\langle \chi_\mu \left| \hat{F} \right| \chi_\nu \right\rangle - c^*_{\mu i} c_{\nu j}\, \varepsilon_i \left\langle \chi_\mu \left| \chi_\nu \right. \right\rangle; \\ \frac{\partial \mathcal{L}}{\partial c} &= 0. \end{aligned} \tag{2.20}$$

Systems with unpaired electrons need separate treatment of the electrons with α and β spin. When the α and β spin-orbitals are allowed to have different orbital expansion coefficients, the method is called unrestricted Hartree–Fock (UHF).

2.6 LINEAR COMBINATIONS OF ATOMIC ORBITALS

The convergence of the energy with respect to the number of basis function is faster when the basis orbitals are of similar type as the exact solution. An obvious choice would be to use Slater–type orbitals (STOs) [54], which are exponential functions $e^{-\zeta r}$ multiplied by a pre-factor consisting of Cartesian coordinates raised to a certain power. The pre-factor can also be expressed using spherical harmonics.

However, it is computationally more efficient to approximate STOs as a sum of Gaussian-type orbitals (GTOs) [55]. The Cartesian Gaussian functions are centred on each atom a and expressed using each Cartesian coordinate raised to a certain power,

$$g_a(\mathbf{r}_a, \zeta, i, j, k) = N x_a^{l_x} y_a^{l_y} z_a^{l_z} e^{-\zeta r_a^2}. \tag{2.21}$$

The sum of the powers l_x, l_y and l_z adds up to the orbital quantum number ℓ, which determines the type of orbital: s, p, d, f.

The core electrons can be approximated by an effective core potential (ECP). This reduces the number of basis functions. ECPs can also account for some relativistic effects [56, 57].

There are a variety of basis sets developed by different research groups [58]. Basis sets which are constructed as linear combinations of individual Gaussian-type functions (primitives) [59, 60] with pre-optimised coefficients and exponents are termed a contracted Gaussian–type orbital (CGTO) basis sets.

Several types of basis sets can be distinguished based on the number of basis functions employed in the approximation of an atomic orbital. When there is only one basis function per orbital, the employed basis set is *minimal*. The obtained results are usually of low accuracy. In split valence (SV) basis sets, each of the valence orbitals are described

using two basis functions. They are suitable for pre-optimisation of the molecular structure. More precise results are obtained by adding more basis functions per atomic orbital. The basis sets are called double-ζ (DZ), triple-ζ (TZ), quadruple-ζ (QZ), etc depending on the number of exponential functions per atomic orbital. Larger exponential factors ζ make the basis function decay faster. Functions with a small exponential factor make the basis function more diffuse, which is necessary, for example, when studying weak interactions and anions. The inclusion of basis functions with higher angular momentum, such as adding p character to an s orbital or d character to a p orbital allows for better flexibility. They are called polarisation (P) functions.

Alternatively, it is possible to use generic interpolation polynomials as a type of a nearly complete numerical basis set. They are employed in the finite-element method (FEM), which is a fully numerical approach [61]. Another option is to employ plane waves which are a natural way of representing extended periodic systems [62]. The size and the quality of the basis set affects the accuracy of the calculation. The point when adding more basis functions barely improves on the result is called the *basis set limit*.

2.7 ELECTRON CORRELATION

The motion of an electron within a molecular system depends on the instantaneous position of all the other electrons. One of the main reasons for inaccuracy in quantum-chemical calculations is the inadequate description of the extent to which the motion of one electron is influenced by the dynamics of the other electrons, known as electron correlation [63]. Physically, it is less likely that an electron will be found in close vicinity to another electron. The volume in which electrostatic repulsion is very high is referred to as a *Coulomb hole*. Further, electrons with parallel spins avoid each other due to Pauli repulsion, a direct consequence of spin statistics. This region is known as a *Fermi hole*.

The Hartree–Fock wave function is defined in terms of a Slater determinant, which considers the exchange interaction of the electrons. The mean-field approximation in the Hartree–Fock method describes the average Coulomb interaction, which is the predominant contribution to the two-electron repulsion.

Hartree–Fock calculations are able to describe more than 99% of the energy of the correlated electronic motion [65]. The remaining 1% which is impossible to obtain at the Hartree–Fock level is referred to as *electron correlation energy*. The calculation of the correlation energy is crucial for achieving accurate energies of chemical bonds and noncovalent interactions. Usually, the chemical accuracy is assumed to be 1 kcal/mol. This corresponds to the experimental accuracy of the measurements of thermodynamic properties [66–70]. In Hartree–Fock-

The correlation energy is defined as the difference between the Hartree–Fock energy and the exact non-relativistic energy. $E_{\text{corr}} = E_{\text{nonrel}} - E_{\text{HF}}$ *[64].*

based methods, the ground state is described with a single determinant. Post-Hartree–Fock methods (second-order Møller–Plesset perturbation theory, configuration interaction, coupled cluster) correct the inability of the mean-field approach to describe the instantaneous electron-electron repulsion. This correlation energy is referred to as *dynamic correlation*.

One way of testing the significance of static correlation is the T_1 diagnostic. It can reveal how important single excitations are [71].

One of the first approximations in Hartree–Fock theory was that the ground state of a system can be described with a single Slater determinant. This is generally a good assumption but it fails for near-degenerate ground states, such as diradicals. *Static correlation* occurs when two or more Slater determinants are needed to describe the long-range spatial interaction of electrons [72].

2.8 PERTURBATION THEORY

A straightforward way of improving the solution of the Schrödinger equation is to introduce a perturbation to the Hamiltonian $\hat{H}_0$. The perturbing Hamiltonian $\hat{H}'$ may not affect the system significantly, otherwise the model becomes inaccurate [33, 73],

$$\hat{H} = \hat{H}_0 + \lambda \hat{H}', \tag{2.22}$$

where the parameter λ is a number which defines the strength of the perturbation. The method is called *Rayleigh–Schrödinger* perturbation theory.

The k^{th}-order correction terms are the respective derivatives at the limit of $\lambda = 0$ i. e.,

$$E_n^{(k)} = \frac{1}{k!} \frac{\mathrm{d}^k E_n}{\mathrm{d}\lambda^k}\bigg|_{\lambda=0}$$

$$\psi_n^{(k)} = \frac{1}{k!} \frac{\mathrm{d}^k \psi_n}{\mathrm{d}\lambda^k}\bigg|_{\lambda=0}$$

The Schrödinger equation for the perturbed state is expanded into powers of λ,

$$\left(\hat{H}_0 + \lambda \hat{H}'\right) \psi_n = E_n \psi_n \tag{2.23}$$

$$\begin{aligned} E_n &= E_n^{(0)} + \lambda E_n^{(1)} + \lambda^2 E_n^{(2)} + \cdots \\ \psi_n &= \psi_n^{(0)} + \lambda \psi_n^{(1)} + \lambda^2 \psi_n^{(2)} + \cdots \end{aligned} \tag{2.24}$$

After substitution in the Schrödinger equation, the first-order corrections to the energy and to the wave function are expressed as

$$\begin{aligned} E_n^{(1)} &= \left\langle \psi_n^{(0)} \middle| \hat{H}' \middle| \psi_n^{(0)} \right\rangle; \\ \psi_n^{(1)} &= \sum_{m \neq n} \frac{\left\langle \psi_m^{(0)} \middle| \hat{H}' \middle| \psi_n^{(0)} \right\rangle}{E_n^{(0)} - E_m^{(0)}}. \end{aligned} \tag{2.25}$$

In the first-order correction term, the perturbing Hamiltonian operates only on the ground-state wave function. However, the second-order

term is evaluated by calculating the matrix elements of $\hat{H}'$ acting on all pairs of different states,

$$E_n^{(2)} = \sum_{m \neq n} \frac{\left| \left\langle \psi_m^{(0)} \left| \hat{H}' \right| \psi_n^{(0)} \right\rangle \right|^2}{E_n^{(0)} - E_m^{(0)}}. \tag{2.26}$$

The expression shows that the unperturbed wave functions suffice to calculate the second-order energy correction.

In second-order Møller–Plesset perturbation theory (MP2), the unperturbed Hamiltonian $\hat{H}_0$ is the sum of all one-electron Fock operators $\hat{f}$ defined according to eq. 2.14 [74]. The difference between the exact molecular Hamiltonian and $\hat{H}_0$ gives the perturbing Hamiltonian $\hat{H}'$. It is applied on the Hartree–Fock wave function Φ_0 in order to calculate the correlation energy. The sum of the zero- and first-order terms gives the HF energy. The second-order term is the correlation correction. The energy calculated at the MP2 level does not follow the variational theorem, so the corrected energy $E_{\mathrm{HF}} + E_n^{(2)}$ can be lower than the exact energy. Higher-order corrections to the energy can be obtained, however, the computational cost increases rapidly and the perturbation series is not guaranteed to be convergent [75, 76].

2.9 CONFIGURATION INTERACTION

A Hartree–Fock calculation produces a set of molecular orbitals, whose total number is equal to the number of basis functions. It is possible to construct Slater determinants where one or more electrons have been excited from an occupied Hartree–Fock orbital to a vacant orbital with a higher energy (a virtual orbital). The weighted sum of the determinants for all possible configurations gives a wave function called *full configuration interaction (FCI)* wave function,

$$\Psi_{\mathrm{FCI}} = C_0 \Phi_{\mathrm{HF}} + \sum_{a,i} C_i^a \Phi_i^a + \sum_{\substack{a>b \\ i>j}} C_{ij}^{ab} \Phi_{ij}^{ab} + \cdots + \sum_{\substack{a>b>c>\ldots \\ i>j>k>\ldots}} C_{ijk\ldots}^{abc\ldots} \Phi_{ijk\ldots}^{abc\ldots}. \tag{2.27}$$

The indices $a, b, c, \ldots$ span the virtual orbitals, while the occupied orbitals are labelled as $i, j, k, \ldots$. The indices in determinant Φ_{ij}^{ab} mean that the electron from the orbitals i and j occupied in the Hartree–Fock ground state are moved to the orbitals a and b which are vacant at the Hartree–Fock level.

The complete set of Slater determinants in a given basis can be used as an ansatz to the Schrödinger equation. Applying the variational principle produces the exact non-relativistic solution in the employed basis set. The difficulty of the method lies in the exponentially growing

number of terms. The FCI ansatz can be truncated to include only singly- and doubly-excited states (configuration interaction singles and doubles (CISD)) [77]. The limited number of excited states makes the solution tractable but also introduces two problems. The energy of a molecular system consisting of two isolated fragments is not equal to the sum of the energies of each fragment alone, therefore, the truncated CI method is not *size consistent*. In addition, the limited number of excited configurations makes the result less accurate as the system size grows. This problem is called *size extensivity*.

2.10 COUPLED CLUSTER

Another way to introduce correlation is to define an exponential cluster operator acting on the HF wave function Φ_0,

The exponential ansatz ensures size-extensivity.

$$\psi_{\text{exact}} = e^{\hat{T}}\Phi_0. \tag{2.28}$$

The CC method was originally devised for the purposes of nuclear physics [78], and later on applied to molecular electronic structure theory [79]. The exponential is expanded into a Taylor series,

$$e^{\hat{T}} = 1 + \hat{T} + \frac{\hat{T}^2}{2!} + \frac{\hat{T}^3}{3!} + \cdots, \tag{2.29}$$

and subsequently the cluster operator $\hat{T}$ is expressed as the sum of operators for the excitation of a different number of electrons (from 1 to their total number n) from the HF determinant to an excited Slater determinant,

The one-electron operator acts on the HF wave function $\hat{T}_1\Phi_0$ to give $\sum_i^n \sum_{a=n+1}^{\infty} t_i^a \Phi_i^a$.

$$\hat{T} = \hat{T}_1 + \hat{T}_2 + \cdots + \hat{T}_n. \tag{2.30}$$

In analogy with the expression for the CI ansatz, the excitation operator generates a linear combination of all possible excited Slater determinants. When all contributions to the cluster operator up to order N are included, coupled cluster theory is exact in the given basis set. The goal of the method is to find the expansion coefficients (amplitudes) $t_{ijk\ldots}^{abc\cdots}$ of the molecular wave function, where $i, j, k, \ldots$ denote the occupied orbitals and $a, b, c, \ldots$ cover all virtual orbitals. The inclusion of each additional excitation operator $\hat{T}_i$ in the expansion leads to a rapidly growing number of determinants. Usually, only the first few terms are included. Employing only the $\hat{T}_2$ operator gives rise to the coupled cluster doubles (CCD) method. The advantage of CCD over configuration interaction doubles (CID) is that the double-excitation operator $\hat{T}_2$ after the expansion in a Taylor series yields quadruply and higher-order excited determinants:

The $\hat{T}_i$ operators are commonly defined in second quantisation formalism [80] using creation $\hat{a}^\dagger$ and annihilation $\hat{a}$ operators, e. g.*,: $\hat{T}_2 = \frac{1}{4} t_{ij}^{ab} \hat{a}_a^\dagger \hat{a}_b^\dagger \hat{a}_i \hat{a}_j$.*

$$e^{\hat{T}_2}|\Phi_0\rangle = 1 + \hat{T}_2|\Phi_0\rangle + \frac{1}{2}\hat{T}_2^2|\Phi_0\rangle + \cdots. \tag{2.31}$$

Employing both the $\hat{T}_1$ and $\hat{T}_2$ operators gives coupled cluster singles and doubles (CCSD). Adding the triple-excitation operator makes the calculations increasingly expensive. Instead, triples can be included as a perturbation, yielding the popular method coupled cluster singles and doubles with perturbative inclusion of triples (CCSD(T)) [81]. The working equations are very complicated. Their derivation can also be done using a diagrammatic approach [82].

The coupled cluster method is not variational, however, given the good representation of electron correlation, the results are usually excellent. Problems arise when molecules are not well described by the ground state Hartree–Fock wave function. Improving on them is expensive while at the same time being futile [83]. They are called multireference systems and require special treatment.

2.11 ELECTRON DENSITY

The molecular wave function is a function of the three spatial coordinates and the spin coordinate of each electron, making it a function of $4N$ arguments for a molecule with N electrons. The high dimensionality increases the level of complexity. An alternative approach to wave-function methods is to employ the electron density. It is expressed as the integral of the square of the molecular wave function over the spin coordinate of the electron and the spatial coordinates of the other electrons,

$$\rho(\boldsymbol{r}) = N \int \mathrm{d}\boldsymbol{r}_2 \cdots \int \mathrm{d}\boldsymbol{r}_N d\sigma_1 \left|\Psi(\boldsymbol{r}_1, \boldsymbol{r}_2 \ldots \boldsymbol{r}_N; \sigma_1 \ldots \sigma_N)\right|^2 . \quad (2.32)$$

The number of electrons is obtained by integrating the electron density over the volume: $N = \int \rho(\boldsymbol{r}) \mathrm{d}\boldsymbol{r}$.

2.11.1 *The Thomas–Fermi model*

A semiclassical method for the calculation of the electron density in a many-electron atom is the *Thomas–Fermi model* [47, 84]. It is based on the approximation that the electron density is homogeneous in a small volume of space in the vicinity of the nucleus. As such, the kinetic energy is related to the electron density as

$$T = \frac{3}{10}(3\pi^2)^{2/3} \int \rho(\boldsymbol{r})^{5/3} \mathrm{d}^3\boldsymbol{r}. \quad (2.33)$$

The electronic repulsion can be expressed using Coulomb's law,

$$V_{ee} = \frac{1}{2} \int \mathrm{d}^3\boldsymbol{r}\ \mathrm{d}^3\boldsymbol{r}'\ \frac{\rho(\boldsymbol{r})\rho(\boldsymbol{r}')}{|\boldsymbol{r} - \boldsymbol{r}'|}. \quad (2.34)$$

An inherent problem in eq. 2.34 is that the Coulomb repulsion does not vanish for the same electron – there is a self-interaction error.

Even with the corrections for the exchange energy introduced by Dirac, and for the kinetic energy by Weizsäcker, the Thomas–Fermi model

usually yields unacceptably large errors for the purpose of chemistry [48, 85, 86]. However, the one-electron solutions in a Thomas–Fermi field can be used to as the first step in atomic calculations [87].

2.11.2 *Hohenberg–Kohn theorems*

$$v_{\text{ext}} = \sum_{i,A} \frac{-Z_A}{|\boldsymbol{r}_i - \boldsymbol{R}_A|}$$

where r_i is the coordinate of electron i and R_A is the coordinate of nucleus R_A. Z_A is the nuclear charge.

The Hohenberg–Kohn (HK) theorem states that the electron density contains all the information about a quantum system [88]. Namely, if the exact electron density were known, the external potential of the nuclei $v_{\text{ext}}(\boldsymbol{r})$ in which the electrons are moving would be uniquely defined up to a constant. The exact energy of the system is calculated as a functional of the electron density $E[\rho(\boldsymbol{r})]$. The true ground-state electron density minimises the ground-state energy, making the calculation variational. This is the second Hohenberg–Kohn theorem.

The exact electron density is unknown which makes it impossible to calculate the exact density functional. However, $E[\rho(\boldsymbol{r})]$ can be split into three terms. The first two terms are the universal functional $F[\rho(\boldsymbol{r})]$, independent of $v_{\text{ext}}(\boldsymbol{r})$. The third term V_{eN} is system-specific.

$$E_{\text{HK}}[\rho(\boldsymbol{r})] = T[\rho(\boldsymbol{r})] + V_{ee}[\rho(\boldsymbol{r})] + V_{eN}[\rho(\boldsymbol{r})] \tag{2.35}$$

where T is the kinetic energy functional, V_{ee} is the electronic repulsion functional, and V_{eN} is the electronic-nuclear attraction functional. It can be expressed as $V_{eN} = \int v_{\text{ext}}(\boldsymbol{r})\rho(\boldsymbol{r})\mathrm{d}^3\boldsymbol{r}$.

2.12 KOHN–SHAM EQUATIONS

Upon inspection of the Hohenberg–Kohn functional E_{HK} in eq. 2.35, it appears that some of the terms can describe a fictitious system of the nuclei and N non-interacting electrons such that the electron density is the same as in the actual molecule [89]. This idea does not involve any approximations, and is thus exact. One can express the energy as the Kohn–Sham (KS) functional E_{KS} which involves the kinetic energy of the non-interacting electrons T_s, the classical electrostatic (Coulomb) energy of the electrons J (as in eq. 2.34), and an unknown quantity covering the electron correlation and exchange interactions which the previous terms do not take into account properly (the exchange–correlation (XC) functional E_{XC}),

Formally,

$$E_{XC} = T[\rho] - T_s[\rho] + E_{ee}[\rho] - J[\rho]$$

.

$$E_{KS}[\rho(\boldsymbol{r})] = T_s[\rho(\boldsymbol{r})] + J[\rho(\boldsymbol{r})] + E_{XC}[\rho(\boldsymbol{r})]\,. \tag{2.36}$$

The exchange–correlation functional represents the difference between the exact and the fictitious systems. It has both kinetic-energy and potential-energy contributions. It is associated with the Kohn–Sham potential v_{KS}. It is the sum of the external potential created by the

nuclei v_{ext}, the electrostatic repulsion of the electrons v_J, and the exchange–correlation potential v_{XC},

$$v_{\text{KS}}(\boldsymbol{r}) = v_{\text{ext}}(\boldsymbol{r}) + v_{\text{J}}(\boldsymbol{r}) + v_{\text{XC}}(\boldsymbol{r}). \tag{2.37}$$

Each of the potentials v_{KS}, v_{J}, and v_{XC} in eq. 2.37 is the functional derivative of the respective energy over the electron density:

$$v_i = \frac{\delta E_i\left[\rho(\boldsymbol{r})\right]}{\delta\rho(\boldsymbol{r})}$$

.

When the Kohn–Sham potential is substituted into the Schrödinger equation, the ground-state electron density $\rho(\boldsymbol{r})$ is calculated as the sum of the squares of the orbitals,

$$\rho(\boldsymbol{r}) = \sum_{i=1}^{N} \left|\psi_i(\boldsymbol{r})\right|^2. \tag{2.38}$$

The self-consistent solution to this Schrödinger equation leads to the set of *Kohn–Sham equations*,

$$\left[-\frac{1}{2}\nabla^2 + v_{\text{KS}}(\boldsymbol{r})\right]\psi_i(\boldsymbol{r}) = \varepsilon_i\psi_i(\boldsymbol{r}). \tag{2.39}$$

2.13 DENSITY FUNCTIONAL THEORY

In order to apply the Kohn–Sham equations to real systems, it is necessary to find a reasonable approximation to the exchange–correlation functional. The possibilities for that are endless since E_{XC} is unknown. The freedom to choose the parametrisation is classified into the well-known Jacob's ladder of the density functionals by Perdew [90]. In contrast to HF theory, in density functional theory (DFT), it is generally impossible to trace the source of errors caused by the approximations.

2.13.1 *Local-density approximation*

LDA tends to overbind – chemical bonds become shorter and bond energies are larger than the exact values [91].

The simplest way of describing the exchange–correlation functional is to adopt the homogeneous electron gas model of Fermi, Thomas and Dirac. The exchange–correlation energy is obtained by integrating the exchange-correlation energy density per electron, $\varepsilon_{\text{xc}}(\rho)$, scaled by the electron density at each point in space,

$$E_{\text{xc}}^{\text{LDA}} = \int \rho(\boldsymbol{r})\varepsilon_{\text{xc}}(\rho)\mathrm{d}^3\boldsymbol{r}. \tag{2.40}$$

The exchange energy functional in LDA is known analytically,

$$E_{\text{x}}^{\text{LDA}} = -\frac{3}{2}\left(\frac{3}{4\pi}\right)^{1/3}\int \rho(\boldsymbol{r})^{4/3}\mathrm{d}^3\boldsymbol{r}, \tag{2.41}$$

while the correlation energy functional can be parametrised based on quantum Monte Carlo calculations. This method is called the local-density approximation (LDA). Some notable parametrisations of the

correlation functional are given by Vosko, Wilk, and Nusair, and by Perdew and Wang [92, 93].

In systems with unpaired electrons (open-shell systems), the α- and β-spin electrons have a different spin density – there is spin polarisation. The exchange-correlation energy density per atom is a function of both the α- and β-spin densities ($\varepsilon_{xc}(\rho_\alpha, \rho_\beta)$). Two Kohn–Sham equations are solved for each spin case and the resulting energies from eq. 2.41 summed. The method is called local-spin-density approximation (LSDA).

2.13.2 *Generalised-gradient approximation*

Generalised-gradient approximation (GGA) density functionals are routinely used in quantum chemistry and give reliable results for structure optimisation.

The non-homogeneity of the electron distribution in space can be considered by taking the derivative of electron density $\rho(\boldsymbol{r})$ with respect to the Cartesian coordinates. As a result, $\rho(\boldsymbol{r})$ in the vicinity of point r is taken into account, which makes the method *semi-local*. In the generalised-gradient approximation (GGA), the exchange-correlation energy is defined using the gradient of the electron density $\nabla\rho(\boldsymbol{r})$ in addition to $\rho(\boldsymbol{r})$. It takes the form:

$$E_{xc}^{GGA} = \int \rho(\boldsymbol{r})\varepsilon_{xc}(\rho, \nabla\rho)\mathrm{d}^3\boldsymbol{r}. \tag{2.42}$$

Becke was the first to suggest an empirically scaled term involving the gradient of the electron density to the exchange functional [94]. In particular, his work from 1988 gave a formulation for the exchange energy with "correct asymptotic behaviour" [95]. The approach is expressed in its generalised form [96] as

Correct asymptotic behaviour [95] of the electron density refers to the density reaching a hydrogen-type solution: $\lim_{r\to\infty}\rho_\sigma = e^{-ar}$.

$$E_x^{GGA} = E_x^{LDA} - \beta\sum_\sigma \int \frac{(\nabla\rho_\sigma)^2}{\rho_\sigma^{4/3}}\,\mathrm{d}^3\boldsymbol{r}. \tag{2.43}$$

where the factor β is a fitting parameter [97], and σ refers to α- and β-spin densities. The dimensionless fraction in eq. 2.43 is known as the reduced density gradient. The significant improvement on the accuracy led the way towards a plethora of exchange and correlation functionals.

Parameter-free expressions for exchange and correlation density functionals have also been developed. Perdew, Burke, and Ernzerhof have derived the popular PBE functional [98].

Further improvement on the energy calculated with density functional theory can be done by incorporating the Laplacian of the electron density in the exchange–correlation potential or the kinetic energy density $\tau = \frac{1}{2}\sum_i(\nabla\psi_i)^2$ [99]. These so-called meta-generalised-gradient approximation (mGGA) functionals are probing the long-range behaviour of the electron density, which GGA functionals struggle with. A typical example is the TPSS exchange–correlation functional [100]. Fitting the XC functional to various molecular properties

can produce a large set of parameters for the particular expression of XC, for example in the Minnesota mGGA density functional family [101, 102]. However, the applicability might be limited to molecules similar to the set of fitting molecules [103–105].

2.13.3 *Hybrid functionals*

The Hartree–Fock (HF) method accurately describes the electronic exchange for a single-determinant problem, however it does not involve any explicit correlation terms. In a sense, the Hartree–Fock (HF) method can be considered as an extreme case of DFT where $E_c = 0$ and E_x is exact. There is small tendency for GGA functionals to overbind, which can be reduced by including a fraction of exact HF exchange [106].

One of the most popular DFT functionals is B3LYP. It is parametrised by taking Becke's B88 exchange functional [95], Lee, Yang, and Parr's LYP correlation functional [107]. The energy can be obtained as

$$E_{xc}^{hybrid} = E_{xc}^{LDA} + a(E_x^{HF} - E_x^{LDA}) + b\Delta E_x^{GGA} + c\Delta E_c^{GGA}, \qquad (2.44)$$

and setting the three parameters as $a = 0.20$, $b = 0.72$, and $c = 0.81$.

Another notable family of hybrid functionals are developped in Berkley which are optimised to include long-range and dispersion interactions [108, 109].

An attempt to improve further on the obtained energies is to combine second-order Møller–Plesset perturbation theory (MP2) with GGA density functionals to obtain double-hybrid functionals [110, 111]. The expression for the energy is given as

$$E_{xc}^{dh} = (1 - a_x)E_x^{GGA} + a_x E_x^{HF} + bE_c^{GGA} + cE_c^{PT2}, \qquad (2.45)$$

where the last term is calculated according to eq. 2.26 for the occupied orbitals i, j and the virtual orbitals a, b. Orbital energies are denoted by ϵ [111],

$$E_c^{PT2} = \frac{1}{4}\sum_{i,a}\sum_{j,b}\frac{[(ia|jb) - (ib|ja)]^2}{\epsilon_i + \epsilon_j - \epsilon_a - \epsilon_b}. \qquad (2.46)$$

2.14 METHODOLOGICAL ERRORS AND CORRECTIONS

2.14.1 *Basis-set problems*

A finite number of basis functions are used for the expansion of each orbital. This gives rise to several kinds of basis-set errors. Working at the complete basis set limit is ideally the best option in terms of accuracy [112, 113].

basis-set truncation error (BSTE) – the basis set is not capable of accurately describing the molecule [114]. The BSTE also reduces the accuracy of high-level correlated methods such as coupled cluster.

basis-set superposition error (BSSE) – basis functions for some part of a molecule end up being also basis functions for neighbouring atoms. Effectively, the basis set for them is larger, which artificially lowers the energy and causes overbinding.

basis-set incompleteness error (BSIE) – the basis set is not big enough to describe all interactions and leads to underbinding. Generally, it refers to the error which remains after applying a correction for BSSE.

counterpoise correction – a method to eliminate BSSE [115]. Four calculations are done to obtain the energy of the system AB with basis set A and basis set B. Then the energy of the fragments A and B are calculated with their respective basis set. The counterpoise correction is formed as the difference between the contribution of basis set A to the system, as well as the contribution from basis set B to the system.

$$E_{\mathrm{CP}}^{\mathrm{BSSE}} = (E_{\mathrm{A}}(AB) - E_{\mathrm{A}}(A)) + (E_{\mathrm{B}}(AB) - E_{\mathrm{B}}(B))$$

2.14.2 *System-size problems*

As the system size grows, it is necessary to ensure that the whole molecule is treated equally well as in the case when its building blocks are investigated individually [116].

size extensivity – A size-extensive method ensures that the energy of a system scales linearly with the number of the electrons. It is used to quantify the extent to which a method handles electron correlation [117, 118].

size consistency – A system is separable into non-interacting fragments without affecting the accuracy of the calculations [119]. The energy obtained for a system consisting of non-interacting fragments A and B should be exactly equal to the sum of the energies obtained from calculations of the fragments A and B alone.

2.14.3 *Problems in density functional theory*

The accuracy of the DFT method depends on the choice of the functional. Performance varies when investigating different properties – molecular geometry, thermochemistry, strength of hydrogen bonds

and weak interactions [120]. Even though "chemical accuracy" cannot always be reached, the balance between computational cost and accuracy makes it a popular tool in quantum chemistry nowadays. The success of DFT is, to some extent, based on cancellation of errors introduced in the exchange and the correlation functionals [104]. *Self-interaction error* is a major flaw in Kohn–Sham density functional theory. The Hartree–Fock method does not suffer from self-interaction error because it incorporates the Coulomb and the exact exchange integrals for the interaction between two electrons (eq. 2.12 and eq. 2.13). In KS-DFT there is no exact way of excluding the interaction of an electron with itself unless the exchange–correlation (XC) functional is known exactly.

2.14.4 *Dispersion correction*

In density functional theory (DFT), interactions based on orbital overlap are treated in a satisfactory fashion [96]. Hydrogen bonds are generally described well despite their weak magnitude, however dispersion interactions are not electrostatic by nature, and are completely absent in the typical LDA, GGA and mGGA models. Dispersion forces (also called London forces and van-der-Waals forces) arise between any pair of atoms, inducing a short-lasting weak dipole moment [121, 122]. Van-der-Waals (dispersion) interactions hold together non-covalently bound systems and are crucial for obtaining the correct spatial orientation of the functional groups in a molecule. Arguably the most famous semi-empirical dispersion correction is developed by Grimme [123–126]. It involves the calculation of the n-th order coefficients C_n^{AB} for atoms A and B at a distance R_{AB} away from each other, multiplied by the s_n scaling factors. The coefficients are derived based on electronic-structure calculations. The general form of the pairwise correction is

$$E^{\mathrm{disp}} = \frac{1}{2} \sum_{A \neq B} \frac{s_6 C_6^{\mathrm{AB}}}{R_{\mathrm{AB}}^6} f_{\mathrm{damp}}(R_{\mathrm{AB}}), \tag{2.47}$$

where f_{damp} is known as the damping function,

$$f_{\mathrm{damp}}(R_{\mathrm{AB}}) = \frac{1}{1 + 6 \left(\frac{R_{\mathrm{AB}}}{s_{r,6} R_0} \right)^{-\alpha_n}}. \tag{2.48}$$

The damping function ensures that the dispersion correction does not become singular at $\boldsymbol{r} \to 0$ [127–129]. The α_n exponent is a fitting parameter [109]. The energy correction E^{disp} is then added to the KS energy: $E_{\mathrm{DFT-D}} = E_{\mathrm{KS}} + E_{\mathrm{disp}}$. The R^{-6} expression is part of the multipole expansion of the Coulomb force between two atoms. It is the van-der-Waals interaction, originating from instantaneous dipoles.

2.14.5 *Resolution-of-the-identity approximation*

The resolution of the identity (RI) approximation is a method to increase computational efficiency when calculating two-electron four-centre integrals, at a negligible price of accuracy [130, 131]. The two-electron bra and ket states are expanded into an *auxiliary basis set* labelled with capital letters as

$$(ij|kl) = \sum_{K,L} (ij|L) \left(L|K\right)^{-1} (K|kl) \,. \tag{2.49}$$

The method can be implemented for calculations at any level of theory, including Hartree–Fock, DFT and MP2.

2.14.6 *Spin-component-scaled electron correlation*

The accuracy of the MP2 method can be improved by employing the spin-component scaled correlation correction [132, 133]. The technique is based on the idea that the correlation between electrons with parallel spins is different from the correlation of electrons with opposite spins. These correlation energies are scaled by coefficients, so as to reproduce CCSD(T) results. Even thought the method is no longer strictly *ab initio*, the good accuracy and the lower computational cost compared to more sophisticated post-HF methods make it a valuable tool for studying medium-sized molecules.

2.14.7 *Explicitly correlated methods*

Arguably one of the most accurate techniques for electronic-structure calculations is the explicitly correlated coupled cluster (CCSD-F12) method [134, 135]. The basis set problems related to conventional coupled cluster theory are treated by adding terms with explicit dependence on the interelectron distance r_{12} to the wavefunction ansatz in an attempt to recover the remaining dynamic correlation in the basis set limit [136, 137].

$$F_{12}(r_{12}) = -\frac{1}{\gamma} e^{-\gamma r_{12}} \tag{2.50}$$

The F_{12} correction reduces the basis-set truncation error. It is possible to achieve accuracy superior to the CCSD(T)/aug-cc-pV5Z method by employing the triple-ζ correlation consistent basis set with the F_{12} correction [138, 139].

2.15 MOLECULAR PROPERTIES

Perturbations cause changes in the energy of the molecule. The total energy can be expanded in Taylor series and if the perturbation is static, or time-independent, then the change in energy describes a molecular property.

$$E(\mu) = E^{(0)} + E^{(1)}\mu + \frac{1}{2}E^{(2)}\mu^2 + \cdots \tag{2.51}$$

$$E^{(1)} = \frac{\mathrm{d}E}{\mathrm{d}\mu}\Big|_{\mu=0} \tag{2.52}$$

$$E^{(2)} = \frac{\mathrm{d}^2E}{\mathrm{d}\mu^2}\Big|_{\mu=0} \tag{2.53}$$

According to the Hellmann–Feynman theorem, the derivative of the total energy can be calculated as the expectation value of the derivative of the Hamiltonian acting upon the eigenstate ψ_μ depending on the μ parameter [56, 140, 141].

$$\frac{\mathrm{d}E}{\mathrm{d}\mu} = \left\langle \psi_\mu \middle| \frac{\mathrm{d}\hat{H}}{\mathrm{d}\mu} \middle| \psi_\mu \right\rangle \tag{2.54}$$

Perturbations to the geometry, such as bond stretching, are characterised with force constants of the vibration mode. External electromagnetic fields interact with the magnetic and electric moments of particles, resulting in properties such as polarisability, magnetisability, and optical activity. An extensive description of magnetism and molecular properties in magnetic fields is given in Chapter 3.

3

MAGNETIC FIELDS

3.1 CLASSICAL ELECTROMAGNETISM

Electromagnetic interactions are one of the four fundamental forces in nature. Classical electromagnetism studies how electromagnetic fields arise and interact with particles. Stationary positive or negative electric charges generate an electric field, whereas moving charges also give rise to a magnetic field. The electromagnetic force acts upon a point charge q moving with velocity $\boldsymbol{v}$ in an electric field $\boldsymbol{E}$ and a magnetic field $\boldsymbol{B}$. It is known as the Lorentz force $\boldsymbol{F}$,

In fact, according to the special theory of relativity, electromagnetism is not separable into electric and magnetic phenomena but instead they are perceived as the one or the other, or a mixture of both, depending on the frame of reference.

$$\boldsymbol{F} = q\boldsymbol{E} + q\boldsymbol{v} \times \boldsymbol{B}. \tag{3.1}$$

Electromagnetic fields are generated by the scalar electric potential φ and the magnetic vector potential $\boldsymbol{A}$,

$$\boldsymbol{E} = -\nabla\varphi - \frac{\partial \boldsymbol{A}}{\partial t}; \tag{3.2}$$

$$\boldsymbol{B} = \nabla \times \boldsymbol{A}. \tag{3.3}$$

The vector potential $\boldsymbol{A}$ is not uniquely defined because for any function f, the curl of which vanishes,

$$\nabla \times (\boldsymbol{A} + \nabla f) = \nabla \times \boldsymbol{A}. \tag{3.4}$$

This property of a class of vector potentials to describe the same magnetic field is called gauge invariance. Usually, $\boldsymbol{A}$ is defined in the Coulomb gauge such that $\nabla \cdot \boldsymbol{A} = 0$. Likewise, the electric potential φ is defined up to a constant and is also gauge invariant. For the sake of convenience, φ is typically chosen to vanish at infinity. Given that the physical system does not change through the choice of the gauge origin implies that gauge invariance is a type of symmetry. And, as per Noether's theorem, gauge invariance of the electromagnetic field leads to charge conservation [142].

The physical meaning of φ is the potential energy of the electric field acting on a charged particle, while the magnetic vector potential $\boldsymbol{A}$ expresses the potential energy of the magnetic field interacting with an electric current flowing through a wire in one or the other direction.

A	ampere (electric current)
$\mathrm{J} = \mathrm{kg} \cdot \mathrm{m}^2 \cdot \mathrm{s}^{-2}$	joule (energy)
$\mathrm{N} = \mathrm{kg} \cdot \mathrm{m} \cdot \mathrm{s}^{-2}$	newton (force)
$\mathrm{C} = \mathrm{A} \cdot \mathrm{s}$	coulomb (electric charge)
$\mathrm{V} = \mathrm{J} \cdot \mathrm{C}^{-1}$	volt (electric potential)
$\mathrm{T} = \mathrm{N} \cdot \mathrm{A}^{-1} \cdot \mathrm{m}^{-1}$	tesla (magnetic flux density, SI)
$\mathrm{G} = 10^{-4}\,\mathrm{T}$	gauss (magnetic flux density, cgs)
$B_0 = 2.350\,517\,42 \times 10^5\,\mathrm{T}$	atomic unit of magnetic field strength

Table 3.1: Commonly used units in electromagnetism.

3.1.1 *Notation and units*

Some of the commonly used units in electromagnetism are listed in Table 3.1. An additional unit of magnetic flux density, from now on referred to as magnetic field strength, is the atomic unit $B_0 = m_e^2 e^3 c/\hbar^3$, where m_e is the electron mass, e is the electron charge, c is the speed of light, and $\hbar$ is the reduced Planck constant.

3.1.2 *Maxwell's equations*

The concept of an electric point charge can be generalised to the charge distribution ρ in a certain volume, whereas the flow of electric charge evolves to the current density $\boldsymbol{J}$ – the electric current I per unit area,

$$I = \int \boldsymbol{J} \cdot \mathrm{d}\boldsymbol{A}. \tag{3.5}$$

The core of electrodynamics is summarised by Maxwell's equations [143–146], here presented in differential form along with their individual name.

Boundary conditions are applied such that static electric and magnetic fields vanish infinitely far away from the source or current respectively.

$$\nabla \cdot \boldsymbol{E} = \frac{\rho}{\varepsilon_0} \tag{3.6}$$
Gauss's law – Describes the static electric field that arises from a charge density ρ. The field diverges from a positive point charge.

$$\nabla \cdot \boldsymbol{B} = 0 \tag{3.7}$$
Gauss's law for magnetism – Forbids the existence of magnetic charges (monopoles).

From Maxwell's equations, the speed of light depends on the vacuum permittivity ε_0 and the vacuum permeability μ_0.

$$\nabla \times \boldsymbol{E} = -\frac{\partial \boldsymbol{B}}{\partial t} \tag{3.8}$$
Faraday's law – Electric fields are generated by magnetic fields which changes in time.

$$\nabla \times \boldsymbol{B} = \mu_0 \left(\boldsymbol{J} + \varepsilon_0 \frac{\partial \boldsymbol{E}}{\partial t} \right) \tag{3.9}$$
Ampère's law – Magnetic fields arise from electric currents or by changing electric fields. Magnetic fields curl around the current flow.

3.1.3 *Electromagnetic induction*

A measure of the strength of an electromagnetic field through a surface is given by the concept of flux. A higher flux density corresponds to a stronger force with which the field acts on another particle. The magnetic flux Φ_B is the vector field defined by the magnetic flux density $\boldsymbol{B}$ through a surface, expressed as

$$\Phi_B = \boldsymbol{B} \cdot \boldsymbol{S} = BS\cos(\theta), \tag{3.10}$$

where $\boldsymbol{S}$ is the oriented area which the flux flows through, or, as the normal component of the magnetic field through the area. Alternatively, it can be expressed as the integral of the magnetic flux density over the infinitesimal surface elements,

$$\Phi_B = \int_S \boldsymbol{B} \cdot \mathrm{d}\boldsymbol{S}. \tag{3.11}$$

From Gauss's law for magnetism it follows that the magnetic flux through a closed surface (enclosing a volume without any holes) is zero. This notion follows from the observation that there are no magnetic monopoles. The third Maxwell equation shows that magnetic fields which change in time interact with charges moving in a closed contour by generating voltage, or electromotive force, in the current loop. This process called *electromagnetic induction* was studied by Michael Faraday and the principle is known nowadays as *Faraday's law of induction*. It states that the change of the magnetic flux Φ_B gives rise to an electromotive force $\mathcal{E}$ in a conductive loop. It denotes the intensity of the electric field and is measured in volts. The electromotive force can be interpreted as the work done on a charged particle if it makes one loop around the conducting wire. The induced current opposes the changing external magnetic field, which is known as *Lenz's law*. It leads to a negative sign in the mathematical expression

$$\mathcal{E} = -\frac{\mathrm{d}\Phi_B}{\mathrm{d}t}. \tag{3.12}$$

The electromotive force vanishes in an electrostatic field.

$$\mathcal{E} = \oint_C \boldsymbol{E}' \mathrm{d}\boldsymbol{l} = 0$$

.

3.1.4 *Electrostatic fields*

Stationary charges give rise to electric fields that do not change in time. They are studied by electrostatics. Coulomb's law describes the electrostatic repulsion or attraction between two charged particles. Effectively, it is a case of Gauss's law. The scalar form of Coulomb's law for the force $\boldsymbol{F}$ exerted by particle 1 on particle 2, with an interparticle distance $\boldsymbol{r}$, is the inverse-square law

$$|\boldsymbol{F}| = \frac{1}{4\pi\varepsilon_0}\frac{|q_1 q_2|}{r^2}. \tag{3.13}$$

ε_0 is the dielectric permittivity of vacuum.

$\varepsilon_0 = 8.854\,187\,8128(13) \times 10^{-12}\ \mathrm{F \cdot m^{-1}}$

By defining $\boldsymbol{r}_1 - \boldsymbol{r}_2 = \boldsymbol{r}_{12}$ and $\hat{\boldsymbol{r}}_{12} = \boldsymbol{r}_{12}/|\boldsymbol{r}_{12}|$ as the unit vector showing the direction of the force, Coulomb's law in vector form becomes

$$\boldsymbol{F} = \frac{q_1 q_2}{4\pi\varepsilon_0} \frac{1}{|\boldsymbol{r}_{12}|^2} \hat{\boldsymbol{r}}_{12} = \frac{q_1 q_2}{4\pi\varepsilon_0} \frac{\boldsymbol{r}_1 - \boldsymbol{r}_2}{|\boldsymbol{r}_1 - \boldsymbol{r}_2|^3}. \tag{3.14}$$

A test charge q' at position $\boldsymbol{r}$ interacts with a charge with a continuous distribution $\rho(\boldsymbol{r}')$ in the volume $\mathrm{d}V'$ with the Coulomb force

$$\boldsymbol{F} = \frac{q'}{4\pi\varepsilon_0} \int \mathrm{d}V' \rho(\boldsymbol{r}') \frac{\boldsymbol{r} - \boldsymbol{r}'}{|\boldsymbol{r} - \boldsymbol{r}'|^3}. \tag{3.15}$$

3.1.5 *Magnetostatic fields*

Electric currents which do not change with time (*steady currents*) induce constant magnetic fields. They are an object of interest of magnetostatics. The magnetic vector potential generated by an arbitrary current density $\boldsymbol{J}(\boldsymbol{r})$ in volume V is given by

$$\boldsymbol{A}(\boldsymbol{r}, t) = \frac{\mu_0}{4\pi} \int \frac{\boldsymbol{J}(\boldsymbol{r}')}{|\boldsymbol{r} - \boldsymbol{r}'|} \mathrm{d}V. \tag{3.16}$$

The analogue of Coulomb's law in magnetostatics describes the relation between a steady current and the magnetic field which it induces. Maxwell's equations simplify to *Biot–Savart's law*,

$$\begin{aligned} \boldsymbol{B}(\boldsymbol{r}) =& \frac{\mu_0}{4\pi} \oint \frac{I \mathrm{d}\boldsymbol{l}' \times (\boldsymbol{r} - \boldsymbol{r}')}{|\boldsymbol{r} - \boldsymbol{r}'|^3} \\ =& \frac{\mu_0}{4\pi} \int_V \frac{\boldsymbol{J}(\boldsymbol{r}') \times (\boldsymbol{r} - \boldsymbol{r}')}{|\boldsymbol{r} - \boldsymbol{r}'|^3} \mathrm{d}V'. \end{aligned} \tag{3.17}$$

It shows the contribution of each element of the wire $\mathrm{d}\boldsymbol{l}'$ to the magnetic field at a given point. Or, equivalently, the contribution of the current density $\boldsymbol{J}$ in a volume element $\mathrm{d}V'$ to the magnetic field.

Charge is a conserved quantity, therefore the current density $\boldsymbol{J}(\boldsymbol{r})$ in a given volume must be equal to the current flowing into the volume minus the outflow charge,

$$\nabla \cdot \boldsymbol{J} + \frac{\partial \rho}{\partial t} = 0. \tag{3.18}$$

Steady currents do not change in time, thus

$$\frac{\partial \rho}{\partial t} = 0; \ \frac{\partial \boldsymbol{J}}{\partial t} = 0, \tag{3.19}$$

and as a result, the continuity equation can be derived,

$$\nabla \cdot \boldsymbol{J} = 0. \tag{3.20}$$

3.1.6 *Magnetic pressure*

Electric and magnetic fields store energy, which in vacuum is expressed as

$$u = \frac{\varepsilon_0}{2}\boldsymbol{E}^2 + \frac{1}{2\mu_0}\boldsymbol{B}^2, \tag{3.21}$$

$\mu_0 = 1.256\,637\,062\,12(19) \times 10^{-6}\ \mathrm{N \cdot A^2}$

where u is the energy density measured in J/m^3, ε_0 is the vacuum permittivity and μ_0 is the vacuum permeability. The second term is known as *magnetic pressure* (Maxwell stress). Magnetic pressure causes the straightening and the resistance against compression of the magnetic field lines. The effect is clearly exhibited when two magnets are pushed head-to-head. Magnetic pressure puts a practical limit to the strength of a magnetic field which can be generated in laboratory conditions [147]. The pressure exerted on the material the magnet is constructed from can rise enough to cause self-destruction of the equipment.

Magnetic pressure is responsible for solar flares. Sunspots are areas characterised by a strong magnetic field. As the magnetic flux density increases, an arc of plasma is thrown up from the solar surface.

3.1.7 *Precession in a magnetic field*

Magnetism arises either because of electric current flow or from the spin magnetic moments of elementary particles. The magnetic moment $\boldsymbol{m}$ is an inherent property of an object to align itself to be parallel to the magnetic field vector $\boldsymbol{B}$. This alignment is a result of the torque $\boldsymbol{\tau}$,

Multipole (Taylor) expansion of the magnetic vector potential $\boldsymbol{A}$ shows that the magnetic dipole moment $\boldsymbol{\mu}$ is the most significant contribution to $\boldsymbol{m}$ for electrons.

$$\boldsymbol{\tau} = \boldsymbol{m} \times \boldsymbol{B}, \tag{3.22}$$

because the magnetic potential energy $U(\theta)$ is at a minimum in parallel orientation (the angle $\theta = 0$),

$$U(\theta) = -\boldsymbol{m} \cdot \boldsymbol{B}. \tag{3.23}$$

The torque created by the magnetic field causes the magnetic moment vector to rotate around an axis parallel to the magnetic field in a process called *Larmor precession*.

Torque for rotational motion is the equivalent of force for linear motion.

The angular momentum $\boldsymbol{L}$ is a characteristic of the rotational motion of an object with linear momentum $\boldsymbol{p} = m\boldsymbol{v}$ along a circle with radius r from the axis of rotation,

$$\boldsymbol{L} = \boldsymbol{r} \times \boldsymbol{p}. \tag{3.24}$$

Due to isotropy of space – the fact that rotation is independent of the orientation of the system – total angular momentum is a conserved

quantity (from Noether's theorem) [142], *i.e.*, a rotating object will continue rotating, unless external torque is applied, such as from an external field.

The gyromagnetic ratio γ is the coefficient which relates the magnetic moment to the angular momentum $\boldsymbol{L}$,

$$\boldsymbol{m} = -\frac{e}{2m_e}\boldsymbol{L} = \gamma \boldsymbol{L}, \tag{3.25}$$

Torque is the rate of change of angular momentum, $\boldsymbol{\tau} = \frac{\mathrm{d}\boldsymbol{L}}{\mathrm{d}t}$.

and consequently, the torque to the angular momentum,

$$\boldsymbol{\tau} = \gamma \boldsymbol{L} \times \boldsymbol{B}. \tag{3.26}$$

The negative sign in eq. 3.25 reflects the fact that the magnetic moment orients itself to be antiparallel to the external magnetic field.

3.1.8 *Classical diamagnetism*

From a classical point of view, electrons orbiting around the atomic nuclei can be approximated as a steady electric current. An electron as a charged particle rotating about the axis of its angular momentum possesses a magnetic moment. Any current loop placed in a magnetic field experiences torque, which causes the magnetic moment of the object to precess around the axis of the magnetic field (eq. 3.22).

The magnetic moments of the electrons in the atoms comprising a material define the material's response to an external magnetic field. Orbital motion is described by the Coulomb force. However, in a magnetic field, Lorentz force (eq. 3.1) also acts upon the electrons and causes a small increase or decrease in the distance at which they are orbiting the nucleus. As a result, the angular momentum and consequently the velocity are affected slightly. The change in angular momentum is associated with torque (eq. 3.26), which in turn affects the magnetic moment. The magnetic moment vector aligns itself against the external magnetic field according to Lenz's law. Typically the magnetic moments of electrons in a pair are aligned such that they cancel out according to the Pauli principle. In open-shell systems, the magnetic moments of the unpaired electrons point randomly in space.

3.1.9 *Magnetisation*

Magnetisation is also called magnetic polarisation.

Upon application of a magnetic field, the magnetic moments of electrons can line up and produce a net magnetic moment in the whole object, or in other words, the material becomes *magnetised*. Magnetisation can be seen as the density of the net magnetic dipole moments in a material. The alignment of the magnetic dipole moments produces a secondary magnetic field. Materials in which this magnetic field opposes the external one are called *diamagnetic* [148]. The unpaired

electrons of a material placed in an external magnetic field align their magnetic moment with the field and reinforce the external magnetic field. These materials are *paramagnetic*. Closed-shell paramagnetism is also known [149–151]. There are materials – ferromagnets, which have permanent magnetic polarisation even without the presence of a magnetic field.

3.1.10 *Magnetic permeability*

The strength of a magnetic field can be defined in two ways. It can be measured in amperes per meter and denoted by $\boldsymbol{H}$. However, it is more common to use the *magnetic flux density* $\boldsymbol{B}$ to quantify the magnetic field strength. In vacuum, $\boldsymbol{B}$ is proportional to $\boldsymbol{H}$, whereas in materials, there is an additional term describing the magnetic dipole moment density in the material, or magnetisation ($\boldsymbol{M}$),

$$\boldsymbol{B} = \mu_0(\boldsymbol{H} + \boldsymbol{M}), \tag{3.27}$$

where μ_0 is the permeability of vacuum. Permeability is the ability of a material to sustain a magnetic field within itself.

Another quantity, *magnetisability*, ξ, gives the induced magnetic moment $\boldsymbol{m}_i$ in a material for a given magnetic flux density $\boldsymbol{B}$,

$$\xi = \frac{\boldsymbol{m}}{\boldsymbol{B}}. \tag{3.28}$$

The magnetisation of a material is related to the magnetic field strength via the *magnetic susceptibility* coefficient χ_m [152, 153],

$$\boldsymbol{M} = \chi_\mathrm{m}\boldsymbol{H}, \tag{3.29}$$

which shows the tendency of the material to become magnetised in a magnetic field. Paramagnetic materials have positive magnetic susceptibility. Their energy becomes lower, so they are attracted to a magnet. When the magnetic susceptibility is negative, the material is diamagnetic and its magnetic moment opposes the magnetic field. In other words, it expels the magnetic field lines. Its energy is higher in the magnetic field, so it is repelled by a magnet. Molecules and crystals often have different magnetic susceptibility components in the three Cartesian directions. This anisotropy determines the preferred orientation of the molecule in the magnetic field. Classical physics fails to describe magnetisation, implying that it is a purely quantum effect [154]. Magnetic susceptibility is an experimentally measurable quantity.

3.2 QUANTUM-MECHANICAL TREATMENT OF MAGNETIC FIELDS

The Hamiltonian for a quantum-mechanical system is derived from the classical Hamiltonian through *canonical quantisation* [155]. Position is expressed as the vector operator $\hat{\boldsymbol{r}}$, whereas momentum is expressed as a differential operator with respect to the Cartesian coordinates, $\hat{\boldsymbol{p}} = -i\hbar\nabla$. These definitions lead to the canonical commutation relation for position $\hat{r}_i$ and conjugate momentum $\hat{p}_j$ [38],

A commutator of two operators $\hat{A}$ and $\hat{B}$ is the expression:

$$[\hat{A}, \hat{B}] = [\hat{A}\hat{B} - \hat{B}\hat{A}]$$

$$\left[\hat{r}_i, \hat{p}_j\right] = i\hbar\delta_{ij}\,, \tag{3.30}$$

where the indices i and j are a pair of Cartesian coordinates and δ_{ij} is the Kronecker delta. Subsequently, eq. 3.30 can be used to derive the uncertainty principle [156]. In the x direction, it is expressed as

$$\delta_{ij} = \begin{cases} 1 \text{ if } i = j \\ 0 \text{ if } i \neq j \end{cases}$$

$$\Delta x \Delta p_x \geq \hbar/2. \tag{3.31}$$

3.2.1 *Angular momentum in quantum mechanics*

In analogy with its classical definition in eq. 3.24, angular momentum can be defined in operator form as the cross product of the position operator and the vector operator nabla,

$$\hat{\boldsymbol{L}} = \hat{\boldsymbol{r}} \times \hat{\boldsymbol{p}} = -i\hbar(\hat{\boldsymbol{r}} \times \nabla). \tag{3.32}$$

Two operators commute if $\left[\hat{A}, \hat{B}\right] = 0$. If the operators commute then their expectation values can be measured at the same time.

The square of $\hat{\boldsymbol{L}}$, commutes with its vector components L_n as

$$\left[L^2, L_n\right] = 0, \quad \text{where} \tag{3.33}$$

$$\hat{L}^2 = \sum_n \hat{L}_n^2, \quad n \in \{x, y, z\}. \tag{3.34}$$

The components of $\hat{\boldsymbol{L}}$ do not commute with each other since

$$\left[\hat{L}_l, \hat{L}_m\right] = i\hbar \sum_n \varepsilon_{lmn} L_n, \quad l, m, n \in \{x, y, z\}, \tag{3.35}$$

where ε_{lmn} is the Levi–Civita symbol for cyclic permutations. In 3D its values follow the definition:

$$\varepsilon_{lmn} = \begin{cases} +1 & \text{for} \quad (l,m,n) = [(1,2,3);(2,3,1);(3,1,2)] \\ -1 & \text{for} \quad (l,m,n) = [(1,3,2);(3,2,1);(2,1,3)] \\ 0 & \text{for} \quad l = m \quad \text{or} \quad l = n \quad \text{or} \quad m = n \end{cases}$$

3.2.2 *Quantisation of angular momentum*

Spherical harmonics are the solution to the Laplace equation, $\nabla^2\psi = 0$.

The eigenfunctions of the orbital angular momentum operator are the spherical harmonics:

$$Y_\ell^m(\theta,\phi) = (-1)^m \sqrt{\frac{(2\ell+1)}{4\pi}\frac{(\ell-m)!}{(\ell+m)!}} P_\ell^m(\cos\theta) e^{im\varphi}\,, \tag{3.36}$$

where $P_{\ell m}(u)$ are the associated Legendre polynomials [157],

$$P_{\ell m}(u) = \frac{(-1)^m}{2^\ell\,\ell!}\left(1-u^2\right)^{m/2}\frac{\mathrm{d}^{(\ell+m)}}{\mathrm{d}u^{(\ell+m)}}(u^2-1)^\ell. \tag{3.37}$$

Spherical harmonics are the angular component of the atomic orbitals of one-electron atoms. The eigenvalues of the $\hat{L}^2$ operator applied on the spherical harmonics are $\ell(\ell+1)\hbar$ where ℓ are the orbital angular quantum numbers $\ell = 0, 1, 2, \ldots$. The ℓ quantum number defines the type of atomic orbital: s, p, d, f, ...

Ladder operators $\hat{L}_\pm$ are employed to represent the transitions between states with different angular momentum.

The eigenvalues of the z-projection of the angular momentum operator $\hat{L}_z$ are the magnetic quantum numbers $m = -\ell, -\ell+1, \ldots, \ell-1, \ell$. Their name comes from the fact that in the presence of a magnetic field the states with different m quantum numbers have different energies. This is known as the *Zeeman effect*. The Coulomb potential is rotationally invariant, therefore in the field-free case, the states with a given ℓ quantum number are degenerate. The degeneracy is m-fold.

Electrons possess magnetic moment associated with their orbital angular momentum. A constant called the electron orbital g-factor $g_\mathrm{L} = 1$. The g-factor appears as an additional proportionality factor in the classical expression for magnetic moment in eq. 3.25.

$$\boldsymbol{m}_\mathrm{L} = -\frac{e}{2m_e} g_\mathrm{L} \hat{\boldsymbol{L}} = -\frac{\mu_\mathrm{B}}{\hbar}\hat{\boldsymbol{L}}, \tag{3.38}$$

where $\mu_\mathrm{B} = e\hbar/2m_e$ is the Bohr magneton. It serves as a unit for the magnetic moment of an electron, as discussed in Chapter 1.

3.2.3 *Spin angular momentum*

In relativistic quantum mechanics, the wave function is a four-component quantity. Two of the components account for the two spin states of the electron and the other two describe the spin states of the positron. The spin operators are called Pauli matrices. [158]

The angular momentum operator $\hat{\boldsymbol{L}}$ describes the spatial motion of a microscopic particle. In addition to it, elementary particles possess an intrinsic *spin angular momentum* $\hat{\boldsymbol{S}}$, which is a quantity without an analogue in the classical world [159]. The corresponding spin magnetic moment $\boldsymbol{m}_\mathrm{s}$ can be expressed similarly to the orbital magnetic moment in eq. 3.38, however multiplied by the constant factor g_s which is called the *electron spin g-factor*,

$$\boldsymbol{m}_\mathrm{s} = -\frac{e}{2m_e} g_\mathrm{s} \hat{\boldsymbol{S}} = -g_\mathrm{s}\frac{\mu_\mathrm{B}}{\hbar}\hat{\boldsymbol{S}}. \tag{3.39}$$

At the relativistic level, g_s is exactly equal to 2, however, quantum electrodynamics has shown that there is a deviation from the value, making it equal to 2.002319 [160, 161].

Spin angular momentum is not associated with the strength of the external magnetic field, and in fact, exists also in the absence of a magnetic field. The relations in eq. 3.34, eq. 3.33 and eq. 3.35 which are valid for the angular momentum operator $\hat{\boldsymbol{L}}$ also hold for the spin angular momentum operator $\hat{\boldsymbol{S}}$. The eigenvalues of the z-projection of the spin angular momentum $\hat{S}_z$ for the electron are $\pm\hbar/2$. Fermions possess half-integer spin, whereas bosons are characterised by integer spin [47, 48].

3.2.4 *Total angular momentum*

Classically, angular momenta can couple. The total angular momentum is simply the vector sum of the coupled angular momenta. In quantum mechanics, angular momentum coupling occurs if a set of angular momentum operators $\hat{\boldsymbol{J}}_i$ and their Cartesian components $\hat{J}_{n,i}$ with $n = \{x, y, z\}$ obey the commutation relations in eq. 3.33 and eq. 3.35. Furthermore, each Cartesian component of a coupled angular momentum operator $\hat{J}_{n,i}$ commutes with the components of all the other coupled angular momentum operators $\hat{J}_{n,k}$. The eigenvalues of $\hat{\boldsymbol{J}}$ are calculated as a sum of the eigenvalues of the individual angular momentum operators.

Electron configurations are marked in the term-symbol notation, based on the combined angular momentum quantum numbers for the atom : ${}^{2S+1}L_J$

According to Russell and Saunders, in multielectron atoms, the spins of the electrons couple to each other and give the total spin quantum number S [162]. It defines the multiplicity of the atom. In operator form, $\hat{\boldsymbol{S}} = \sum_i \hat{\boldsymbol{s}}_i$. Similarly, the orbital angular momenta $\hat{\boldsymbol{\ell}}_i$ are coupled, and the sum of their eigenvalues gives the total orbital quantum number L. This is known as *LS coupling*. The combined spin angular momenta can further couple to the combined orbital angular momenta, known as *spin-orbit coupling*. Their sum is the total angular momentum $\hat{\boldsymbol{J}}$ of the atom. The eigenvalues of the total angular momentum operator follow the relation

$$J = L + S. \tag{3.40}$$

In light atoms (with nuclear charge $Z \leq 30$), spin-orbit interaction is small, meaning that L and S give an accurate representation of the state. In other words, they are *good quantum numbers* because rotation does not change their value. In heavier atoms, spin-orbit coupling is stronger than spin-spin and orbital-orbital interactions. This is caused by the electric field of the nucleus, and is often referred to as *relativistic effects*. For coupled states, orbital angular momentum and spin angular momentum are not necessarily conserved, however, their sum, the total angular momentum, is indeed conserved. Thus,

the eigenvalues J and M_J of the operators $\hat{\boldsymbol{J}}$ and $\hat{J}_z$ are good quantum numbers because rotation does not affect them whereas L and M_L are not. The energies of the electronic states are determined by the eigenvalues of the $\hat{\boldsymbol{J}}$ operator and those of its z-projection $\hat{J}_z$. Spin-orbit coupling occurs without an external electromagnetic field. The energy splitting is known as the *fine structure* of the atom.

3.2.5 *Zeeman effect*

Depending on whether there is spin-orbit coupling, the Zeeman effect is based on the total angular quantum number m_j or on separate orbital-Zeeman and spin-Zeeman splittings. It is determined from the expression for the potential energy of the precessing electron in a magnetic field in eq. 3.23, employing the definition of the magnetic moment of the electron through its angular momentum given in eq. 3.25. In weak magnetic fields, there is a linear relation between energy and field strength, scaled by the magnetic quantum number m,

In strong magnetic fields, there is also a quadratic Zeeman effect [163].

$$\Delta E = \mu_\mathrm{B} m B, \tag{3.41}$$

where μ_B is the Bohr magneton. The expression shows that electrons with a negative spin magnetic quantum number m_s will lower their energy compared to the corresponding state with $m_\mathrm{s} = \hbar/2$. Furthermore, orbitals with high angular momentum and a negative m_ℓ quantum number will have lower energy than orbitals with $m_\ell \geq 0$.

In the presence of a sufficiently strong magnetic field, the coupling between the total angular momentum with the magnetic field becomes comparable to the strength of the coupling of the spin and angular orbital momenta. This breaks down the Zeeman effect and $\boldsymbol{L}$ and $\boldsymbol{S}$ decouple. The eigenvalues j of the total angular momentum operator are no longer good quantum numbers. Energy splitting depends on the projections of the angular orbital momentum and the spin orbital momentum. The spectroscopically observed pattern is known as the Paschen-Back effect.

3.2.6 *The Hamiltonian in a uniform magnetic field*

Placing an electron in a magnetic field originating from the vector potential $\boldsymbol{A}$ gives rise to the kinetic momentum $\boldsymbol{\pi}$, which includes the canonical momentum $\boldsymbol{p}$ and a term reflecting the interaction with the external field,

$$\boldsymbol{\pi} = \boldsymbol{p} + e\boldsymbol{A}. \tag{3.42}$$

The kinetic momentum operator,

$$\hat{\boldsymbol{\pi}} = -i\hbar\nabla + e\boldsymbol{A}, \tag{3.43}$$

is applied in the Schrödinger equation employing the Coulomb gauge $\nabla \cdot \boldsymbol{A} = 0$ in order to reduce the number of terms in the Hamiltonian. It leaves the freedom to choose a gauge origin $\boldsymbol{O}$ since the same constant uniform magnetic field $\boldsymbol{B}$ is generated by the magnetic vector potential $\boldsymbol{A}$ irrespective of $\boldsymbol{O}$ as discussed in Section 3.1. If the distance between a coordinate $\boldsymbol{r}$ and the gauge origin $\boldsymbol{O}$ is expressed as $\boldsymbol{r}_O = (\boldsymbol{r} - \boldsymbol{O})$, the magnetic vector potential of an external uniform magnetic field $\boldsymbol{A}$ for the gauge origin $\boldsymbol{O}$ can be obtained as

$$\boldsymbol{A}(\boldsymbol{r}) = \frac{1}{2}\boldsymbol{B} \times \boldsymbol{r}_O. \tag{3.44}$$

A wave function $\psi(\boldsymbol{r})$ is not a gauge-invariant object and obtains a complex phase pre-factor upon gauge transformation. The transformation $\boldsymbol{A} \mapsto \boldsymbol{A}' = \boldsymbol{A} + \nabla\Lambda(\boldsymbol{r})$ where $\Lambda(\boldsymbol{r})$ is an arbitrary real function, transforms the wave function $\psi(\boldsymbol{r}) \mapsto \psi'(\boldsymbol{r})$, so that

$$\psi'(\boldsymbol{r}) = \exp(-i(e/\hbar c)\Lambda)\psi(\boldsymbol{r}). \tag{3.45}$$

However, physical observables such as the probability density are conserved under gauge transformation since $|\psi(\boldsymbol{r})|^2 = |\psi'(\boldsymbol{r})|^2$, therefore it is physically indistinguishable whether the probability density corresponds to the problem in the magnetic field generated by $\boldsymbol{A}$ or by $\boldsymbol{A}'$.

The inclusion of the magnetic vector potential in the one-electron Hamiltonian $\hat{H}$ results in three terms – the field-free Hamiltonian $\hat{H}^{(0)}$, a term with first-order dependence on the magnetic field $\hat{H}^{(1)}$, and a term with a quadratic dependence on $\boldsymbol{A}$ denoted by $\hat{H}^{(2)}$:

$$\hat{H} = \hat{H}^{(0)} + \hat{H}^{(1)}(\boldsymbol{A}) + \hat{H}^{(2)}(A^2). \tag{3.46}$$

The term linear in $\boldsymbol{A}$ describes the paramagnetic interaction between the external magnetic field and the orbital angular momentum of the electron. It leads to an increase or decrease in the energy depending on $\hat{\boldsymbol{L}}$. $\hat{H}^{(1)}$ is then obtained by taking the expression for the magnetic moment in eq. 3.25,

The angular momentum operator depends on the gauge origin: $\hat{\boldsymbol{L}} = -i\boldsymbol{r}_O \times \nabla$.

$$\hat{H}^{(1)} = \frac{e}{m_e}\boldsymbol{A} \cdot \boldsymbol{p} = \frac{e}{2m_e}\boldsymbol{B} \cdot \boldsymbol{L}. \tag{3.47}$$

The second-order term in the magnetic-field Hamiltonian describes the diamagnetic interaction of the electron with the field. It is a parabolic confinement term which always raises the energy,

$$\hat{H}^{(2)} = \frac{e^2}{2m_e}A^2 = \frac{e^2}{8m_e}\left(B^2r^2 - (\boldsymbol{B}\cdot\boldsymbol{r})^2\right). \tag{3.48}$$

It is convenient to use $\boldsymbol{B} \parallel z$, so that

$$\hat{H}^{(2)} = \frac{e^2}{8m_e}B^2(x^2+y^2). \tag{3.49}$$

Spin angular momentum does not appear naturally when deriving the Schrödinger equation from the classical Hamiltonian since electron spin is a purely quantum-mechanical property and vanishes in the classical limit. The interaction between the electron spin and the external magnetic field can be interpreted using the spin magnetic moment $\boldsymbol{m}_s$ from eq. 3.39. Therefore, the spin Zeeman effect can be modelled with the Hamiltonian

$$\hat{H}_{Zeeman} = -\boldsymbol{B}\cdot\boldsymbol{m}_s. \tag{3.50}$$

Electron spin can be expressed through the dot product of the Pauli spin matrices $\boldsymbol{\sigma}$ with the kinetic momentum. The Pauli spin matrices for electrons are a set of three 2×2 matrices (one for each spatial coordinate). The spin operator can be defined as $\hat{\boldsymbol{S}} = \frac{\hbar}{2}\boldsymbol{\sigma}$. Hence, the one-electron Hamiltonian in the Coulomb gauge takes the form [164]

The eigenvalues of the Pauli spin matrices are ± 1.

$$\begin{aligned}\hat{H} &= \frac{(\boldsymbol{\sigma}\cdot\boldsymbol{\pi})^2}{2m_e} \\ &= \frac{1}{2m_e}p^2 + \frac{e}{2m_e}\boldsymbol{B}\cdot\hat{\boldsymbol{L}} + \frac{e}{m_e}\boldsymbol{B}\cdot\hat{\boldsymbol{S}} + \frac{e^2}{8m_e}\left(B^2r^2 - (\boldsymbol{B}\cdot\boldsymbol{r})^2\right).\end{aligned} \tag{3.51}$$

In an n-electron system, $\hat{\boldsymbol{L}} = \sum_i^n \hat{\ell}_i$ and $\hat{\boldsymbol{S}} = \sum_i^n \hat{s}_i$ where $\hat{\ell}_i$ and $\hat{s}_i$ are the orbital and spin angular momenta of electron i.

,

3.2.7 *Magnetically induced current density*

Electrons are particles in motion even without the presence of an external field. Their velocity is related to the linear momentum $\boldsymbol{p}$ as in classical mechanics, $\boldsymbol{v} = \frac{\boldsymbol{p}}{m_e}$. Scaling the velocity with the probability of finding the electron at point $\boldsymbol{r}$ and with the electron charge gives the current density $\boldsymbol{j}$ at point $\boldsymbol{r}$,

$$\boldsymbol{j}(\boldsymbol{r}) = -\frac{e}{2m_e}\left(\psi\hat{\boldsymbol{p}}\psi^* + \psi^*\hat{\boldsymbol{p}}\psi\right). \tag{3.52}$$

The complex conjugate ensures that the current density is real.

The integral of the current density in a certain volume is the probability that an electron will pass through the given region of space. Electron density and current density are subobservables, meaning that they are the expectation values of quantum-mechanical operators [165]. Electron density is a scalar function, whereas current density is a vector function in 3D. Current density is a conserved quantity and obeys the canonical continuity equation for charge conservation in eq. 3.18, which can be derived in the hydrodynamical representation of the Schrödinger equation [34, 166].

Magnetic fields give rise to induced current density in atoms and molecules according to Faraday's law in eq. 3.12 [27, 167]. It has been shown that the electron density flux forms quantised vortices surrounded by the nodes of the wave function [168–171]. Current vortices arising in the presence of a homogeneous magnetic field are classified as axial by Hirschfelder if they have orbital angular momentum dipole moments, whereas the interactions with a non-homogeneous magnetic field can generate toroidal vortices which possess orbital angular momentum quadrupole moments [171].

As shown in eq. 3.42, the interaction between the electron and the magnetic field is expressed by adding the magnetic vector potential $\boldsymbol{A}$ to the linear momentum operator $\boldsymbol{p}$. Upon substitution in the definition of current density in eq. 3.52, an additional term appears which has an explicit dependence on $\boldsymbol{A}$,

$$\boldsymbol{J}^B = -\frac{e}{2m_e}\left(\psi^*\boldsymbol{p}\psi + \psi\boldsymbol{p}\psi^*\right) - \frac{e^2}{m_e c}\boldsymbol{A}\psi^*\psi. \tag{3.53}$$

Magnetic fields perturb the wave function. The interaction of a molecule with a weak magnetic field can be described by the solution of the Schrödinger equation with the first-order correction to the Hamiltonian for the magnetic vector potential $\boldsymbol{A}$ (eq. 3.47). The presence of the orbital angular momentum operator in the Hamiltonian makes the wave function complex. The magnetically perturbed wave function can be expanded as

$$\psi_n = \psi_n^{(0)} + \psi_n^{(1)} + \cdots \quad \text{, where} \tag{3.54}$$

$$\psi_n^{(1)} = \sum_{n\neq 0} a_n \psi_n^{(0)}. \tag{3.55}$$

The orbitals can be assumed to be real, while the expansion coefficients a_n are complex. Formally, there are two contributions to the magnetically induced current density – diamagnetic $\boldsymbol{J}_d^B$ and paramagnetic $\boldsymbol{J}_p^B$. The diamagnetic current density depends only on the ground-state wave function ψ_0, whereas the paramagnetic component is related

to the response to the magnetic field exhibited as the mixing of the excited states ψ_n with ψ_0. Thus, the total current density is expressed as

$$\boldsymbol{J}^B = \begin{cases} \boldsymbol{J}_d^B & = -\dfrac{e^2}{m_e}\boldsymbol{A}\psi_0^2 \\ \boldsymbol{J}_p^B & = -i\hbar\dfrac{e^2}{2m_e}\displaystyle\sum_{n\neq 0}\left(a_n - a_n^*\right)\left(\psi_n\nabla\psi_0 - \psi_0\nabla\psi_n\right), \end{cases} \tag{3.56}$$

where a_n are the off-diagonal elements of the angular momentum operator. By convention, the magnetic field is chosen to point in the z direction so the L_z component is employed in calculations, yielding

$$a_n = \frac{\left\langle n \left| \hat{L}_z \right| 0 \right\rangle}{E_n - E_0}. \tag{3.57}$$

The diamagnetic term corresponds to the classical interpretation of the Larmor precession of an electron in a magnetic field given in eq. 3.25. The paramagnetic term does not a have a classical counterpart. The diamagnetic and paramagnetic contributions alone do not have a physical meaning. They depend on the choice of gauge origin of the magnetic vector potential. For example, a certain gauge origin can cause the paramagnetic current to vanish completely [150, 172]. Only the total current density is a physical quantity and it is independent of the gauge origin.

3.2.8 *Current density topology*

The magnetically induced current density $\boldsymbol{J}^B$ for is a particular magnetic field direction is a vector field with complicated topology [27, 173–176]. There are multiple singular points where the current density vanishes. Nodal surfaces called separatrices can be identified, which separate the current density field into various domains [173]. Each domain is a vortex in which the current traces a closed loop around a singular axis. As a consequence of charge conservation, domains may exist inside one another but their separatrices may not cross. Using graph theory, Gomes showed that there is necessary a vortex which completely surrounds the entire molecule [173]. Methods of fluid mechanics can be adapted to distinguish between different current vortices [177]. Streamlines are a useful visualisation tool as an analogue to classical trajectories.

In the concept of tropicity, a vortex is labelled as *diatropic* when the direction of the current is clockwise when looking towards the negative direction of the magnetic field vector, in accordance with Lenz's law (eq. 3.12) and the right-hand rule [150, 178]. A current vortex exhibiting flow in the counter-clockwise direction is termed

paratropic. Current tropicity does not depend on the gauge origin, unlike the classification into diamagnetic and paramagnetic currents, making it a physical observable. Comprehensive visual analyses are presented in Chapter 4.

Diamagnetic (classical) currents $\boldsymbol{J}_d^B$ always correspond to diatropic current vortices, however no direction can be assigned to paramagnetic (non-classical) currents $\boldsymbol{J}_p^B$, *i. e.*, they give rise to both diatropic and paratropic current density domains. Dia/paramagnetism is a characteristic of the response of a material to an external field, however, it is out of historical rather than physical reason to use the term to assign two contributions to magnetic properties derived through perturbation theory, especially given that only the sum of them is a physical observable [150]. Originally, molecules exhibiting a diamagnetic response were called diatropic molecules while molecules with paramagnetic characteriseds were termed paratropic [178]. Nowadays tropicity is only used in the context of current density distribution and direction since there can be both diatropic and paratropic ring currents in the same molecule.

3.2.9 *Nuclear magnetic vector potential*

Atomic nuclei with non-zero spin give rise to a magnetic vector potential $\boldsymbol{A}_{\text{nuc}}$,

$$\boldsymbol{A}_{\text{nuc}} = \frac{\mu_0}{4\pi} \frac{\boldsymbol{m}_{\text{nuc}} \times \boldsymbol{r}}{r^3}. \tag{3.58}$$

The corresponding nuclear magnetic moment $\boldsymbol{m}_{\text{nuc}} = \gamma_N \boldsymbol{I}$ is related to the spin angular momentum $\boldsymbol{I}$ of the nucleus as in eq. 3.25, where γ_N is the gyromagnetic ratio of the nucleus. Therefore, in an external magnetic field, the magnetic vector potential experienced by electron i is

$$\boldsymbol{A}_i = \frac{1}{2}\boldsymbol{B} \times \boldsymbol{r}_{iO} + \alpha^2 \sum_K \frac{\boldsymbol{m}_K \times \boldsymbol{r}_{iK}}{r_{iK}^3}. \tag{3.59}$$

where $\boldsymbol{r}_{iO} = \boldsymbol{r}_i - \boldsymbol{O}$ with $\boldsymbol{O}$ being the gauge origin of the external magnetic field, α is the fine structure constant, the indices K span all nuclei, $\boldsymbol{m}_K$ is the magnetic moment of nucleus K, and r_{iK} is the distance between electron i and nucleus K.

Gauge transformations act as unitary transformations on the Hamiltonian, thus its eigenvalues are also gauge invariant.

The Schrödinger equation is gauge-invariant, however a large number of the available approximate solutions often do not fulfill this requirement [179, 180]. Expansion of the wave function to a finite basis set can lead to current leakage, *i. e.*, charge conservation is violated, and subsequently, magnetic properties depend on the choice of the origin of the coordinate system [181]. There is no optimal gauge origin for studying molecular systems [182]. Keith and Bader showed

that the gauge origin does not have to be the same for every point at which magnetic properties of molecules are calculated [183]. A common way of handling the gauge-origin dependence is to employ gauge-including atomic orbitals (GIAOs), also known as London orbitals [184]. They involve a complex exponential pre-factor to ordinary GTO basis functions $\chi_K(\boldsymbol{r})$. The definition is physically meaningful since such a pre-factor also appears in the wave function of a single electron in a magnetic field as well as in a wave function after a gauge transformation as in eq. 3.45. The gauge origin of each orbital is set at the nucleus of the atom the orbital belongs to [185, 186]. GIAOs do not ensure gauge invariance of the current density but lead to gauge-origin independence and fast basis-set convergence [179, 187]. Expressing the magnetic vector potential at each point as $\boldsymbol{A}_K^B = \frac{1}{2}\boldsymbol{B} \times (\boldsymbol{R}_K - \boldsymbol{O})$ defines a gauge-including atomic orbital:

$$\omega_K(\boldsymbol{r}, \boldsymbol{A}_K^B) = \exp(-i\boldsymbol{r} \cdot \boldsymbol{A}_K^B)\chi_K(\boldsymbol{r}). \tag{3.60}$$

3.2.10 *Nuclear shielding*

The magnetically induced current density gives rise to a secondary magnetic field which couples with the nuclear magnetic moment [27]. The local magnetic field $\boldsymbol{B}_{\text{loc}}$ in the vicinity of a nucleus is related to the applied external field through the *shielding tensor* $\boldsymbol{\sigma}$ [188, 189]. The average of the diagonal elements of of the shielding tensor is the observed isotropic shielding constant σ for that nucleus,

$$\sigma = \frac{1}{3}\left(\sigma_{xx} + \sigma_{yy} + \sigma_{zz}\right). \tag{3.61}$$

therefore,

$$\boldsymbol{B}_{\text{loc}} = (1 - \sigma)\,\boldsymbol{B} \tag{3.62}$$

When $\boldsymbol{A}_{\text{nuc}}$ is added to the Hamiltonian involving an external magnetic field in eq. 3.46, the energy with first-order dependence on the magnetic vector potential is expressed as the coupling between the nuclear magnetic moment m_I and the magnetically induced current density $\boldsymbol{J}^B(\boldsymbol{r})$,

$$E^{m_I B} = -\int \boldsymbol{A}_{\text{nuc}}(\boldsymbol{r}) \cdot \boldsymbol{J}^B(\boldsymbol{r})\,\mathrm{d}\tau. \tag{3.63}$$

The local magnetic field arising from the interaction between the nuclear magnetic moment and the current density in the presence of an external magnetic field can be expressed as

$$\boldsymbol{B}_{\text{loc}} = \frac{\mu_0}{4\pi}\int \frac{\boldsymbol{r} \times \boldsymbol{J}(\boldsymbol{r})}{r^3}\mathrm{d}\tau. \tag{3.64}$$

It is the sum of the external magnetic field and the magnetic field which the magnetically induced currents give rise to, $\boldsymbol{B} = \boldsymbol{B}_{\text{ext}} + \boldsymbol{B}_{\text{ind}}$.

Computationally, time-independent molecular properties which are the result of a perturbation to the system can be calculated as derivatives of the total energy, as shown in eq. 2.51, eq. 2.52 and eq. 2.53 in the limit of zero magnetic field. Nuclear shielding is a second-order property. The elements of the shielding tensor $\sigma^K_{\alpha\beta}$ for nucleus K can be calculated as the mixed second derivative of the total energy of the perturbed molecule with respect to the components of the magnetic field and the magnetic moments of the nuclei,

$$\sigma^K_{\alpha\beta} = \left.\frac{\partial^2 E}{m^K_\alpha \partial B_\beta}\right|_{m^K_\alpha, B_\beta = 0}, \text{ where } \alpha, \beta \in \{x, y, z\}. \tag{3.65}$$

The above expression can be re-written in the language of second quantisation, employing the matrix elements of the one-electron Hamiltonian $h_{\mu\nu}$, the density matrix $D_{\mu\nu}$ and its derivatives with respect to the external magnetic field which are called the magnetically perturbed density matrices [179],

$$\sigma^K_{\alpha\beta} = \sum_{\mu\nu} D_{\mu\nu} \frac{\partial^2 h_{\mu\nu}}{\partial m^K_\alpha \partial B_\beta} + \sum_{\mu\nu} \frac{\partial D_{\mu\nu}}{\partial B_\beta} \frac{\partial h_{\mu\nu}}{\partial m^K_\alpha}. \tag{3.66}$$

The indices μ and ν give the respective matrix elements in the atomic-orbital representation, and m^K_α are the Cartesian components of the magnetic moment of nucleus K.

The tensor components of the shielding tensor are difficult to measure experimentally because molecules are tumbling as a result of thermal motion. Nuclear shielding constants are indirectly probed by measuring chemical shifts in nuclear magnetic resonance (NMR). Therefore, the NMR spectrum is also an indirect experimental method for the measurement of magnetically induced currents and the assessment of the electronic structure of the molecule [27, 190, 191]. Chemical shifts δ are defined as the resonance frequency ν_{mol} of a nucleus relative to a standard ν_{ref} [190, 191]. They can be calculated as the difference between the shielding constant of a nucleus in a reference molecule versus the shielding constant of the same nucleus in the investigated molecule, $\delta = \sigma_{\text{ref}} - \sigma_{\text{mol}}$. Chemicals shifts are reported in parts per million (ppm).

$$\delta = \frac{\nu_{\text{mol}} - \nu_{\text{ref}}}{\nu_{\text{ref}}}$$

3.2.11 *The gauge-including magnetically induced currents method*

The current density can be expanded in a Taylor series for each of the vector components of the magnetic field at the limit of $|\boldsymbol{B}| \to 0$,

$$\boldsymbol{J}^B(\boldsymbol{r}) = \boldsymbol{j}_0(\boldsymbol{r}) + \sum_{\beta \in \{x,y,z\}} \left. \frac{\partial \boldsymbol{J}^B(\boldsymbol{r})}{\partial B_\beta} \right|_{B_\beta = 0} B_\beta + \mathcal{O}\left(B_\beta^2\right). \tag{3.67}$$

where $\boldsymbol{J}^B(\boldsymbol{r})$ is the sum of the field-free current density $\boldsymbol{j}_0(\boldsymbol{r})$ and the magnetically induced current density. The derivatives of the components of the current density and the magnetic field give the tensor elements of the first-order current density susceptibility tensor [192],

$\boldsymbol{j}_0(\boldsymbol{r}) = 0$ for closed-shell molecules.

$$\mathcal{J}_\alpha^{B_\beta} = \frac{\partial J_\alpha^{B_\beta}(\boldsymbol{r})}{\partial B_\beta} \text{ , where } \alpha, \beta \in \{x, y, z\}. \tag{3.68}$$

The current density for a particular magnetic field direction can subsequently be obtained by contracting the current density susceptibility tensor with the Cartesian components of the magnetic field. The SI unit for current density is $\mathrm{nA} \cdot \mathrm{T}^{-1} \cdot \mathrm{m}^{-2}$.

The current density susceptibility appears in the expression for the shielding tensor derived from the Biot–Savart law [27, 176, 192],

$$\sigma_{\alpha\beta}^K = -\varepsilon_{\alpha\delta\gamma} \int \frac{r_\delta - R_{K\delta}}{|\boldsymbol{r} - \boldsymbol{R}_K|^3} \frac{\partial J_\gamma^B(\boldsymbol{r})}{\partial B_\beta} \, \mathrm{d}\tau, \tag{3.69}$$

where $\varepsilon_{\alpha\delta\gamma}$ is the Levi–Civita tensor for the three Cartesian directions. The position of nucleus K is given by the vector $\boldsymbol{R}_K$. Combined with the analytical-derivative expression for the shielding tensor in eq. 3.66, it is possible to write the current density susceptibility using the unperturbed and the magnetically perturbed density matrices in the atomic-orbital basis [193, 194],

$$\begin{aligned}\mathcal{J}_\alpha^{B_\beta}(\boldsymbol{r}) = &\sum_{\mu\nu} D_{\mu\nu} \frac{\partial \omega_\mu^*(\boldsymbol{r})}{\partial B_\beta} \frac{\partial \tilde{h}}{\partial m_\alpha^K} \omega_\nu(\boldsymbol{r}) + \sum_{\mu\nu} D_{\mu\nu} \omega_\mu^*(\boldsymbol{r}) \frac{\partial \tilde{h}}{\partial m_\alpha^K} \frac{\partial \omega_\nu(\boldsymbol{r})}{\partial B_\beta} \\ &+ \sum_{\mu\nu} \frac{\partial D_{\mu\nu}}{\partial B_\beta} \omega_\mu^*(\boldsymbol{r}) \frac{\partial \tilde{h}}{\partial m_\alpha^K} \omega_\nu(\boldsymbol{r}) - \varepsilon_{\alpha\beta\delta} \sum_{\mu\nu} D_{\mu\nu} \omega_\mu^*(\boldsymbol{r}) \frac{\partial^2 \tilde{h}_{\mu\nu}}{\partial m_\alpha^K \partial B_\beta} \omega_\nu(\boldsymbol{r}),\end{aligned} \tag{3.70}$$

where ω are the GIAO basis functions which depend on the magnetic vector potential as defined in eq. 3.60. The $|\boldsymbol{r} - \boldsymbol{R}_K|^3$ term in the denominator as in eq. 3.69 is excluded in the newly defined one-electron Hamiltonian $\tilde{h}$ for simplicity. For open-shell systems there are two equations like eq. 3.70 for α or β electron spin [194].

Nuclear shielding calculations are routinely done using various quantum-chemistry codes. The obtained perturbed and unperturbed density matrices can be used in the gauge-including magnetically induced currents (GIMIC) program by Jusélius, Sundholm, and Gauss to calculate the magnetically induced current density susceptibilities in the zero-field limit in eq. 3.68. [193, 195].

The use of approximate wave functions in quantum-chemistry calculations was shown to break charge conservation [181, 185]. The divergence of the current density is an indicator of the completeness of the basis set [193]. However, from practical experience DFT level with a triple-ζ (TZ) basis set can reproduce the magnetically induced currents obtained at MP2 level of theory which consistently match experimental data [151]. Valiev, Fliegl, and Sundholm further showed that paratropic current strength is overestimated at the B3LYP level. The density functionals with more accurate long-range behaviour such as CAM-B3LYP [196] and B97D [197] were found to better reproduce MP2-level data. We showed that the amount of HF exchange in the DFT functional affects the strength of the diatropic and the paratropic currents [198].

3.2.12 *Molecular aromaticity*

Aromaticity is an abstract property of organic and inorganic molecules and clusters, the definition of which is not univocally agreed upon [199–205]. It is not an observable since there is no quantum-mechanical operator corresponding to it. Instead, aromaticity can be regarded as a set of properties. Various techniques can be employed to determine molecular (anti)aromaticity, including chemical reactivity and stability, geometrical planarity, bond length alternation, aromaticity indices, magnetically induced current density, diamagnetic exaltation, and nucleus-independent chemical shift (NICS) among others [28, 200, 206–209].

Diamagnetic anisotropy is historically among the first characteristics for aromatic character [148, 210]. The first quantum-mechanical treatment was developed by London [184]. The simplest condition for aromaticity is the Hückel rule [211–215]. Molecules with $(4n+2)$ number of π electrons are expected to be aromatic. If the number of electrons is a multiple of 4, then the molecule should be antiaromatic. The empirical rule for molecules with Möbius topology is the opposite: when there are $4n$ π electrons the molecule is aromatic while $(4n+2)$ π electrons suggests antiaromatic character [216–219]. Aromaticity (and antiaromaticity) of three-dimensional molecules has also been studied by many authors [220, 221].

According to the ring-current model, magnetic fields induce current density in molecular rings [27, 222]. The net current strength in the molecule determines whether it is aromatic, antiaromatic or

non-aromatic. Aromatic molecules sustain strong net diatropic ring currents, whereas strong net paratropic ring currents are observed in antiaromatic molecules. When the diatropic and paratropic currents are of equal magnitude the net current vanishes; such molecules are non-aromatic [28, 223]. Despite their name, ring currents are observed also in open-chain molecules and even in single atoms [223].

NMR has proven to be the standard experimental method for the assignment of molecular aromaticity. Ring currents induce a secondary magnetic field $\boldsymbol{B}_{\text{ind}}$ perpendicular to the ring-current pathway, similarly to the field induced concentrically around a wire conducting electricity as described by Biot–Savart's law [27, 190, 222]. The direction of the magnetic field is determined by Lenz's law from classical electrodynamics. The magnetic field induced by diatropic currents attenuates the external magnetic field inside the molecular ring, while enhancing the external magnetic field $\boldsymbol{B}_{\text{ext}}$ on the outer perimeter of the molecule. The hydrogen atoms in the benzene molecule lie outside of the carbon skeleton. There is a strong diatropic ring current, thus the hydrogen atoms are *deshielded* and experience a stronger magnetic field. This leads to *downfield shifting* of the nuclear shielding constants. Conversely, paratropic currents induce a secondary magnetic field which is colinear with $\boldsymbol{B}_{\text{ext}}$ inside the ring, whereas $\boldsymbol{B}_{\text{ind}}$ opposes the external field on the outer perimeter of the molecular ring. The hydrogen atoms of pentalene are *shielded* by a strong paratropic current, therefore the nuclear shielding constants are *shifted upfield*.

3.2.13 *Anapole moment*

Magnetic field are usually dipolar, *i. e.*, there is a north and a south pole. This enforces axial symmetry of the field and any interactions depend on the field direction. According to classical electrodynamics, current flowing in a coiled wire which is bent so that the two ends can meet gives rise to a magnetic field inside the volume enclosed by the loops of the coil. Such kind of magnetic field without north and south poles is called an *anapole*. It is associated with an *anapole (toroidal) moment*. It can be shown that the $\boldsymbol{B}_{\text{ind}} \neq 0$ only inside the volume of the torus since the contributions of the magnetic field of each coil cancel each other. Anapole moments of certain particles have been predicted and some have been measured, such as the nuclear anapole moment of cesium [224, 225]. Similarly in molecules, helical magnetically induced current density flowing on a toroidal surface can induce a secondary anapolar magnetic field $\boldsymbol{B}_{\text{ind}}$ inside the volume of the torus [226–228]. The magnetically induced anapole moments of chiral molecules is equal in magnitude but in the opposite direction for the two enantiomers [226, 227, 229].

3.2.14 *The strong-magnetic-field regime*

Classically, an electron in a uniform magnetic field follows a circular trajectory perpendicular to the magnetic field vector, where the radius is a function of the magnetic field strength. Equating the centripetal force to the Lorentz force defines the cyclotron speed. The Larmor radius as well as the cyclotron speed associated with the rotational motion are quantised in the quantum-mechanical description,

$$E = \hbar\omega = \hbar\frac{eB}{m_e c}. \tag{3.71}$$

For hydrogen-like atoms with nuclear charge Ze, the critical magnetic field strength is $B_0 Z^2$ [230].

The spectrum of states in eq. 3.71 is called *Landau energy levels* [231]. Setting the cyclotron radius to be equal to the Bohr radius a_0 defines the atomic unit of magnetic field strength B_0. For magnetic fields several orders of magnitude stronger than B_0, the cyclotron energy $\hbar\omega$ of an electron in an atom becomes much larger than the energy of the Coulomb interaction with the nucleus. This is known as the *Landau regime* in ultrastrong magnetic fields. The electrostatic interaction can then be treated as a perturbation to the magnetic Hamiltonian [232]. The magnetic field confines electronic motion perpendicularly to the field direction. The diamagnetic term in the Hamiltonian, quadratic in B, is confining and enforces cylindrical symmetry. The Larmor radius is only determined by the Coulomb interaction whereas there is little restriction along the field.

3.2.15 *Atoms and molecules in strong and ultrastrong magnetic fields*

The magnetic fields produced in laboratory conditions are typically within four-five orders of magnitude smaller than the atomic unit B_0, so that magnetic interactions can be treated perturbatively. The relative strength between the Coulomb force and the magnetic force can become smaller in solid state for materials with a large dielectric constant [10, 232]. Studying strong magnetic field also finds applications in astrophysics. [233]. Very strong magnetic fields can be found in space Magnetic white dwarfs sustain fields in the order of 1000 T, while neutron stars can generate fields as strong as several atomic units to tens of thousands of atomic units [15, 234].

In ultrastrong magnetic fields, the atomic orbitals become needle-shaped – highly confined perpendicularly to the magnetic field vector but elongated in the parallel direction [235]. In $B \geq 1000\, B_0$, typical for highly magnetised neutron stars and pulsars, there is very strong confinement [234, 236]. Atoms become small and with strongly pronounced cylindrical symmetry parallel to the magnetic field. They align themselves into linear chains similarly to how iron filings visualise the magnetic field lines of a magnet [236]. Bonds form due to the high quadrupole moment of the atoms along the field axis, while

the electrons form a sheath with cylindrical symmetry around the chain of nuclei. The Coulomb interaction is only significant in the parallel direction, therefore there is attraction and repulsion between neighbouring chains. As a result, matter in ultrastrong magnetic fields form a rigid crystal lattice which is a conductor parallel to the field but insulator in the perpendicular direction [236]. Studies on the H_2^+ molecular ion have shown a significant increase in the binding energy and shortening of the equilibrium bond distance [237]. Chen, Ruderman, and Sutherland predicted the binding energy between two iron atoms to be 5-10 $\times$ 10^4 eV on the surface of a neutron star [238].

The significant changes in the shape of the orbitals brought about by strong magnetic fields pose difficulties to the choice of basis set. It is increasingly difficult for GTO basis sets to accurately describe the behaviour, thus finite-field calculations are typically performed for $B \leq B_0$ atomic units [239–241]. Computational studies with orders of magnitude stronger magnetic fields have also been reported [242–255]. We compared the basis-set truncation error for $B = [0;10]\, B_0$ at the Hartree–Fock level of theory using correlation-consistent GTO basis sets and a fully numerical finite-element method [256]. An alternative to ordinary GTO basis sets are anisotropic ones where the coefficients and the exponents of the primitives are different for the parallel and the perpendicular orientation [257, 258]. The computational cost is significantly increased but also optimising the basis set is challenging [259–261].

In the *intermediate regime* when the Coulomb interaction and the magnetic interaction are comparable in energy, perturbation theory is not applicable. The angular momentum operator in the Hamiltonian in a magnetic field (eq. 3.51) sets the requirement that orbitals need to be complex. New *ab initio* quantum-chemistry programs are required, such as LONDON [262], QUEST [263], and BAGEL [264]. They feature implementations of the Hartree–Fock, DFT, full configuration interaction and coupled cluster levels of theory [239–241, 265–272]. Studies of molecules in non-uniform magnetic fields have also been performed [229, 273]. The aforementioned software employs GIAOs to ensure gauge-origin independence.

The energy states of H_2 were first investigated by Detmer et al. and later Lange et al. predicted a new type of interatomic interaction – the *paramagnetic bond* – in the triplet state of the H_2 molecule in perpendicular field [240, 247]. The geometry of the singly charged molecular ion H_3^+ has been studied in magnetic fields in the intermediate regime by Warke and Dutta [274]. They showed that for $B < B_0$, the molecule forms an isosceles triangle, whereas in a stronger field, it becomes linear. At sufficiently strong magnetic fields, the high-spin states of the molecules are bound through the paramagnetic bond mechanism when the C–H bonds are perpendicular to the magnetic field vector.

4

INVESTIGATIONS AND RESULTS

4.1 ELECTRONIC FLOW IN WEAK MAGNETIC FIELDS

The gauge-including magnetically induced currents (GIMIC) method presented in Section 3.2.11 was employed in Articles I, II, III, and IV. Throughout the discussion, the magnetically induced current density susceptibility $\mathcal{J}(\boldsymbol{r})$ will be referred to as current density for simplicity. The current density field is analysed visually to determine the ring-current pathways. The strength of the ring currents is determined by integration of the current density passing through a plane. Atomic units of distance are employed, where 1 bohr $\equiv a_0 = 0.529\,177\,210\,903(80)$ Å [275].

4.1.1 *Visualisation of the current density field*

Recently we developed a visualisation method of the magnetically induced current density vector field using the PARAVIEW program [276]. The tropicity of the ring-current flow as well as the current density vortices and separatrices can be determined visually. A colour scheme is employed to show the strength of the current density, where black corresponds to $|\mathcal{J}(\boldsymbol{r})| \leq 10^{-6}\,\mathrm{nA}\cdot\mathrm{T}^{-1}\cdot\mathrm{m}^{-2}$ and increasing in the order red, orange, yellow, and white which signifies current density larger than $|\mathcal{J}(\boldsymbol{r})| \geq 0.1\,\mathrm{nA}\cdot\mathrm{T}^{-1}\cdot\mathrm{m}^{-2}$. In Figure 4.1, line integral convolution was applied on a plane crossing the current density field in ethane perpendicular to the external magnetic field direction.

Any molecule is enclosed by a global current-density domain which vanishes at increasing distance from the molecule as Gomes showed using topology analysis [173]. Cross-sections of the current density field such as the one in Figure 4.1 reveal the presence of various other smaller domains embedded into the global current-density domain. The outermost global ring current is always diatropic but its strength varies from one molecule to another. In the close vicinity of atomic nuclei, there is a highly concentrated current density due to the core electrons. Such features of the current density field are referred to as atomic ring currents. Their strength correlates with the number of core electrons. Near some atoms there are additional local atomic ring-current pathways which can be either diatropic or paratropic. Other local current-density vortices can be found at chemical bonds called bond currents. They are diatropic and generally weak, about $1\,\mathrm{nA}\cdot\mathrm{T}^{-1}$.

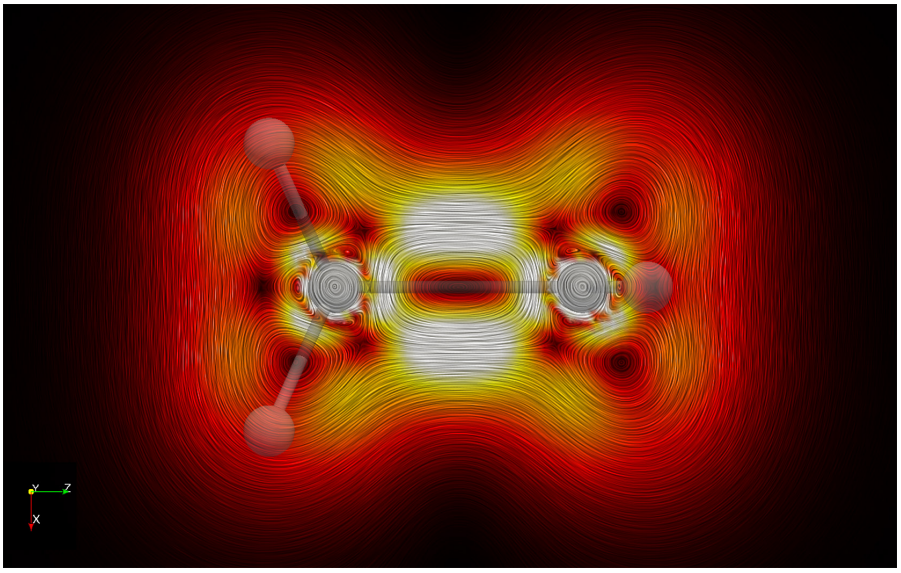

Figure 4.1: The line integral convolution technique is applied to a plane through the C–C bond in ethane perpendicular to the magnetic field to visualise the current vortices. The colour scheme is defined such that white is the strongest current density, whereas black corresponds to vanishing current density.

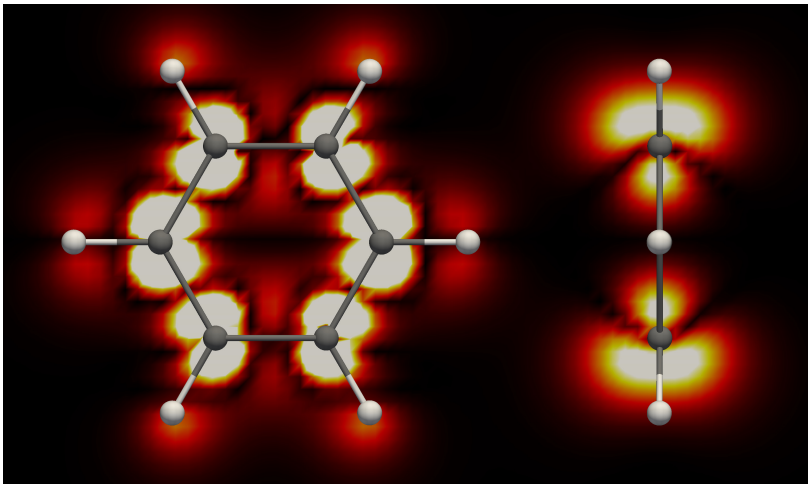

Figure 4.2: A slice through the molecular plane of one of the benzene rings in the T-shaped benzene dimer. The magnetic field is parallel to the ring on the left but perpendicular to the other benzene ring of the dimer. The colour scheme represents the strength of the current density.

Typically, the strongest ring currents in a molecular ring arise when the magnetic field is perpendicular to the ring. This is associated with the alignment of the p orbitals of the atoms involved in the conjugated π-electron pathway in organic molecules. Atomic ring currents and bond ring currents exist in any orientation of the magnetic field due to the symmetry of the atomic and the σ orbitals respectively. However, the paratropic ring current following the contour of a molecular ring vanishes altogether in parallel orientation as shown for the T-shaped benzene dimer in Figure 4.2. There is only a weak global ring current and strong local atomic ring currents, illustrated also for toluene in Figure 4.5.

In polycyclic and non-planar molecules, there are numerous ring currents which are explored in detail in Articles I and II. In particular, the presence of heteroatoms can alter the ring-current pathways depending on the electronegativity of the atom. Two sp^2 carbon atoms are isoelectronic to the pair of a boron atom and a trivalent nitrogen atom. We found that in the vicinity of the nitrogen atoms there are large local atomic current-density domains which enclose the bond current vortices of the neighbouring N–H bonds (Figures 6, 7, 9, and 12 in Article II). They are well visible also in the streamline representation of the current density in triphyrin(2.1.1) with an annelated benzo[b]furan ring illustrated in Figure 4.3, part of our manuscript in Ref. [277]. Heteroatoms cause the formation of complicated patterns of the global ring currents, for example in molecule (2) in Article II where a strand of the global ring current makes a turn inside the 1,2,3-diazaborole rings (illustrated in Figure 6 in Article II).

Ring currents often do not follow a planar trajectory. Streamline plots are useful particularly when investigating non-planar molecules. As we showed in Article III, Figure 6, there are through-space interactions when the opposite sides of the Möbius twisted [40]annulenes meet. Streamline representation of the ring-current pathways in the toroidal carbon nanotubes which we investigated in Article IV was particularly insightful. A strand of the global ring current on the surface of a toroidal nanotube is illustrated in Figure 4.4. We investigated a series of toroidal carbon nanotubes. In one of the biggest chiral toroidal molecules we found that the ring current flows in a helical manner around the tube (Article IV, Figure 9). These findings are very promising for future studies on the magnetically induced anapole moments of chiral molecules as described in Section 3.2.13.

4.1.2 *Calculation of the strength of the current density*

Quantitative current density analysis is performed by placing an integration plane so that it crosses a particular current-density domain. Integration is usually done between $8\,a_0$ above and below the molecular plane in the vertical direction. Horizontally, the integration is

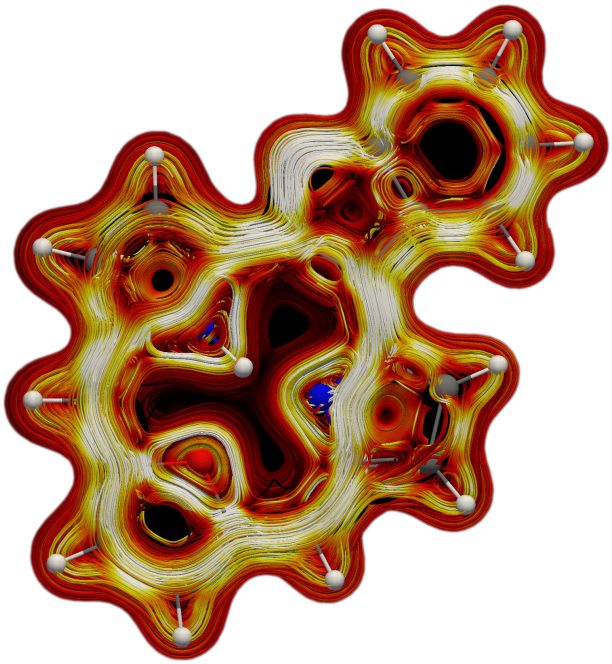

Figure 4.3: A streamline representation of the current density in triphyrin(2.1.1) with an annelated benzo[b]furan ring. The colour scheme is defined such that white is the strongest current density. Some parts of the local paratropic ring currents are not visible. Originally from our manuscript in Ref. [277].

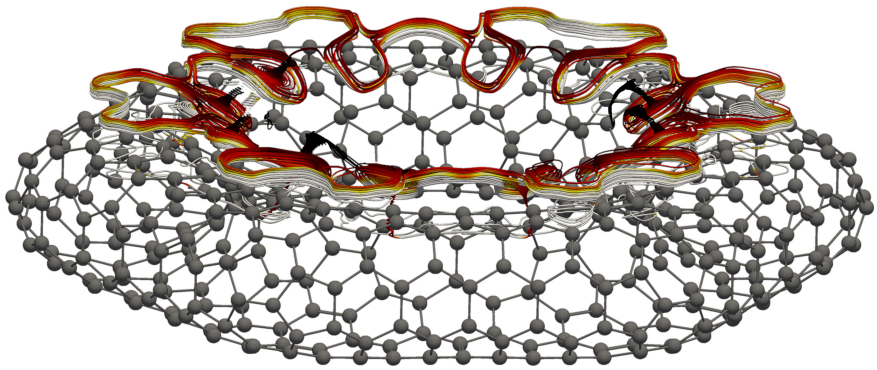

Figure 4.4: A streamline representation of the global ring current in a toroidal carbon nanotube investigated in Article IV.

often started from the centre of a molecular ring and extended out until the current density vanishes. This ensures that the whole cross-section of current density domain will be evaluated. For each grid point on the integration plane, we can assign a positive or a negative sign depending on whether the current appears to be flowing to the left or to the right when seen from above. This alone is not enough to distinguish whether the current density is diatropic or paratropic since tropicity is a global property of the vortex and a single point is not enough to characterise it. When crossing a vortex twice, first it appears to flow in the one direction and after crossing the vortex origin, the returning current appears to flow in the opposite direction as illustrated in Figure 4.5. This is physically sound since, as a result, the net current vanishes.

Two ring-current vortices may have different tropicity but locally at neighbouring grid points on the integration plane, the current density vectors point in the same direction. This is the case, for example, when the integration plane crosses the origins of the two paratropic ring-current vortices in naphthalene as illustrated in Figure 4.6. The diatropic bond current appears to flow in the same direction as the paratropic ring current on each side of the shared C–C bond.

The rationalisation of the current strength becomes increasingly difficult as the size of the molecule grows. As seen in Figure 2 in Article I, there are unexpected crescent-shaped diatropic current loops in the six-membered rings of the naphthalene molecule. Likely they originate from the coalescence of the C–C bond-current vortices. One way of tackling the problem is to define multiple integration planes and do scans of the current strength as a function of distance along the integration plane. These differential current profiles as in Figure 10 from Article I and in Figure 2 from Article II make it possible to integrate the current strength of individual domains of the current density field, and the strength of the ring currents can be obtained using basic algebra.

When an integration plane crosses a bond or an atomic current vortex, the ring current is integrated twice as the it circulates around the vortex origin. Due to charge conservation, the net integrated ring-current strength of the bond or atom vanishes. This makes it possible to calculate the global net ring-current strength in a molecular ring, which is a criterion for its aromatic character. The benzene molecule sustains a net ring current of $11.66\,\mathrm{nA}\cdot\mathrm{T}^{-1}$ while in the pentalene molecule, an example of an antiaromatic structure, the net ring current is $-15.12\,\mathrm{nA}\cdot\mathrm{T}^{-1}$ at the B3LYP/def2-TZVP level of theory, reported in Article II. Molecular rings with a net ring current weaker than about $\pm 3\,\mathrm{nA}\cdot\mathrm{T}^{-1}$ are considered non-aromatic. The magnitude of the current density depends on the employed level of theory. We investigated the dependence of the amount of Hartree–Fock exchange in a series of DFT functionals in Article IV. The plot in Figure 14 in

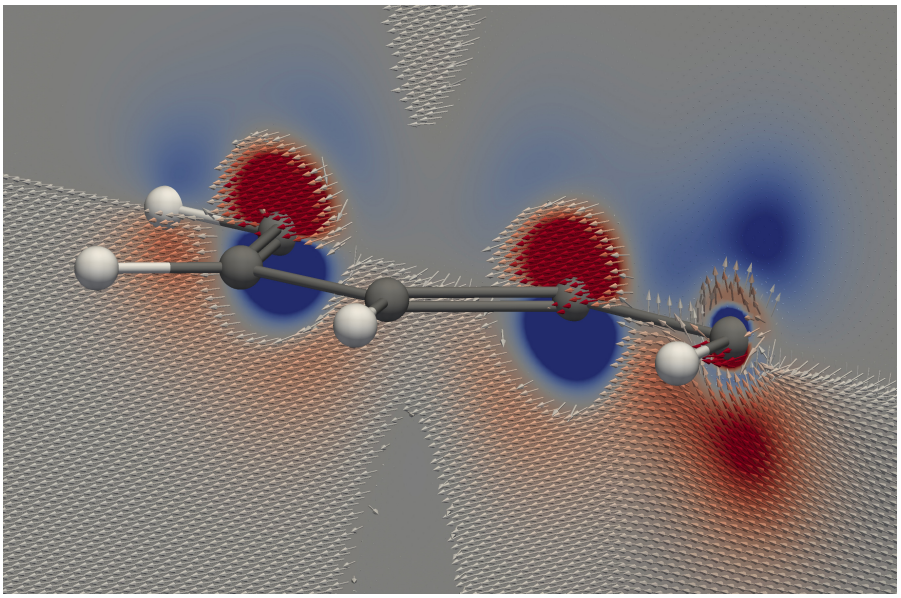

Figure 4.5: Integration plane positioned along the C – C bond to the methyl group in toluene. The red and blue colour show whether the current density vector points towards or away from the integration plane. The magnetic field is parallel to the molecular plane and points along the C–C bond to the methyl group. Originally from our manuscript in Ref. [278].

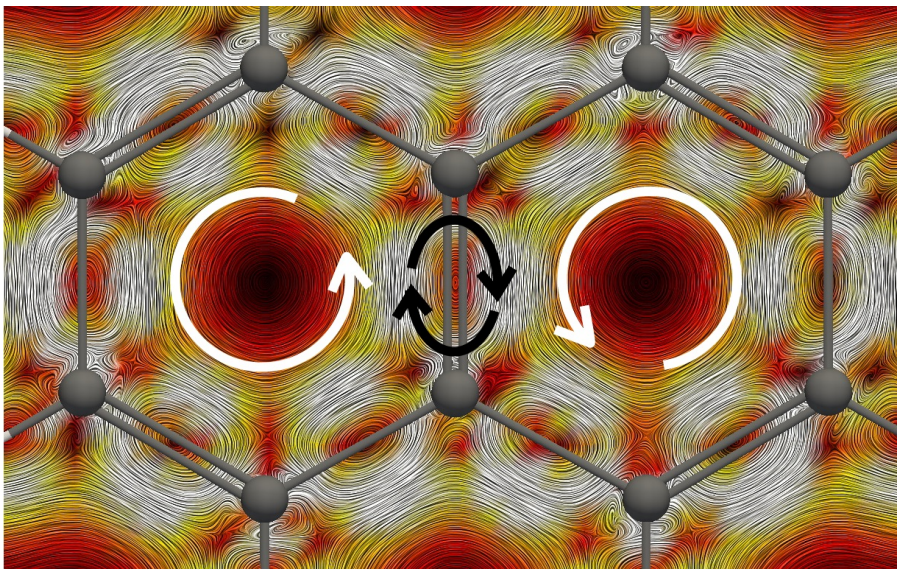

Figure 4.6: Directions of the paratropic (counterclockwise; white arrows) ring current and the diatropic (clockwise; black arrows) bond current. The magnetic field is perpendicular to the molecular plane, pointing away from the viewer.

Article IV shows that the net current density for one of the toroidal carbon nanotubes with 576 carbon atoms changes from $118\,\mathrm{nA}\cdot\mathrm{T}^{-1}$ with a non-hybrid density functional to $165\,\mathrm{nA}\cdot\mathrm{T}^{-1}$ when employing the M06-2X functional with 54% Hartree–Fock exchange. The change was even more significant for the toroidal carbon nanotube with 672 carbon atoms from the same series. Three non-hybrid DFT functionals yielded an average of $-93\,\mathrm{nA}\cdot\mathrm{T}^{-1}$, whereas the molecule became weakly antiaromatic ($-9\,\mathrm{nA}\cdot\mathrm{T}^{-1}$) when employing the M06-2X functional. Given that the strength of the current density cannot be directly measured experimentally, it is hard to say which functional gives the most accurate value. However, the comparison of the calculated chemical shifts to the experimentally measured ones in NMR spectroscopy gives a good indication of the applicability of the DFT functional for current density analysis.

4.1.3 *Applications of the current density analysis*

One of the main applications of the current density analysis is to study molecular aromaticity. In Articles I – IV we studied the aromatic properties of a variety of molecules. Different conformations of a molecule can have a different aromatic character. The conformer with the most strongly pronounced aromaticity is not necessary the most stable one as shown in Article I. Interestingly, in the all-*trans* conformer of [10]annulene, where the p orbitals are parallel to the magnetic field, there is no paratropic ring current inside the ring. However, there is a strong diatropic current which yields a slightly stronger net ring current than that in benzene. When the two shared carbon atoms in naphthalene are replaced by copper atoms, the current density distribution in the resulting macrocycle shows a similarity to the all-carbon [10]annulene. The paratropic ring current follows a pathway along all atoms and there is no indication for the existence of a Cu – Cu bond.

In Article II we investigated the properties of the molecule formally obtained by annelating two benzene rings (the traditional example of an aromatic system with $(4n+2)$ π electrons) to the strongly antiaromatic pentalene molecule with $4n$ π electrons, which, to our knowledge, has not been isolated experimentally. The benzene rings are weakly aromatic with net ring-current strength of about a half of that in the benzene molecule. The heteroatoms in the other three investigated molecules increase the net ring-current strength in the six-membered rings, especially when the benzene ring is annelated to a diazaborole ring when it reaches about 90% of the net ring-current strength in the benzene molecule. The diazaborole rings in molecules (**2**) and (**3**) are non-aromatic with net ring-current strength of about $2.6\,\mathrm{nA}\cdot\mathrm{T}^{-1}$. The azadiborole rings are non-aromatic to weakly antiaromatic. In molecule (**2**) where the nitrogen atoms are fused at

the N–N bond, the pentalene paratropic current is missing altogether, while there is a ribbon-shaped local diatropic ring current surrounding the two nitrogen atoms, visualised in Figure 7 in Article II.

The dependence between the aromaticity and the topology of three series of Möbius all-*trans* [40]annulenes was investigated in Article III. The Hückel rules for (anti)aromaticity are reversed for Möbius twisted molecules – the presence of $(4n+2)$ π electrons predicts antiaromatic character, whereas molecules with $4n$ π electrons are expected to be aromatic. Möbius molecular systems are characterised by the linking number L_k, which describes the twist of the carbon skeleton of the molecule T_w, and the bending of the molecular frame in space as a whole (writhe W_r), such that $L_k = T_w + W_r$. Examples for molecules of the extreme cases with the smallest and with the largest writhe (the largest and the smallest twist, respectively) are given in Figure 2 ($L_k = 0$), Figure 3 ($L_k = 1$) and Figure 5 ($L_k = 2$) in Article III. We showed that L_k is not a definitive criterion for the degree of aromaticity but in fact both the twist and the writhe affect the aromatic properties of the molecule. We found that the strength of the net current density increases with increasing twist (decreasing writhe). The magnetic field was oriented such that the orthographic projection of the molecular ring has a maximum area. The area shrinks proportionally with the increase in W_r, which likely causes the weaker current density in the deformed ring.

In Article IV we studied seven series of toroidal carbon nanotubes (nanotori). Nanotori can be figuratively constructed by folding without twisting a rectangular graphene sheet such that the corners coincide. This creates a problem that the bonds on the inner side of the nanotorus become too short while the bonds on the outside are too long. This problem can be solved by working with very large molecules, such as our three biggest structures with 2016 carbon atoms. Toroidal topology can also be constructed by replacing pairs of hexagons by sets of a pentagon and a heptagon. This alleviates the bond strain since pentagons create positive Gaussian curvature whereas heptagons introduce negative curvature. An example is illustrated in Figure 4.7.

There are two classes of carbon nanotubes which we employed in the construction of the nanotori – *armchair*, with a long acene-like hexagonal lattice along the length of the nanotube, and *zigzag*, where the acene pattern makes a circle around the diameter of the nanotube, perpendicularly to its long side. There are various intermediate alignments of the acene chain with respect to the open end of the nanotube. This concept applies also to toroidal carbon nanotubes. Armchair and zigzag nanotori are illustrated in Article IV, in Figures 7 and 8 respectively. When it comes to ring-current flow, the armchair pattern gives rise to long current pathways surrounding the whole nanotorus. The increase in the length of the acene chain leads to stronger global ring currents as we found in the series I of nanotori. In contrast, the

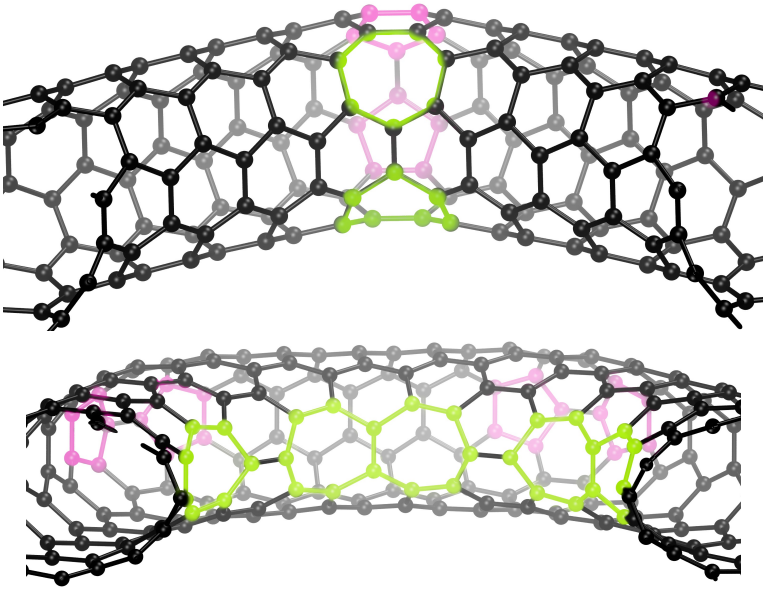

Figure 4.7: The corner with pentagons (magenta) and heptagons (green) in series IV (above) and series VI (below) of the toroidal carbon nanotubes investigated in Article IV [198]. The corners in series V are similar to those in series IV. Series VII has a more complicated structure.

zigzag pattern appears to allow mostly local ring currents and the global ring current is weak. Patterns intermediate between armchair and zigzag are more specific. Series IV and V of nanotori are constructed such that there are six straight fragments of a nanotube of varying length connected by introducing two pairs of pentagons and heptagons at the corners. There were no strong global ring currents in all but one of the investigated molecules, irrespectively of whether the nanotube segments are of armchair or zigzag type. Series VI and VII are constructed from twelve pieces of carbon nanotube of alternating armchair and zigzag types. Pentagons and heptagons are used to connect the corners. No clear trends were found regarding their ring-current strengths. The corner connections of the nanotori of series IV and series VI are illustrated in Figure 4.7. The current density on a toroidal surface can be decomposed into one vector component along the tube and another component perpendicular to it. If the both components are non-zero, the nanotorus sustains helical current-density flow as found for one of the investigated molecules built entirely from hexagons with 2016 carbon atoms. A streamline representation is given in Figure 9 in Article IV.

In our manuscript [278], GIMIC calculations were performed on the toluene and the 3,4,5-trifluorotoluene molecules at the DFT and MP2 levels of theory. The 3D current-density vector field was visualised by placing an integration plane perpendicularly to the molecular ring along the C–C bond to the methyl group as illustrated in Figure 4.5.

The magnetic field vector points along the C–C bond. There is a diatropic atomic current vortex at each nucleus. However, the sp^2 carbon atoms also exhibit a strong paratropic current of about $-14\,\mathrm{nA}\cdot\mathrm{T}^{-1}$ which is entirely local. Interestingly, these paratropic currents can also be found when the magnetic field is perpendicular to the benzene ring. Their existence has been previously investigated through a topology analysis of the current density [27].

4.2 SMALL MOLECULES IN STRONG MAGNETIC FIELDS

Strong magnetic fields act as a confining potential with cylindrical symmetry and thus the binding energies between atoms differ, depending on the mutual orientation of the magnetic field vector and the chemical bond. High-spin states become ever more favourable and state rearrangements occur as the field strength grows. As a result, isolated atoms with parallel electron spin may have lower energy than a molecule bound by a σ bond. In our studies we employed the unrestricted Hartree–Fock level of theory with uncontracted augmented correlation-consistent double-ζ, triple-ζ, quadruple-ζ, and quintuple-ζ basis sets. The Dunning family of basis sets has been designed with dynamic electron correlation in mind [279]. Additional auxiliary functions are introduced in the augmented variety of the basis sets in order to bring additional flexibility, required for the calculation of nuclear shielding constants and spin-spin interactions [280]. The calculations were performed with the LONDON program [262, 267]. Benchmarking was done with the HELFEM program [281–283].

4.2.1 *Basis set evaluation*

In Article V, the accuracy of the aforementioned basis sets consisting of Gaussian-type orbitals (GTOs) was benchmarked to data obtained with a fully numerical implementation based on the finite-element method (FEM) close to the complete basis set limit on the molecules H_2, HeH^+, LiH, BeH^+, BH, and CH^+ with the magnetic field in parallel orientation to the bonds. The interatomic distances were kept constant in the calculations performed with the both programs. We concluded that the basis-set truncation errors (BSTEs) of the employed aug-cc-pVTZ uncontracted GTO basis set is less than $1\,\mathrm{kcal}\cdot\mathrm{mol}^{-1}$ at zero magnetic field, which lies within the chemical accuracy at the UHF level of theory. The error increases as the magnetic field strength grows. At $B = B_0$, the deviation in the energy is within about $3\,\mathrm{kcal}\cdot\mathrm{mol}^{-1}$ for the singlet and triplet states of the investigated molecules with the exception of the triplet H_2 molecule with a BSTE of $11.5\,\mathrm{kcal}\cdot\mathrm{mol}^{-1}$. The quality of the basis set varies for the quintet states between $2.5\,\mathrm{kcal}\cdot\mathrm{mol}^{-1}$ for BeH^+ and $21.1\,\mathrm{kcal}\cdot\mathrm{mol}^{-1}$ for BH. Likely this is due to some basis functions having more suitable exponents than

others to describe the changes in the molecular orbitals brought about by the strong magnetic field. Increasing the magnetic field strength to $B = 10\,B_0$ leads to disastrous performance with a BSTE of about $1000\,\mathrm{kcal \cdot mol^{-1}}$.

We also investigated the significance of the number of high-angular-momentum basis functions by performing calculations with the uncontracted augmented correlation consistent aug-cc-pVDZ, aug-cc-pVTZ, aug-cc-pVQZ, and aug-cc-pV5Z basis sets without g and h functions for the singlet, triplet, and quintet states of BeH^+. The data for $B = [0;10]\,B_0$ are plotted in Figure 4.8. High-multiplicity configurations were the least accurate ones for all investigated molecule, and there were various issues with the quintet BeH^+.

The BSTE at $B = 0$ is large because the FEM calculation converged to state where all orbitals are of σ type, whereas the GTO calculations produced a state with an occupied π orbital. Attempts to converge to the correct state was only done in the calculation performed with the native aug-cc-pVTZ basis set. The BSTE was found to be $1.3\,\mathrm{kcal \cdot mol^{-1}}$. At $B = B_0$, the quintet state of BeH^+ the BSTE with the native aug-cc-pVTZ basis set grew to $2.5\,\mathrm{kcal \cdot mol^{-1}}$ but the aug-cc-pV5Z basis sets without g and h functions yielded an error of barely $0.24\,\mathrm{kcal \cdot mol^{-1}}$. At $B = 2\,B_0$, the numerical calculations produced a configuration with an occupied δ orbital. The aug-cc-pVTZ basis set does not contain enough basis functions to reproduce the same occupation. The configuration was only obtained with the quadruple-ζ and quintuple-ζ basis sets with s, p, d, and f functions. Therefore, both the number and the angular momentum of the primitives in the basis set are an important factor when choosing the level of theory.

4.2.2 *Atoms*

The electronic configuration of atoms undergoes changes as the field strength increases due to the Zeeman effect. Orbitals with high angular momentum become lower in energy. By convention, the orbitals with magnetic quantum number $m < 0$ become stabilised, whereas when m is positive, the orbital energy grows. Similarly, due to the spin Zeeman effect, the orbitals with spin quantum number $m_s = -\frac{1}{2}$ becomes stabilised in the presence of a magnetic field while $m_s = \frac{1}{2}$ leads to an increase in the orbital energy. The dependence of the energy of the singlet, triplet and quintet states of the carbon atom on the magnetic field is plotted in Figure 4.9. In the absence of a magnetic field, the ground state is a triplet with the familiar occupation $1s^2 2s^2 2p^2$. However, at $B = 0.18\,B_0$ there is a state crossing and the quintet state becomes lower in energy than the triplet as originally shown by Hampe and Stopkowicz [241]. They compared the Hartree–Fock results to coupled-cluster data and found that the state crossing should occur at about $B = 0.3\,B_0$ where all three p orbitals

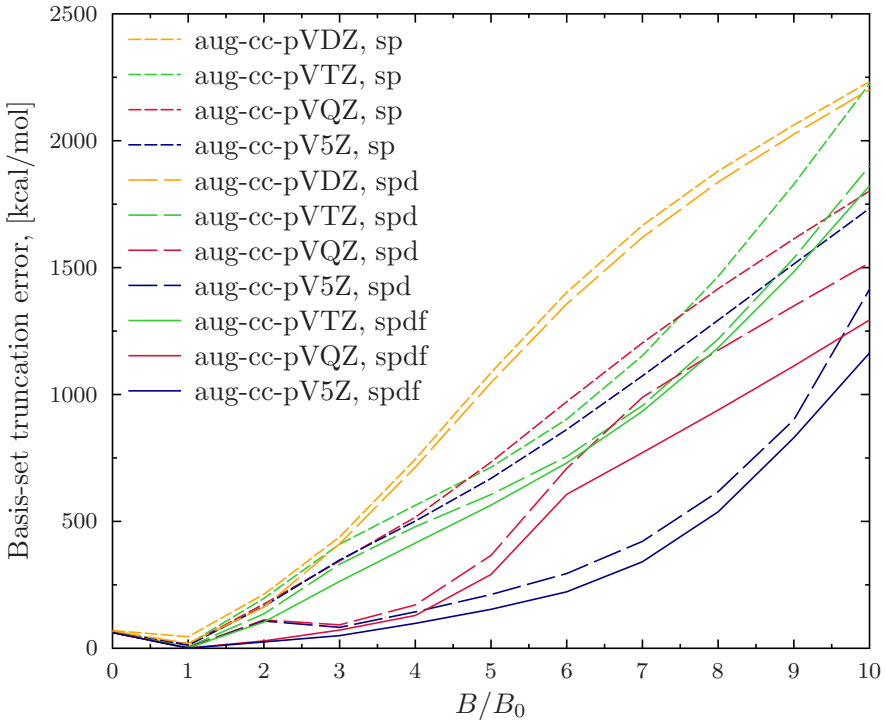

Figure 4.8: Basis-set truncation error comparison of a series of uncontracted Gaussian-type correlation-consistent basis sets for $B = [0; 10]B_0$ calculated for the quintet state of BeH^+. The reference data is obtained using the fully numerical code HELFEM. The aug-cc-pVDZ basis set natively consists of s, p and d primitives only. In the aug-cc-pVTZ basis set there are also f functions. The g and h functions were excluded from the larger basis sets.

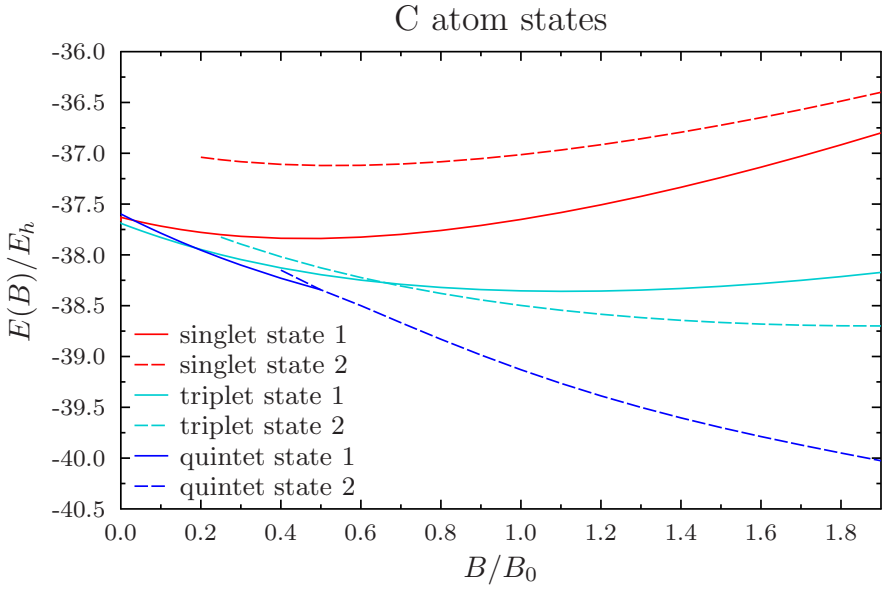

Figure 4.9: The energy of the carbon atom as a function of the magnetic field strength at the UHF/aug-cc-pVTZ level of theory.

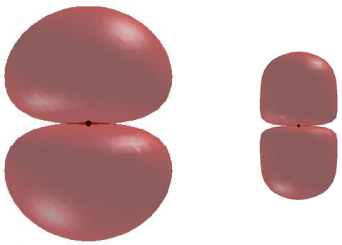

Figure 4.10: A p orbital of the carbon atom at $B = 0$ (left) and at $B = 10\,B_0$ (right). The plots are to scale.

are occupied. Another state crossing was found at $B = 0.5\,B_0$ both at HF and CC level where the d_{-2} orbital becomes lower in energy than p_{+1}. Increasing the magnetic field strength to $B = 10\,B_0$ confines the orbitals as shown in Figure 4.10, however we did not do any further studies at that field strength due to the basis-set truncation error discussed in Section 4.2.1 and Article V.

4.2.3 *Diatomic molecules*

The electron configuration and orbital symmetry of diatomic molecules was investigated in Article V. We showed that for the most part, there is good agreement between the symmetry of the occupied orbitals calculated with GTO basis sets and with the finite-element method. In states with high spin multiplicity such as the quintet configuration of BH and CH^+, a δ orbital becomes occupied at $B = 0.4\,B_0$ and at $B = 0.7\,B_0$ respectively according to the FEM implementation. Tables of the ground-state configurations for the investigated molecules are listed in Tables 1, 2, and 3 in Article V. Symmetry was not enforced in the calculations with the LONDON program unlike for the HELFEM program. In consequence, some symmetry-broken states were obtained at very strong magnetic fields.

Diatomic molecules oriented perpendicularly to the magnetic field vector exhibit paramagnetic bonding, where a state with high spin multiplicity shows a shallow minimum in the potential energy surface (PES) [240]. This is the case in our work in Article VI. The interatomic distance in the doublet, quartet, and sextet CH was investigated for $B \leq B_0$ with both parallel and perpendicular direction of the magnetic field with respect to the chemical bond. The energy state diagram becomes complicated as shown in Article VI, Figure 3 for $B = 0.1\,B_0$ and in Article VI, Figure 4 for $B = 0.7\,B_0$. At $B = 0$, the CH molecule exists in a quartet state. However, between $B = 0.25\,B_0$ and $B = 0.5\,B_0$, the molecule is not bound. Increasing the magnetic field further gives rise to paramagnetic bonding in the sextet state and at $B = 0.7\,B_0$ the binding energy is $6.7\,\mathrm{kcal \cdot mol^{-1}}$.

4.2.4 *Polyatomic molecules*

We have investigated the energies and electron configurations of a series of small CH fragments: CH, CH_2, CH_3, and CH_4 at the UHF level of theory with the uncontracted aug-cc-pVTZ basis set. The smaller CH and CH_2 are studied in Article VI, whereas CH_3 and CH_4 will be explored in more detail in the future. We found that all of the molecules become bound at sufficiently strong magnetic fields when they are aligned perpendicularly to the field vector. The molecular geometry of CH_2 was first optimised as a linear molecule by varying the bond lengths. After the minima were obtained for the lowest states of all multiplicities and magnetic field strengths and directions, the bond angle was varied. We found that there is little preference for the position of the hydrogen atoms. Plots of the energy dependence on the bond angle ϕ are presented in Article VI.

We have done preliminary investigations on CH_3 and CH_4, both of which were enforced to be planar structures with D_{3h} and D_{4h} symmetry respectively. The choice of molecular geometries is based on the finding that the highest binding energy in the CH molecule when the magnetic field is perpendicular to the C – H axis. Bound states were found in the high-spin states where only the $1s$ electrons of the carbon atom. The binding energy of the octet state of CH_3 is largest at $B = 0.7\,B_0$, $14.4\,\mathrm{kcal}\cdot\mathrm{mol}^{-1}$. At increasing field strength, the binding energy starts dropping again. At $B = 0.9\,B_0$, $E_{\mathrm{bind}} = 11.4\,\mathrm{kcal}\cdot\mathrm{mol}^{-1}$. The largest binding energy for the nonet state of CH_4 also occurs at $B = 0.7\,B_0$.

5

CONCLUSION

The work presented in the doctoral thesis follows two main lines – the magnetically induced current density in molecules treated at the zero-field limit using perturbation theory, and the explicit treatment of magnetic fields of finite strength.

We studied the flow and the strength of the magnetically induced current densities in various organic molecules - small annulenes, polycyclic molecules, Möbius twisted annulenes and toroidal carbonanotubes. The aim of the studies was to evaluate the current pathways and determine the aromatic properties of the investigated molecules. We showed that the conformers of [10]annulene have significantly different current-density flow, however, the most stable conformer is non-aromatic. The introduction of two copper atoms instead of two carbon atoms in the [10]annulene ring preserves the ten-atom-ring structure, rather than producing a copper-copper bond as if it were a substituted naphthalene. We found that the presence of the heteroatoms boron and nitrogen disrupts the current density distribution in spite of the same number of electron present in the molecular systems. The aromaticity of Möbius systems was found to be dependent on the topology of the molecular ring, both as the writhe–or the extent to which a ribbon is twisted before its two ends meet–, as well as global twist of the molecule in 3D space. An exotic set of all-carbon molecules formally obtained by twisting and bending a carbon nanotube into a torus were also investigated. The interest in them lies in the possible presence of anapole moment in chiral toroidal molecules.

On the other scale of magnetic field strength, we evaluated the stability of molecules in strong magnetic fields and studied the applicability of the available quantum-chemistry methods for a correct description of the electronic structure of diatomic hydrides. We showed that when a hydrocarbon molecule is oriented perpendicularly to the magnetic field, chemical bonds arise in a high-spin configuration. In the case of methane, the most stable molecule was found to exist at $B = 0.7\,B_0$ with eight electrons with parallel spin.

BIBLIOGRAPHY

[1] P. Zeeman. *Nature* **55** (1897), 347.

[2] G. E. Hale. *J. Geophys. Res.* **13** (1908), 159.

[3] P. Luyten, J. Bulthuis, and C. Maclean. *Chem. Phys. Letters* **89** (1982), 287.

[4] K. Kordás, T. Mustonen, G. Tóth, J. Vähäkangas, H. Jantunen, A. Gupta, K. V. Rao, R. Vajtai, and P. M. Ajayan. *Chem. Mater.* **19** (2007), 787.

[5] S. Takami, S. Furumi, Y. Shirai, Y. Sakka, and Y. Wakayama. *J. Mater. Chem.* **22** (2012), 8629.

[6] M. Iwasaka and S. Ueno. *J. Appl. Phys.* **83** (1998), 6459.

[7] H. Inaba, T. Saitou, K. ichi Tozaki, and H. Hayashi. *J. Appl. Phys.* **96** (2004), 6127.

[8] M. Iino and Y. Fujimura. *Appl. Phys. Letters* **94** (2009), 261902.

[9] National Institute of Standards and Technology (NIST). The NIST Reference on Constants, Units, and Uncertainty. https://physics.nist.gov/cgi-bin/cuu/Value?mub. Accessed: 2019-05-29.

[10] B. N. Murdin et al. *Nat. Comm.* **4** (2013), 1469.

[11] S. Hahn et al. *Nature* **570** (2019), 496.

[12] A. I. Bykov, M. I. Dolotenko, N. P. Kolokolchikov, V. D. Selemir, and O. M. Tatsenko. *Physica B* **294-295** (2001), 574.

[13] C. M. Fowler, W. B. Garn, and R. S. Caird. *J. Appl. Phys.* **31** (1960), 588.

[14] D. Nakamura, A. Ikeda, H. Sawabe, Y. H. Matsuda, and S. Takeyama. *Rev. Sci. Instr.* **89** (2018), 095106.

[15] J. C. Kemp, J. B. Swedlund, J. D. Landstreet, and J. R. P. Angel. *Astrophys. J.* **161** (1970), L77.

[16] J. R. P. Angel. *Astrophys. J.* **216** (1977), 1.

[17] J. Angel. *Ann. Rev. Astron. Astrophys.* **16** (1978), 487.

[18] J. D. Landstreet. *Astron. Astrophys. Rev.* **4** (1992), 35.

[19] W Kundt. *Astron. Astrophys* **98** (1981), 207.

[20] A. Reisenegger. *Astron. Nachr.* **328** (2007), 1173.

[21] S. Xu, M. Jura, D. Koester, B. Klein, and B. Zuckerman. *Astrophys. J. Lett.* **766** (2013), L18.

[22] D. T. Wickramasinghe and L. Ferrario. *PASP* **112** (2000), 873.

[23] S. Jordan, P. Schmelcher, W. Becken, and W. Schweizer. *Astron. Astrophys.* **336** (1998), L33.

[24] D. T. Wickramasinghe, G. Schmidt, L. Ferrario, and S. Vennes. *MNRAS* **332** (2002), 29.

[25] G. D. Schmidt, P. Bergeron, and B. Fegley. *Astrophys. J.* **443** (1995), 274.

[26] J. Liebert et al. *Astrophys. J.* **126** (2003), 2521.

[27] P. Lazzeretti. *Prog. Nucl. Magn. Reson. Spectrosc.* **36** (2000), 1.

[28] D. Sundholm, H. Fliegl, and R. J. F. Berger. *WIREs Comput. Mol. Sci.* **6** (2016), 639.

[29] S. R. Marder, B. Kippelen, A. K.-Y. Jen, and N. Peyghambarian. *Nature* **388** (1997), 845.

[30] J. VandeVondele, U. Borštnik, and J. Hutter. *J. Chem. Theory Comput.* **8** (2012), 3565.

[31] E. Schrödinger. *Ann. Phys. (Berlin)* **384** (1926), 361.

[32] E. Schrödinger. *Ann. Phys. (Berlin)* **384** (1926), 489.

[33] E. Schrödinger. *Ann. Phys. (Berlin)* **385** (1926), 437.

[34] E. Schrödinger. *Ann. Phys. (Berlin)* **386** (1926), 109.

[35] E. Schrödinger. *Ann. Phys. (Berlin)* **384** (1926), 734.

[36] M. Born, W. Heisenberg, and P. Jordan. *Zeits. Phys.* **35** (1926), 557.

[37] W. Heisenberg. *Zeits. Phys.* **33** (1925), 879.

[38] M. Born and P. Jordan. *Zeits. Phys.* **34** (1925), 858.

[39] W. Pauli. *Zeits. Phys.* **36** (1926), 336.

[40] M. Born. *Zeits. Phys.* **37** (1926), 863.

[41] P. A. M. Dirac. *Math. Proc. Cambridge Philos. Soc.* **35** (1939), 416.

[42] M. Born and R. Oppenheimer. *Ann. Phys.* **389** (1927), 457.

[43] D. R. Hartree. *Math. Proc. Cambridge Philos. Soc.* **24** (1928), 89.

[44] D. R. Hartree. *Math. Proc. Cambridge Philos. Soc.* **24** (1928), 111.

[45] J. C. Slater. *Phys. Rev.* **32** (1928), 339.

[46] W. Ritz. *J. Reine. Angew. Math.* **135** (1909), 236.

[47] E. Fermi. *Rend. Accad. Naz. Lincei* **6** (1927), 32.

[48] P. A. M. Dirac. *Math. Proc. Cambridge Philos. Soc.* **26** (1930), 376.

[49] J. C. Slater. *Phys. Rev.* **34** (1929), 1293.

[50] V. Fock. *Zeits. Phys.* **61** (1930), 126.

[51] W. Pauli. *Phys. Rev.* **58** (1940), 716.

[52] C. C. J. Roothaan. *Rev. Mod. Phys.* **23** (1951), 69.

[53] G. G. Hall. *Proc. R. Soc. Lond. A* **205** (1951), 541.

[54] J. C. Slater. *Phys. Rev.* **36** (1930), 57.

[55] S. F. Boys. *Proc. R. Soc. Lond. A* **200** (1950), 542.

[56] H. Hellmann. *J. Chem. Phys.* **3** (1935), 61.

[57] P. Schwerdtfeger. *Chem. Phys. Chem.* **12** (2011), 3143.

[58] F. Jensen. *WIREs Comput. Mol. Sci.* **3** (2012), 273.

[59] E. Clementi and D. R Davis. *J. Comp. Phys.* **1** (1966), 223.

[60] H. Taketa, S. Huzinaga, and K. O-ohata. *J. Phys. Soc. Jpn* **21** (1966), 2313.

[61] F. A. Bischoff and E. F. Valeev. *J. Chem. Phys.* **134** (2011), 104104.

[62] H.-J. Flad, W. Hackbusch, D. Kolb, and R. Schneider. *J. Chem. Phys.* **116** (2002), 9641.

[63] D. P. Tew, W. Klopper, and T. Helgaker. *J. Comp. Chem.* **28** (2007), 1307.

[64] P.-O. Löwdin. Correlation Problem in Many-Electron Quantum Mechanics I. Review of Different Approaches and Discussion of Some Current Ideas. *Advances in Chemical Physics*. John Wiley & Sons, Ltd, 2007. chap. 7, 207.

[65] T. Helgaker and P. Taylor. Gaussian Basis Sets and Molecular Integrals. *Modern Electronic Structure Theory*. ed. by D. R. Yarkony. vol. 2. Advanced Series in Physical Chemistry. World Scientific Publishing Company, 1995. chap. 12, 725.

[66] J. A. Pople, M. Head-Gordon, D. J. Fox, K. Raghavachari, and L. A. Curtiss. *J. Chem. Phys.* **90** (1989), 5622.

[67] L. A. Curtiss, C. Jones, G. W. Trucks, K. Raghavachari, and J. A. Pople. *J. Chem. Phys.* **93** (1990), 2537.

[68] L. A. Curtiss, K. Raghavachari, G. W. Trucks, and J. A. Pople. *J. Chem. Phys.* **94** (1991), 7221.

[69] L. A. Curtiss, K. Raghavachari, P. C. Redfern, V. Rassolov, and J. A. Pople. *J. Chem. Phys.* **109** (1998), 7764.

[70] L. A. Curtiss, P. C. Redfern, and K. Raghavachari. *J. Chem. Phys.* **126** (2007), 084108.

[71] T. J. Lee and P. R. Taylor. *Int. J. Quant. Chem.* **36** (1989), 199.

[72] C. L. Benavides-Riveros, N. N. Lathiotakis, and M. A. L. Marques. *Phys. Chem. Chem. Phys.* **19** (2017), 12655.

[73] J. W. S. B. Rayleigh. *The theory of sound*. vol. 2. Macmillan, 1896, 115.

[74] C. Møller and M. S. Plesset. *Phys. Rev.* **46** (1934), 618.

[75] O. Christiansen, J. Olsen, P. Jørgensen, H. Koch, and P.-Å. Malmqvist. *Chem. Phys. Letters* **261** (1996), 369.

[76] J. Olsen, O. Christiansen, H. Koch, and P. Jørgensen. *J. Chem. Phys.* **105** (1996), 5082.

[77] J. A. Pople, R. Seeger, and R. Krishnan. *Int. J. Quant. Chem.* **12** (1977), 149.

[78] F. Coester and H. Kümmel. *Nucl. Phys.* **17** (1960), 477.

[79] J. Čížek. *J. Chem. Phys.* **45** (1966), 4256.

[80] P. A. M. Dirac. *Proc. R. Soc. Lond. A* **114** (1927), 243.

[81] J. Řezáč and P. Hobza. *J. Chem. Theory Comput.* **9** (2013), 2151.

[82] J. Goldstone. *Proc. R. Soc. Lond. A* **239** (1957), 267.

[83] F. Neese, D. G. Liakos, and S. Ye. *J, Biol. Inorg. Chem.* **16** (2011), 821.

[84] L. H. Thomas. *Math. Proc. Cambridge Philos. Soc.* **23** (1927), 542.

[85] C. F. v. Weizsäcker. *Zeits. Phys.* **96** (1935), 431.

[86] E. Teller. *Rev. Mod. Phys.* **34** (1962), 627.

[87] J. P. Desclaux. *Comput. Phys. Commun.* **9** (1975), 31.

[88] P. Hohenberg and W. Kohn. *Phys. Rev.* **136** (1964), B864.

[89] W. Kohn and L. J. Sham. *Phys. Rev.* **140** (1965), A1133.

[90] J. P. Perdew, A. Ruzsinszky, L. A. Constantin, J. Sun, and G. I. Csonka. *J. Chem. Theory Comput.* **5** (2009), 902.

[91] A. D. Becke. *Phys. Rev. A* **33** (1986), 2786.

[92] S. H. Vosko, L. Wilk, and M. Nusair. *Can. J. Phys.* **58** (1980), 1200.

[93] J. P. Perdew and Y. Wang. *Phys. Rev. B* **45** (1992), 13244.

[94] A. D. Becke. *J. Chem. Phys.* **84** (1986), 4524.

[95] A. D. Becke. *Phys. Rev. A* **38** (1988), 3098.

[96] A. D. Becke. *J. Chem. Phys.* **140** (2014), 18A301.

[97] A. D. Becke. *Int. J. Quant. Chem.* **23** (1983), 1915.

[98] J. P. Perdew, K. Burke, and M. Ernzerhof. *Phys. Rev. Lett.* **77** (1996), 3865.

[99] J. P. Perdew and L. A. Constantin. *Phys. Rev. B* **75** (15 2007), 155109.

[100] J. Tao, J. P. Perdew, V. N. Staroverov, and G. E. Scuseria. *Phys. Rev. Lett.* **91** (2003), 146401.

[101] Y. Zhao, N. E. Schultz, and D. G. Truhlar. *J. Chem. Phys.* **123** (2005), 161103.

[102] Y. Zhao and D. G. Truhlar. *Theor. Chem. Acc.* **120** (2007), 215.

[103] E. G. Hohenstein, S. T. Chill, and C. D. Sherrill. *J. Chem. Theory Comput.* **4** (2008), 1996.

[104] D. E. Taylor et al. *J. Chem. Phys.* **145** (2016), 124105.

[105] N. Mardirossian and M. Head-Gordon. *J. Chem. Theory Comput.* **12** (2016), 4303.

[106] A. D. Becke. *J. Chem. Phys.* **98** (1993), 5648.

[107] C. Lee, W. Yang, and R. G. Parr. *Phys. Rev. B* **37** (1988), 785.

[108] J.-D. Chai and M. Head-Gordon. *J. Chem. Phys.* **128** (2008), 084106.

[109] J.-D. Chai and M. Head-Gordon. *Phys. Chem. Chem. Phys.* **10** (2008), 6615.

[110] Y. Zhao, B. J. Lynch, and D. G. Truhlar. *J. Phys. Chem. A* **108** (2004), 4786.

[111] S. Grimme. *J. Chem. Phys.* **124** (2006), 034108.

[112] J. W. Ochterski, G. A. Petersson, and J. A. Montgomery. *J. Chem. Phys.* **104** (1996), 2598.

[113] M. P. de Lara-Castells, R. V. Krems, A. A. Buchachenko, G. Delgado-Barrio, and P. Villarreal. *J. Chem. Phys.* **115** (2001), 10438.

[114] D. Feller and D. A. Dixon. *J. Phys. Chem. A* **122** (2018), 2598.

[115] S. F. Boys and F. Bernardi. *Mol. Phys.* **19** (1970), 553.

[116] M. Nooijen, K. R. Shamasundar, and D. Mukherjee. *Mol. Phys.* **103** (2005), 2277.

[117] R. J. Bartlett and G. D. Purvis. *Int. J. Quant. Chem.* **14** (1978), 561.

[118] R. J. Bartlett. *Annu. Rev. Phys. Chem.* **32** (1981), 359.

[119] J. A. Pople, J. S. Binkley, and R. Seeger. *Int. J. Quant. Chem.* **10** (2009), 1.

[120] S. F. Sousa, P. A. Fernandes, and M. J. Ramos. *J. Phys. Chem. A* **111** (2007), 10439.

[121] R. Eisenschitz and F. London. *Zeits. Phys.* **60** (1930), 491.

[122] F. London. *Zeits. Phys.* **63** (1930), 245.

[123] S. Grimme. *J. Comp. Chem.* **27** (2006), 1787.

[124] S. Grimme, J. Antony, S. Ehrlich, and H. Krieg. *J. Chem. Phys.* **132** (2010), 154104.

[125] S. Grimme, S. Ehrlich, and L. Goerigk. *J. Comp. Chem.* **32** (2011), 1456.

[126] E. Caldeweyher, C. Bannwarth, and S. Grimme. *J. Chem. Phys.* **147** (2017), 034112.

[127] A. D. Becke and E. R. Johnson. *J. Chem. Phys.* **122** (2005), 154104.

[128] A. D. Becke and E. R. Johnson. *J. Chem. Phys.* **123** (2005), 154101.

[129] E. R. Johnson and A. D. Becke. *J. Chem. Phys.* **124** (2006), 174104.

[130] S. F. Boys and I. Shavitt. *University of Wisconsin Naval Research Laboratory Tech. Rept*. tech. rep. WIS-AF-13, 1959.

[131] R. A. Kendall and H. A. Früchtl. *Theor. Chem. Acc.* **97** (1997), 158.

[132] S. Grimme. *J. Chem. Phys.* **118** (2003), 9095.

[133] S. Grimme, L. Görigk, and R. F. Fink. *WIREs Comput. Mol. Sci.* **2** (2012), 886.

[134] J. Rychlewski. *Explicitly Correlated Wave Functions in Chemistry and Physics: Theory and Applications*. Progress in Theoretical Chemistry and Physics. Springer Netherlands, 2013.

[135] W. Klopper and C. C. M. Samson. *J. Chem. Phys.* **116** (2002), 6397.

[136] W. Kutzelnigg. *Theor. Chem. Acc.* **68** (1985), 445.

[137] E. A. Hylleraas. *Zeits. Phys.* **54** (1929), 347.

[138] T. B. Adler, G. Knizia, and H.-J. Werner. *J. Chem. Phys.* **127** (2007), 221106.

[139] D. P. Tew, W. Klopper, C. Neiss, and C. Hättig. *Phys. Chem. Chem. Phys.* **9** (2007), 1921.

[140] P. Güttinger. *Zeits. Phys.* **73** (1932), 169.

[141] R. P. Feynman. *Phys. Rev.* **56** (1939), 340.

[142] E. Noether. ger. *Gott. Nachr.* **1918** (1918), 235.

[143] J. C. Maxwell. *Trans. Cambridge Philos. Soc.* **10** (1855).

[144] J. C. Maxwell. *Philos. Mag.* **90** (1861), 11.

[145] J. C. Maxwell. *A treatise on electricity and magnetism*. vol. 1. Oxford: Clarendon Press, 1873.

[146] J. C. Maxwell. *A treatise on electricity and magnetism*. vol. 2. Oxford: Clarendon Press, 1873.

[147] M. Motokawa. *Rep. Prog. Phys.* **67** (2004), 1995.

[148] L. Pauling. *J. Chem. Phys.* **4** (1936), 673.

[149] R. A. Hegstrom and W. N. Lipscomb. *Rev. Mod. Phys.* **40** (1968), 354.

[150] S. Pelloni, P. Lazzeretti, and R. Zanasi. *J. Phys. Chem. A* **113** (2009), 14465.

[151] R. R. Valiev, H. Fliegl, and D. Sundholm. *Chem. Comm.* **53** (2017), 9866.

[152] K. S. Krishnan, B. C. Guha, and S. Banerjee. *Phil. Trans. Royal Soc.* **231** (1933), 235.

[153] K. S. Krishnan, N. C. Chakravorty, and S. Banerjee. *Phil. Trans. Royal Soc.* **232** (1934), 99.

[154] J. Van Vleck. *The Theory of Electric and Magnetic Susceptibilities*. The International series of monographs on physics. Clarendon Press, 1932.

[155] P. A. M. Dirac. *Proc. R. Soc. Lond. A* **109** (1925), 642.

[156] W. Heisenberg. *Zeits. Phys.* **43** (1927), 172.

[157] M. Abramowitz and I. A. Stegun. *Handbook of Mathematical Functions with Formulas, Graphs, and Mathematical Tables*. Ninth Revised Ed. New York: Dover, 1964. chap. 8.

[158] W. Pauli. *Zeits. Phys.* **43** (1927), 601.

[159] G. E. Uhlenbeck and S. Goudsmit. *Nature* **117** (1926), 264.

[160] B. Odom, D. Hanneke, B. D'Urso, and G. Gabrielse. *Phys. Rev. Lett.* **97** (2006).

[161] G. Gabrielse, D. Hanneke, T. Kinoshita, M. Nio, and B. Odom. *Phys. Rev. Lett.* **97** (2006).

[162] H. N. Russell and F. A. Saunders. *Astrophys. J.* **61** (1925), 38.

[163] L. I. Schiff and H. Snyder. *Phys. Rev.* **55** (1939), 59.

[164] J.-M. Lévy-Leblond. *Commun. Math. Phys.* **6** (1967), 286.

[165] J. O. Hirschfelder. *J. Chem. Phys.* **68** (1978), 5151.

[166] E. Madelung. *Zeits. Phys.* **40** (1927), 322.

[167] E. Steiner and P. W. Fowler. *J. Phys. Chem. A* **105** (2001), 9553.

[168] P. A. M. Dirac. *Proc. R. Soc. Lond. A* **133** (1931), 60.

[169] J. O. Hirschfelder, A. C. Christoph, and W. E. Palke. *J. Chem. Phys.* **61** (1974), 5435.

[170] J. O. Hirschfelder, C. J. Goebel, and L. W. Bruch. *J. Chem. Phys.* **61** (1974), 5456.

[171] J. O. Hirschfelder. *J. Chem. Phys.* **67** (1977), 5477.

[172] D. F. Heller and J. O. Hirschfelder. *J. Chem. Phys.* **66** (1977), 1929.

[173] J. A. N. F. Gomes. *J. Chem. Phys.* **78** (1983), 4585.

[174] T. A. Keith and R. F. W. Bader. *J. Chem. Phys.* **99** (1993), 3669.

[175] P. Lazzeretti. *Phys. Chem. Chem. Phys.* **18** (2016), 11765.

[176] P. Lazzeretti. *J. Chem. Phys.* **148** (2018), 134109.

[177] R. L. Ricca. Tropicity and complexity measures for vortex tangles. *Quantized Vortex Dynamics and Superfluid Turbulence*. Springer, 2001, 366.

[178] F. Sondheimer. *Acc. Chem. Res.* **5** (1972), 81.

[179] J. Gauss and J. F. Stanton. Electron-Correlated Approaches for the Calculation of NMR Chemical Shifts. *Advances in Chemical Physics*. John Wiley & Sons, Inc., 2003, 355.

[180] S. T. Epstein. *Isr. J. Chem.* **19** (1980), 154.

[181] P. W. Atkins and J. A. N. F. Gomes. *Mol. Phys.* **32** (1976), 1063.

[182] W. Kutzelnigg. *J. Mol. Struct. (THEOCHEM)* **202** (1989), 11.

[183] T. A. Keith and R. F. Bader. *Chem. Phys. Letters* **210** (1993), 223.

[184] F. London. *J. Phys. Rad.* **8** (1937), 397.

[185] S. T. Epstein. *J. Chem. Phys.* **58** (1973), 1592.

[186] S. T. Epstein. *J. Chem. Phys.* **42** (1965), 2897.

[187] T. Helgaker, M. Jaszuński, and K. Ruud. *Chem. Rev.* **99** (1999), 293.

[188] N. F. Ramsey. *Phys. Rev.* **78** (1950), 699.

[189] J. C. Facelli. *Prog. Nucl. Magn. Reson. Spectrosc.* **58** (2011), 176.

[190] J. A. Pople. *J. Chem. Phys.* **24** (1956), 1111.

[191] H. J. Bernstein, W. G. Schneider, and J. A. Pople. *Proc. R. Soc. Lond. A* **236** (1956), 515.

[192] P. Lazzeretti, M. Malagoli, and R. Zanasi. *Chem. Phys. Letters* **220** (1994), 299.

[193] J. Jusélius, D. Sundholm, and J. Gauss. *J. Chem. Phys.* **121** (2004), 3952.

[194] S. Taubert, D. Sundholm, and J. Jusélius. *J. Chem. Phys.* **134** (2011), 054123.

[195] J. Jusélius, D. Sundholm, and co-workers. GIMIC, Gauge-Including Magnetically Induced Currents, a stand-alone program for the calculation of magnetically induced current density. https://github.com/qmcurrents/gimic.

[196] T. Yanai, D. P. Tew, and N. C. Handy. *Chem. Phys. Letters* **393** (2004), 51.

[197] S. Grimme and M. Waletzke. *J. Chem. Phys.* **111** (1999), 5645.

[198] K. Reiter, F. Weigend, L. N. Wirz, M. Dimitrova, and D. Sundholm. *J. Phys. Chem. C* **123** (2019), 15354.

[199] G. Binsch. *Naturwissenschaften* **60** (1973), 369.

[200] P. R. von Schleyer and H. Jiao. *Pure Appl. Chem.* **68** (1996), 209.

[201] T. M. Krygowski, M. K. Cyrañski, Z. Czarnocki, G. Häfelinger, and A. R. Katritzky. *Tetrahedron* **56** (2000), 1783.

[202] T. M. Krygowski and M. K. Cyrański. *Chem. Rev.* **101** (2001), 1385.

[203] A. T. Balaban, P. von Ragué Schleyer, and H. S. Rzepa. *Chem. Rev.* **105** (2005), 3436.

[204] R. Hoffmann. *Am. Sci.* **103** (2015), 10.

[205] D. Lloyd. *J. Chem. Inf. Comput. Sci.* **36** (1996), 442.

[206] R. Breslow. *Acc. Chem. Res.* **6** (1973), 393.

[207] J.-i. Aihara. *Bulletin of the Chemical Society of Japan* **77** (2004), 2179.

[208] Z. Chen, C. S. Wannere, C. Corminboeuf, R. Puchta, and P. v. R. Schleyer. *Chem. Rev.* **105** (2005), 3842.

[209] R. Gershoni-Poranne and A. Stanger. *Chem. Soc. Rev.* **44** (2015), 6597.

[210] K. Lonsdale. *Proc. R. Soc. Lond. A* **159** (1937), 149.

[211] E. Hückel. *Zeits. Phys.* **70** (1931), 204.

[212] E. Hückel. *Zeits. Phys.* **72** (1931), 310.

[213] E. Hückel. *Zeits. Phys.* **76** (1932), 628.

[214] E. Hückel. *Grundzüge der Theorie ungesättigter und aromatischer Verbindungen.* Verlag Chemie, 1938, 77.

[215] W. von E. Doering and F. L. Detert. *J. Am. Chem. Soc.* **73** (1951), 876.

[216] E. Heilbronner. *Tetrahedron Lett.* **5** (1964), 1923.

[217] H. S. Rzepa. *Chem. Rev.* **105** (2005), 3697.

[218] C. Castro, C. M. Isborn, W. L. Karney, M. Mauksch, and P. von Ragué Schleyer. *Org. Lett.* **4** (2002), 3431.

[219] R. Herges. *Nature* **450** (2007), 36.

[220] M. Bühl and A. Hirsch. *Chem. Rev.* **101** (2001), 1153.

[221] D. Sundholm. *Phys. Chem. Chem. Phys.* **15** (2013), 9025.

[222] J. Pople. *Mol. Phys.* **1** (1958), 175.

[223] H. Fliegl, D. Sundholm, S. Taubert, J. Jusélius, and W. Klopper. *J. Phys. Chem. A* **113** (2009), 8668.

[224] Y. B. Zel'dovich. *Sov. Phys. JETP* **9** (1959), 682.

[225] C. S. Wood. *Science* **275** (1997), 1759.

[226] I. B. Khriplovich and M. E. Pospelov. *Zeits. Phys.* **17** (1990), 81.

[227] A. Ceulemans, L. F. Chibotaru, and P. W. Fowler. *Phys. Rev. Lett.* **80** (1998), 1861.

[228] S. Pelloni, P. Lazzeretti, G. Monaco, and R. Zanasi. *Rend. Fis. Acc. Lincei* **22** (2011), 105.

[229] E. I. Tellgren and H. Fliegl. *J. Chem. Phys.* **139** (2013), 164118.

[230] M. Robnik. *J. Phys. Colloq.* **43** (1982), C2.

[231] L. Landau. *Zeits. Phys.* **64** (1930), 629.

[232] D. Lai. *Rev. Mod. Phys.* **73** (2001), 629.

[233] R. H. Garstang. *Rep. Prog. Phys.* **40** (1977), 105.

[234] R. C. Duncan and C. Thompson. *Astrophys. J.* **392** (1992), L9.

[235] R. C. Duncan. Physics in ultra-strong magnetic fields. *AIP conference proceedings*. vol. 526. AIP. 2000, 830.

[236] M. Ruderman. *Phys. Rev. Lett.* **27** (19 1971), 1306.

[237] C. P. Melo, R. Ferreira, H. S. Brandi, and L. C. M. Miranda. *Phys. Rev. Lett.* **37** (1976), 676.

[238] H.-H. Chen, M. A. Ruderman, and P. G. Sutherland. *Astrophys. J.* **191** (1974), 473.

[239] S. Stopkowicz, J. Gauss, K. K. Lange, E. I. Tellgren, and T. Helgaker. *J. Chem. Phys.* **143** (2015), 074110.

[240] K. K. Lange, E. I. Tellgren, M. R. Hoffmann, and T. Helgaker. *Science* **337** (2012), 327.

[241] F. Hampe and S. Stopkowicz. *J. Chem. Phys.* **146** (2017), 154105.

[242] D. Neuhauser, S. E. Koonin, and K. Langanke. *Phys. Rev. A* **36** (1987), 4163.

[243] P. Schmelcher and L. S. Cederbaum. *Int. J. Quant. Chem.* **64** (1997), 501.

[244] M. V. Ivanov and P. Schmelcher. *Phys. Rev. A* **57** (1998), 3793.

[245] M. V. Ivanov and P. Schmelcher. *Phys. Rev. A* **60** (1999), 3558.

[246] M. V. Ivanov and P. Schmelcher. *Eur. Phys. J. D* **14** (2001), 279.

[247] T. Detmer, P. Schmelcher, F. K. Diakonos, and L. S. Cederbaum. *Phys. Rev. A* **56** (1997), 1825.

[248] T. Detmer, P. Schmelcher, and L. S. Cederbaum. *Phys. Rev. A* **57** (1998), 1767.

[249] W Becken, P Schmelcher, and F. K. Diakonos. *J. Phys. B* **32** (1999), 1557.

[250] W. Becken and P. Schmelcher. *J. Phys. B* **33** (2000), 545.

[251] W. Becken and P. Schmelcher. *Phys. Rev. A* **63** (2001), 053412.

[252] O.-A. Al-Hujaj and P. Schmelcher. *Phys. Rev. A* **70** (2004), 033411.

[253] O.-A. Al-Hujaj and P. Schmelcher. *Phys. Rev. A* **70** (2004), 023411.

[254] P. Schmelcher. *Science* **337** (2012), 302.

[255] E. R. Smith, R. J. W. Henry, G. L. Surmelian, R. F. O'Connell, and A. K. Rajagopal. *Phys. Rev. D* **6** (1972), 3700.

[256] S. Lehtola, M. Dimitrova, and D. Sundholm. *Mol. Phys. (published online)* (2019).

[257] P. Schmelcher and L. S. Cederbaum. *Phys. Rev. A* **37** (1988), 672.

[258] C. Aldrich and R. L. Greene. *Phys. Stat. Sol. (b)* **93** (1979), 343.

[259] A. Kubo. *J. Phys. Chem. A* **111** (2007), 5572.

[260] W. Zhu, L. Zhang, and S. B. Trickey. *Phys. Rev. A* **90** (2014), 022504.

[261] W. Zhu and S. B. Trickey. *J. Chem. Phys.* **147** (2017), 244108.

[262] E. Tellgren, T. Helgaker, and co-workers. LONDON, a quantum-chemistry program for plane-wave/GTO hybrid basis sets and finite magnetic field calculations. https://londonprogram.org.

[263] A. Teale and co-workers. QUEST, QUantum Electronic Structure Techniques. A rapid development platform for electronic structure methods in quantum chemistry. https://quest.codes/.

[264] T. Shiozaki and co-workers. BAGEL, Brilliantly Advanced General Electronic-structure Library. https://nubakery.org.

[265] G. Vignale and M. Rasolt. *Phys. Rev. Lett.* **59** (1987), 2360.

[266] C. J. Grayce and R. A. Harris. *Phys. Rev. A* **50** (1994), 3089.

[267] E. I. Tellgren, A. Soncini, and T. Helgaker. *J. Chem. Phys.* **129** (2008), 154114.

[268] E. I. Tellgren, S. S. Reine, and T. Helgaker. *Phys. Chem. Chem. Phys.* **14** (2012), 9492.

[269] E. I. Tellgren, A. M. Teale, J. W. Furness, K. K. Lange, U. Ekström, and T. Helgaker. *J. Chem. Phys.* **140** (2014), 034101.

[270] E. I. Tellgren, A. Laestadius, T. Helgaker, S. Kvaal, and A. M. Teale. *J. Chem. Phys.* **148** (2018), 024101.

[271] R. D. Reynolds and T. Shiozaki. *Phys. Chem. Chem. Phys.* **17** (2015), 14280.

[272] J. W. Furness, J. Verbeke, E. I. Tellgren, S. Stopkowicz, U. Ekström, T. Helgaker, and A. M. Teale. *J. Chem. Theory Comput.* **11** (2015), 4169.

[273] S. Sen and E. I. Tellgren. *J. Chem. Phys.* **148** (2018), 184112.

[274] C. S. Warke and A. K. Dutta. *Phys. Rev. A* **16** (5 1977), 1747.

[275] National Institute of Standards and Technology (NIST). The NIST Reference on Constants, Units, and Uncertainty. https://physics.nist.gov/cgi-bin/cuu/Value?bohrrada0. Accessed: 2019-09-13.

[276] C. L. J. Ahrens B. Geveci. ParaView: An End-User Tool for Large Data Visualization, Visualization Handbook, Elsevier, 2005, ISBN-13: 978-0123875822. https://www.paraview.org.

[277] K. Bartkowski, M. Dimitrova, P. J. Chmielewski, D. Sundholm, and M. Pawlicki. *(submitted)* (2019).

[278] D. Jia, Y. Yang, M. Dimitrova, Y. Man, and D. Sundholm. *(in preparation)* (2019).

[279] T. H. Dunning. *J. Chem. Phys.* **90** (1989), 1007.

[280] T. Helgaker, M. Jaszuński, K. Ruud, and A. Górska. *Theor. Chem. Acc.* **99** (1998), 175.

[281] S. Lehtola. HelFEM – Finite element methods for electronic structure calculations on small systems Helsinki (Finland 2018). https://github.com/susilehtola/HelFEM.

[282] S. Lehtola. *Int. J. Quant. Chem.* (2019), e25945.

[283] S. Lehtola. *Int. J. Quant. Chem.* (2019), e25944.

TEXTBOOKS

[1] A. Szabo and N. S. Ostlund. *Modern Quantum Chemistry*. Revised ed. Dover Publications, 2012.

[2] I. Levine. *Quantum Chemistry*. Pearson Education, 2013.

[3] F. Jensen. *Introduction to Computational Chemistry*. 2nd ed. Wiley, 2007.

[4] P. W. Atkins and R. S. Friedman. *Molecular Quantum Mechanics*. 5th ed. Oxford University Press, 2011.

[5] D. Griffiths. *Introduction of Quantum Mechanics*. 1st ed. Prentice Hall, 1994.

[6] D. J. Griffiths. *Introduction to Electrodynamics*. 4th ed. Cambridge University Press, 2017.

[7] L. D. Landau and L. M. Lifshitz. *Quantum Mechanics: Non-Relativistic Theory*. 3rd ed. vol. 3. Butterworth-Heinemann, 1981.

APPENDIX

[1] M. Dimitrova and D. Sundholm. The aromatic character of [10]annulenes and dicupra[10]annulenes from current density calculations. *Phys. Chem. Chem. Phys.* **20** (2018), 1337.

[2] M. Dimitrova, H. Fliegl, and D. Sundholm. The influence of heteroatoms on the aromatic character and the current pathways of B_2N_2-dibenzo[a,e]pentalenes. *Phys. Chem. Chem. Phys.* **19** (2017), 20213.

[3] L. N. Wirz, M. Dimitrova, H. Fliegl, and D. Sundholm. Magnetically Induced Ring-Current Strengths in Möbius Twisted Annulenes. *J. Phys. Chem. Lett.* **9** (2018), 1627.

[4] K. Reiter, F. Weigend, L. N. Wirz, M. Dimitrova, and D. Sundholm. Magnetically Induced Current Densities in Toroidal Carbon Nanotubes. *J. Phys. Chem. C* **123** (2019), 15354.

[5] S. Lehtola, M. Dimitrova, and D. Sundholm. Fully numerical electronic structure calculations on diatomic molecules in weak to strong magnetic fields. *Mol. Phys. (published online)* (2019).

[6] M. Dimitrova, S. Lehtola, D. Sundholm, T. Helgaker, and S. Stopkowicz. Small hydrocarbons in strong magnetic fields: CH and CH_2. *(in preparation)* (2019).